E-24-605

FINAL STATUS REPORT

EXPLORATORY STUDY OF SEVERAL ADVANCED NUCLEAR-MHD POWER PLANT SYSTEMS

NASA RESEARCH GRANT NGR-11-002-145

CO-PROJECT DIRECTORS:

J. RICHARD WILLIAMS
SCHOOL OF MECHANICAL ENG.

JOSEPH D. CLEMENT
SCHOOL OF NUCLEAR ENG.

Prepared for the
National Aeronautics and Space Administration
Washington, D. C.

GEORGIA INSTITUTE OF TECHNOLOGY
Atlanta, Georgia

EXPLORATORY STUDY OF SEVERAL ADVANCED NUCLEAR-MHD POWER PLANT SYSTEMS

Final Status Report

NASA Grant NGR-11-002-145

Co Project Directors:

Dr. J. R. Williams
School of Mechanical Eng.

Dr. J. D. Clement
School of Nuclear Eng.

Georgia Institute of Technology
Atlanta, Georgia 30332

March 1973

TABLE OF CONTENTS

ILLUSTRATIONS

page

TABLES

ABSTRACT

In order for efficient multi-megawatt closed cycle nuclear-MHD systems to become practical, long-life gas cooled reactors with exit temperatures of about 2500°K or higher must be developed. Four types of nuclear reactors which have the potential of achieving this goal are the NERVA-type solid core reactor, the colloid core (rotating fluidized bed) reactor, the "light bulb" gas core reactor, and the "coaxial flow" gas core reactor. Research programs aimed at developing these reactors have progressed rapidly in recent years so that prototype power reactors could be operating by 1980. Three types of power plant systems which use these reactors have been analyzed to determine the operating characteristics, critical parameters and performance of these power plants. Overall thermal efficiencies as high as 80% are projected using an MHD turbine-compressor cycle with steam bottoming, and slightly lower efficiencies are projected for an MHD motor-compressor cycle. Nuclear analyses of several reactor configurations have shown that these reactors are capable of breeding, that is, they can produce more fissile fuel than is used. Applications of these plants include terrestrial power generation, space power in the multimegawatt range, and power for proposed satellite nuclear power stations.

INTRODUCTION

J. R. Williams

WHY NUCLEAR-MHD?

It is generally acknowledged today that the world is facing an energy crisis. Electric power requirements have been doubling every ten years, and the demand for transportation and heating fuels has been increasing rapidly. The rapidly increasing demand for fossil fuels has pushed prices up and reduced their availability. In view of the higher costs of fossil fuels and increasingly tight restrictions on the emission of atmospheric pollutants from fossil fuel combustion, nuclear power has become competative and hundreds of nuclear plants are built, planned or under construction. However, serious questions are being raised about the safety and possible adverse environmental effects of these power plants.

The main objections to nuclear power are as follows:
(1) Radioactive emissions during normal plant operation - This is really not a problem in that these emissions can be reduced so that exposure to the public is far below background. This objection can be resolved by proper plant construction, proper plant maintenance, and education. (2) Thermal pollution from nuclear power plants - This is a problem with all thermal power plants (including geothermal). Heat rejection to rivers upsets the ecology of the rivers, wet cooling towers produce local fogging conditions, and dry cooling towers produce thermal plumes which can be a significant hazard to aircraft and which also effect local meteorological conditions. The ultimate heat rejection

method may be radiation to space. However, as the heat rejection temperature is raised, plant efficiency drops and the total thermal discharge increases. Various ideas have been advanced about how the waste heat might be used constructively, but it is difficult to find a practical use for such large amounts of low grade heat. (3) Accidents involving a reactor or a fuel reprocessing plant which result in a release of fission products are a major concern. If such an accident occurs, it could deal a severe setback to the development of nuclear power. (4) Fuel element shipping is a major problem with respect to nuclear power plants. Highly radioactive fuel elements must be removed from the power reactors and transported to a reprocessing plant. An accident which released fission products or plutonium could constitute a major hazard to the public. (5) Safeguards present perhaps one of the greatest long-term problems of nuclear power plants. Unauthorized use of fissionable materials for the development of weapons must be prevented. The necessity of shipping fuel elements to and from reprocessing plants aggrivates the safeguards problem. This problem would be alleviated if fuel reprocessing occured on-site in such a way as to prevent fissionable materials from being removed from the site except under carefully controlled conditions. (6) Disposal of radioactive wastes is presently of major concern to environmentalists. In spite of the elaborate safety precautions that are taken, local governments tend to be strongly opposed to the disposal of radioactive wastes in their area.

The advanced nuclear-MHD power systems described in this report have the potential of alleviating the problems of nuclear power while,

at the same time, reducing its cost. The thermal discharge per electrical megawatt is reduced substantially because of the high overall cycle efficiency projected for advanced nuclear MHD. The heat discharged per MWe from such a plant operating with an 80% efficiency is only 1/4 of the thermal discharge from a gas-turbine topped nuclear plant operating at 50% efficiency, and only 1/6 of the heat release from today's most efficient thermal plants. Also, the efficiency of the nuclear-MHD plant decreases only slightly when the heat rejection temperature is raised (such as by switching from wet to dry cooling towers) whereas other types of thermal power plants are much more strongly affected. Nuclear-MHD plants using colloid-core or gas-core reactors could reject less heat per MWe than fossil-fired MHD power plants.

The safety of colloid-fueled and gas core reactors is enhanced by the continuous removal of fission products from the gas and from the recirculating fuel. In the event of a major accident, only very small amounts of long-lived gaseous fission products would be released. The fuel cycle is simplified since the uranium is handled only as a powder and there are no reactor fuel elements to fabricate or disassemble. This improves the economics of on-site fuel reprocessing, with UF_4 extracted from the ThF_4 in the reactor blanket and reduced to uranium powder which is recirculated through the reactor system. On-site fuel reprocessing elliminates the problem of shipping fuel elements. The safeguards problem is also reduced by on-site fuel reprocessing. Once the reactor is operating, only fertile thorium need be supplied, and the only time fissionable materials need be transported would be an occassional shipment of excess bred fuel.

The problem of radioactive waste disposal is reduced somewhat by the high plant efficiency. An 80% efficient plant produces only 1/2 as much radioactive waste per MWe as a 40% efficient plant.

In order to compete in the breeder economy of the future, advanced nuclear MHD power plants must breed their own fuel from plentiful fertile materials. As was demonstrated so dramatically by the MIT study entitled Limits to Growth, a society which depends for its existance on the consumption of non-renewable resources has a finite lifetime, and the lifetime projected for our society tended to be less than a hundred years, with the end resulting from resource depletion or excessive pollution. The breeder reactor is an essentially non-polluting energy source with over a thousand years of fuel supply readily available. Much of this energy can be used for recycling wastes, so the breeder reactor may permit the development of a closed-cycle (spaceship) economy in which the consumption of non-renewable resources is minimal and pollution is nil, and the lifetime of our society is extended indefinitely. Nuclear-MHD with NERVA-type, colloid core or gas core breeder reactors offer the potential of lower cost power with enhanced safety and reduced environmental impact when compared with current nuclear breeder power plants.

ADVANCED REACTORS FOR NUCLEAR-MHD

In order for efficient multi-megawatt closed cycle nuclear-MHD systems to become practical, long-life gas cooled reactors with exit temperatures of about 2500°K or higher must be developed. Four types of nuclear reactors which have the potential of achieving this goal are the NERVA-type solid core reactor, the colloid core (rotating fluidized bed) reactor, the "light bulb" gas core reactor, and the "coaxial flow" gas core reactor.

The solid core NERVA type reactor,[1,2] which is already well developed, offers the promise of almost immediate application for MHD power generation. The colloid core reactor[3,4] has been studied by the Air Force Aerospace Research Laboratories for the past eight years, and their developmental program has now reached the point that a contract has been given to the Battelle Memorial Institute for an in-reactor test of a fission-heated colloid core reactor experiment using UO_2 particles in a confined vortex.[5] This two year experimental study is the logical step prior to the development of a full scale colloid core reactor. The colloid core reactor uses a rotating fluidized bed of uranium dioxide particles in a confined vortex to heat a gaseous working fluid to as high as 3200°K, temperatures which are ideal for closed cycle MHD power generation. The nuclear fuel cycle, in comparison with present fuel cycles, is greatly simplified since there are no fuel elements.

Two types of gaseous core nuclear reactors also show promise for MHD power generation, the nuclear "light bulb" reactor[6-10] and the coaxial flow reactor.[8-11] In the light bulb reactor, gaseous nuclear fuel is confined within a transparent partition and the working fluid is heated by the absorption of thermal radiation transmitted through the transparent partition from the fissioning gaseous fuel.

Prior to the recent NASA cutback in January, 1973, the United Aircraft Research Laboratories was preparing to conduct a small scale fission heated light bulb reactor experiment in the Nuclear Furnace reactor.[12] Uranium gas was to be confined in a transparent partition and heated by fission to a very high temperature, while a gas such as argon, helium, or hydrogen flowing around the partition is heated to about 3500°K by the thermal radiation from the hot uranium gas inside the partition. The NASA-Lewis Research Center was also proceeding with plans for a Fissioning Uranium Plasma Test Facility to be located at the Nuclear Rocket Development Station. This reactor would have used MTR type fuel elements surrounding a two-foot diameter cavity, and was to be used to test the various gas core and colloid core systems, to demonstrate MHD power generation with these reactors, and to study other applications of fissioning uranium plasmas. Since it now appears that NASA will no longer be involved in the development of nuclear reactors, it is hoped that another agency will continue the development of these high temperature reactor systems for power generation. If such

development is continued, construction of prototype test reactors could begin very soon and they would probably be operating by 1980. The fissioning uranium plasma test facility proposed by NASA would cost about 16 million dollars to build, and could be used to confirm the technical feasibility of larger colloid core and gaseous reactor systems, and to study the performance of MHD generators operating with these reactors.

POWER PLANT SYSTEMS

For the past 1 1/2 years the authors, with NASA support, have been evaluating MHD power plant systems utilizing these high temperature reactors. Some preliminary results have been reported, [13,14] and earlier papers[15-21] describe previous studies of gas core reactor MHD power plant concepts. Some of these earlier studies[17,20] were aimed at determining whether or not a gas core reactor can breed its own fuel. The first calculations considered gas core fast breeder reactors, and showed that although the breeding ratio was high, the critical mass was also large. Gas core thermal breeder reactors, moderated by hydrogen gas, were shown to have much lower critical masses and reasonable breeding ratios.

Three different types of closed cycle nuclear MHD power plant systems have been analyzed to determine the operating characteristics, critical parameters, and performance of these power plant systems. The basic power cycles which have been studied are illustrated by Figures 1-3. Each of these power plant systems may be subdivided into three component subsystems (Figure 4): 1) the high temperature reactor with attached MHD generator and uranium separator (if required), 2) the compressor system and 3) the heat rejection system, which is a steam bottoming cycle.

The first subsystem, which is the same for all 3 plant configurations studied, consists of the nuclear reactor, the MHD generator, uranium separator (if required) and all associated

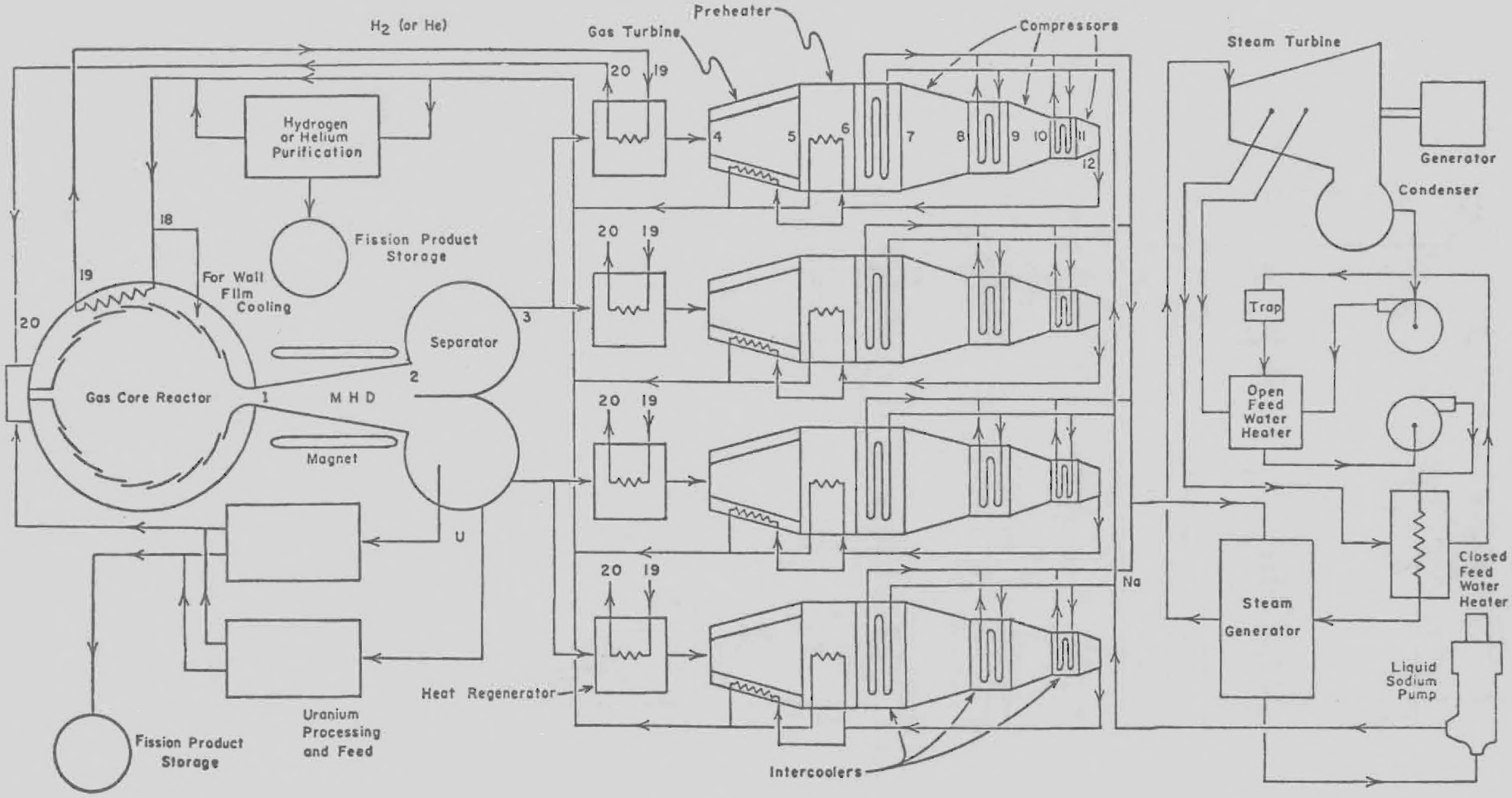

MODE I

Figure 1. Terrestrial Regenerative Turbine-Compressor (Mode I) MHD Power Plant.

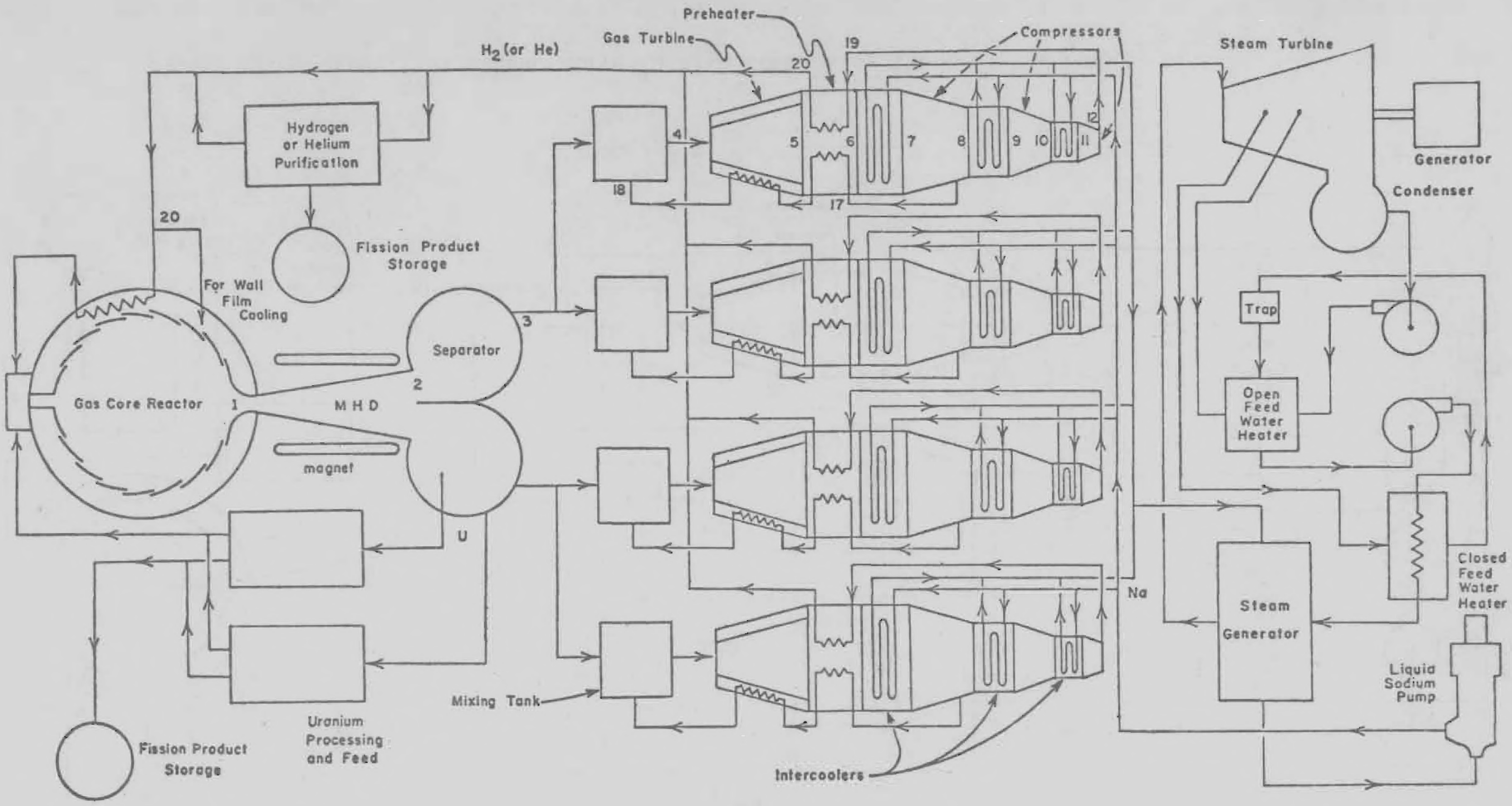

MODE II

Figure 2. Terrestrial Turbine-Compressor (Mode II) MHD Power Plant.

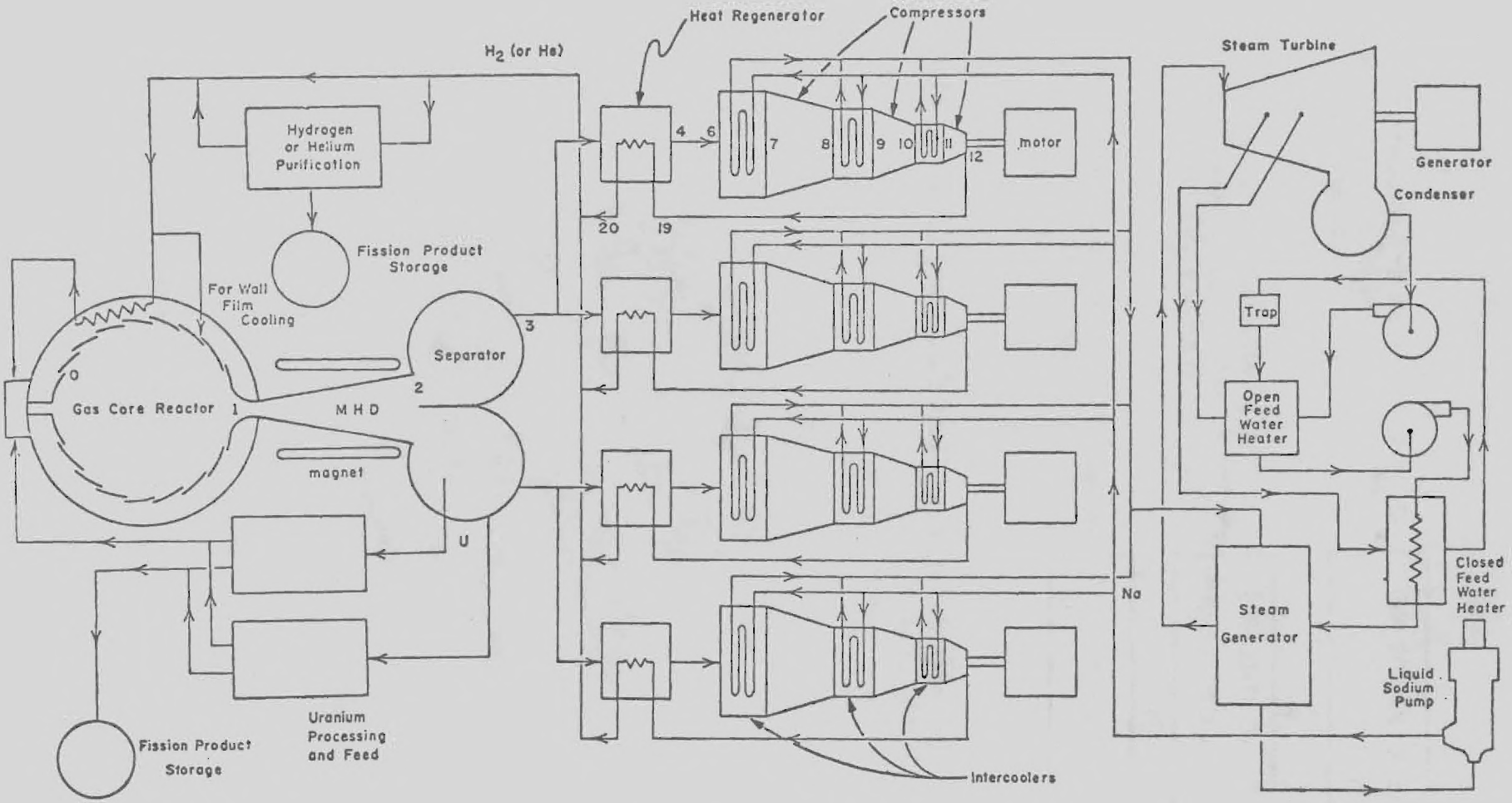

MODE III

Figure 3. Terrestrial Regenerative Motor-Compressor (Mode III) MHD Power Plant.

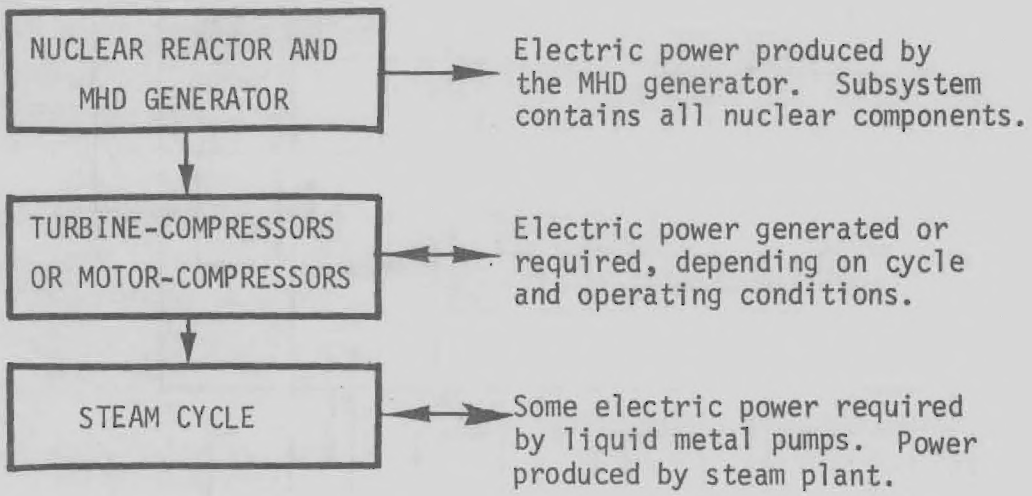

Figure 4. The Three Major Power Plant Subsystems Common to All Three Cycles

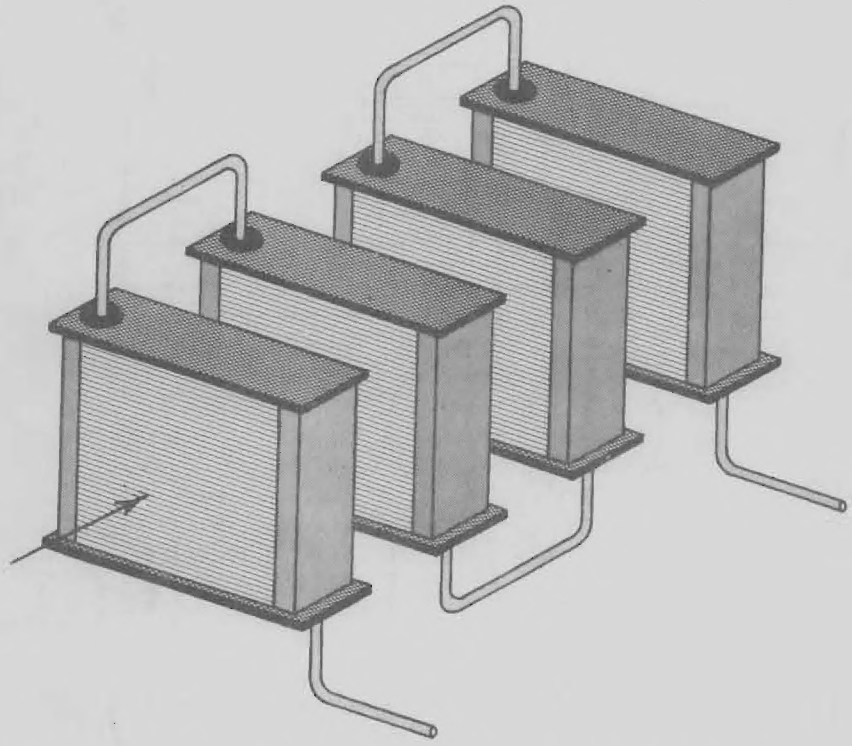

Figure 5. Four Pass Tube-Fin Gas-to-Sodium Crossflow Heat Exchanger

uranium recycling and reprocessing facilities. Figures 1-3 show a gas core reactor of the "coaxial flow" type, but any of the four reactor systems could be used. Both the coaxial flow gas core reactor and the colloid core reactor would require uranium separators, as shown in figures 1-3. The light bulb and NERVA type reactors would not require separators, since the uranium fuel would not become mixed with the working fluid. This first subsystem contains all the nuclear components of the power plant and the components that require the most technological development. These are the components that would be developed with a uranium plasma test facility of the type proposed by NASA.

The second subsystem consists of the turbine, compressor, and associated heat exchangers for Modes I and II; and the compressor, electric motor and heat exchangers in the case of Mode III. In Mode I (figure 1) a regenerative heat exchanger is used to cool the gas from the MHD exit temperature to an acceptable turbine inlet temperature, while the compressed gas returning to the reactor is heated. In Mode II, (figure 2) the regenerator is removed and the temperature of the gas exiting the MHD generator is reduced to the turbine inlet temperature by mixing with cooler gas from the first stage compressor. This avoids the problems associated with the high temperature regenerator, but at the expense of cycle efficiency. Cooling is provided by gas-to-sodium tube-fin heat exchangers. Mode III (figure 3) uses a high temperature regenerator but eliminates the turbine. The major advantage of this cycle is that there are no

moving parts at high temperature, and the efficienty is only two or three percent less than Mode I.

In general, the Mode III cycle appears to be the most attractive because of its simplicity and potential for high reliability, but it will require the development of efficient high power (probably cryogenic) electric motors. Mode I is the most attractive cycle if such motors are not developed, and provides the highest cycle efficiency. However, if regenerator problems prove insurmountable, Mode II can be used. Mode II can use current technology components for this subsystem.

The third subsystem rejects the heat removed by the liquid sodium from the sodium heat exchangers. The sodium is circulated through steam generators to power a conventional steam cycle. In Mode III this steam can drive the compressors.

Figures 1-3 show a "coaxial flow" gas core reactor in the first subsystem, although any of the other three reactor types could be used. Uranium fuel separators would not be needed with the solid core or the "light bulb" gas core reactor. All these reactors, except the solid core, require continuous fuel recirculation, and also permit continuous fuel reprocessing and the removal of gaseous fission products. The probable reactor operating temperature range is given in Table 1.

Table 1. Reactor Exit Temperatures for Advanced Power Reactors

Reactor	Temperature ^{o}K
Solid Core (NERVA type)	$2200^{o}K$ - $2500^{o}K$
Colloid Core	$3000^{o}K$ - $3200^{o}K$
"Light Bulb" Gas Core	$3500^{o}K$ - $4000^{o}K$
"Coaxial Flow" Gas Core	$3700^{o}K$ - $5000^{o}K$

The compressor subsystem uses either a turbine (Modes I and II) or a cryogenic electric motor (Mode III) to drive the multi-stage compressor. Cylindrical plate-fin counterflow surface compact heat exchangers are used for regeneration and four pass gas-to-sodium crossflow type heat exchangers (Figure 5) are used for primary heat rejection and intercooling between compressor stages. The surface characteristics of these heat exchangers are given by Tables 2 and 3.

Table 2. Gas-Gas Heat Exchanger Characteristics

	Hot Side	Cold Side
Surface	plate-fins	plate-fins
Plate spacing (ft)	0.25	0.204
Hydraulic radius (ft)	0.00253	0.000943
Fin thickness (in)	0.006	0.006
Heat transfer area/vol. (ft^2/ft^3)	367	855.6
Fin area/total area	0.756	0.884

Table 3. Gas-Na Heat Exchanger Characteristics

Surface	Gas Side continuous fin	Na Side flat tubes
Frontal Area per tube (in^2)		0.434
Fin thickness (in)	0.004	
Free flow area/frontal area	0.780	0.129
Fin area/total area	0.845	
Hydraulic radius (ft)	0.00288	0.00306
Heat transfer area/vol. (ft^2/ft^3)	270	42

Experimentally determined correlations between Reynolds number and friction factor and heat transfer characteristics are used to evaluate the performance of the heat exchanger for each specific plant operating condition.

Figure 6 illustrates a Mode II power plant, and a Mode III plant is illustrated by Figure 7.

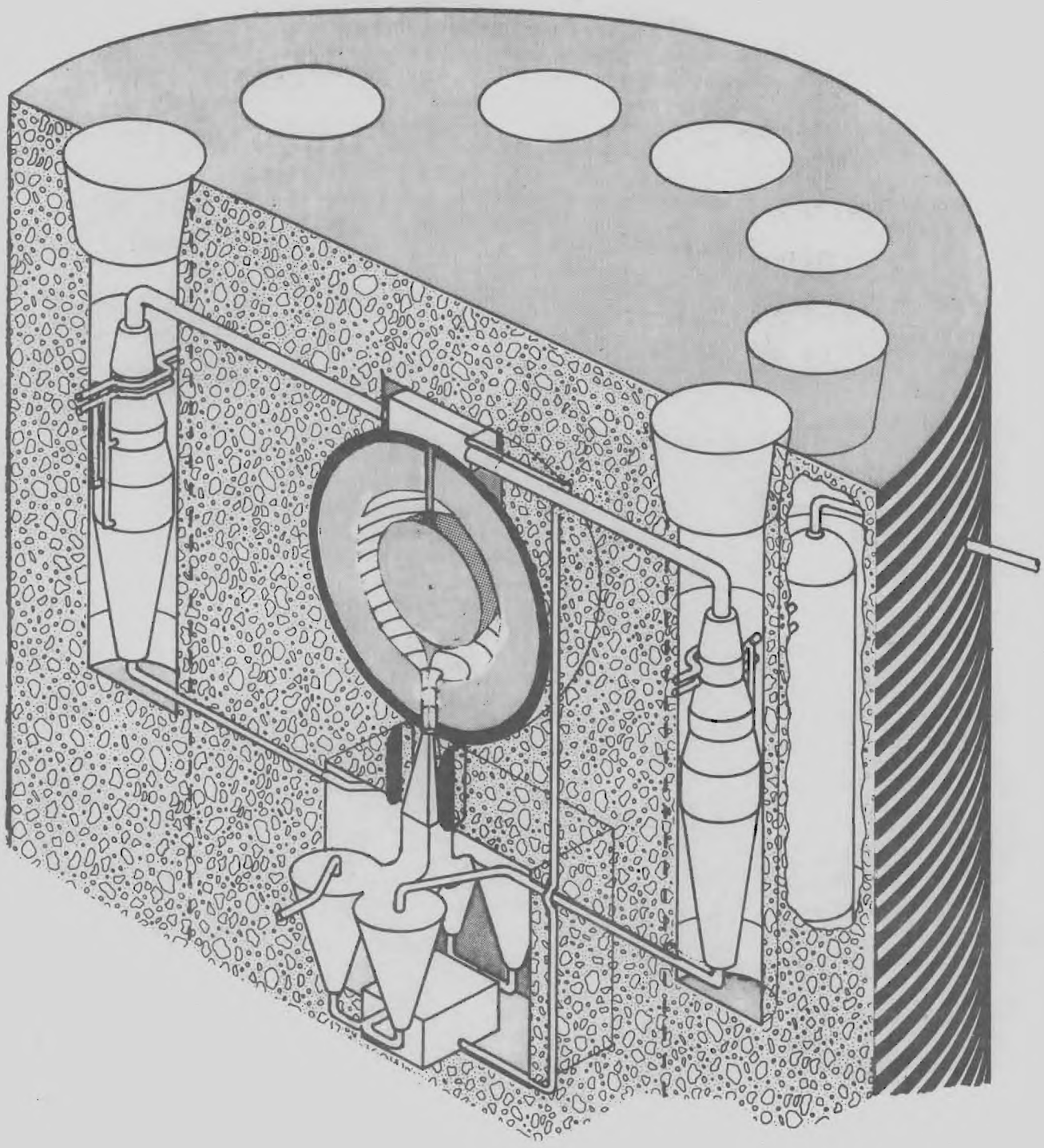

Figure 6. Terrestrial MODE II Power Plant (steam generator shown behind turbine-compressor unit on right, fuel separators located under nuclear reactor).

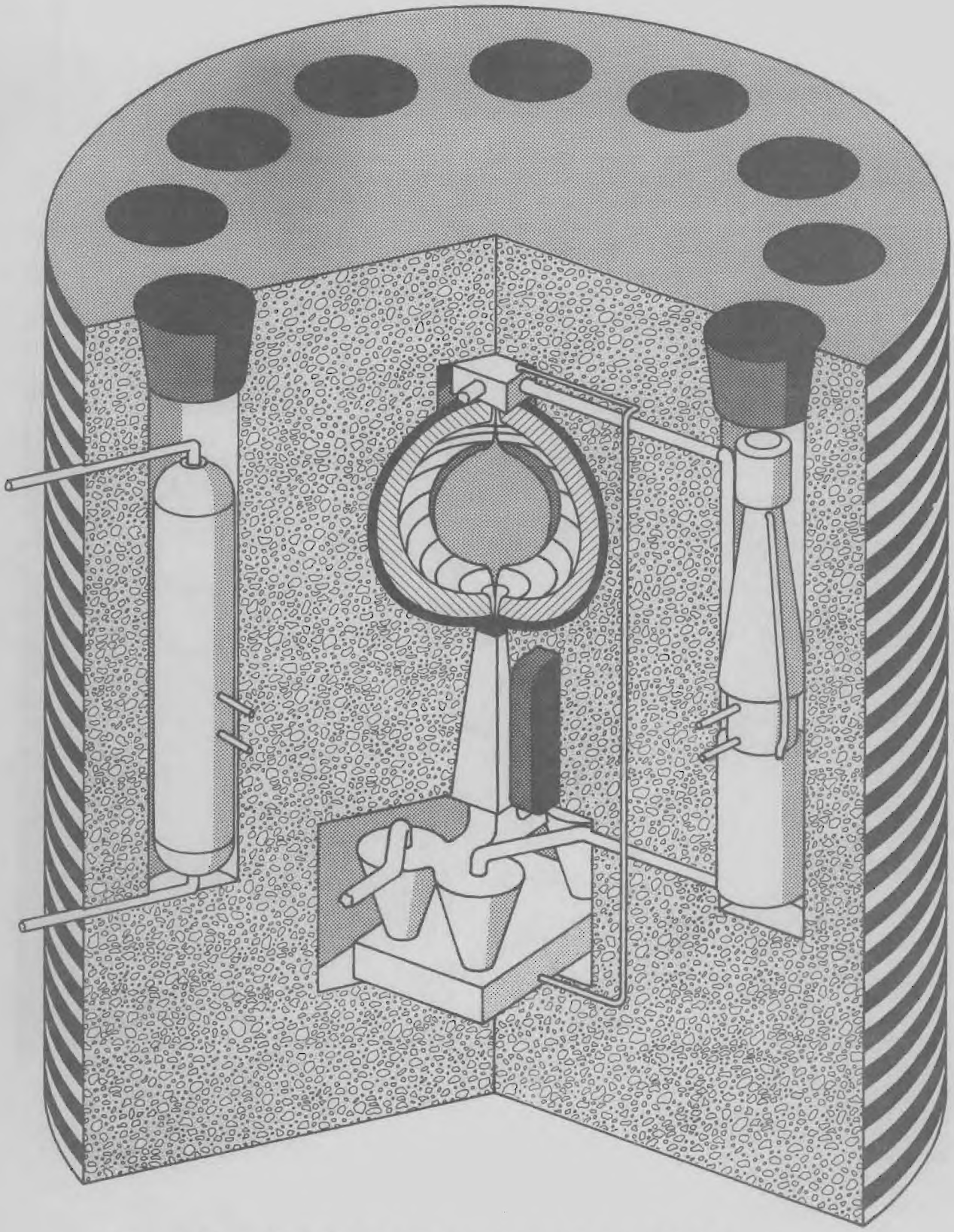

Figure 7. MODE III Motor-Compressor Terrestrial Power Plant (motor-compressor-regenerator on right, steam generator shown on left).

MHD GENERATOR PERFORMANCE LIMITATIONS

R. J. Rosa

MHD GENERATOR PERFORMANCE LIMITATIONS

The electrical properties of the gas are the primary determinant of whether a generator can be operated at a high loading factor without excessive length or field strength requirements. The electrical properties of a plasma that are relevant to MHD are the conductivity and the Hall parameter. Assuming that a given level of electrical power is sought, and that the generator L/D is fixed, for each pressure there is a minimum temperature that is necessary. The parameter L/D is determined largely by the boundary layer growth. Experience has shown L/D~10 to be about right in inert gas generators.

Figures 8 and 9 assume that L/D=10, and show the maximum allowable pressure at several given levels of power extraction, vs. temperature. These plots show the basic advantage of higher temperature as it relates to conductivity; there are two additional factors to be considered.

First, as temperature increases we can increase pressure to a level higher than before available, and boundary layers become much better behaved. L/D = 10 is probably a conservative estimate of what is allowable.

Secondly, the higher pressures available above ~3500 °K lower the Hall parameter, $\omega\tau$, so that a continuous electrode generator becomes a possibility. The power extracted from a continous channel as opposed to an infinitely finely segmented one is given by the factor $\frac{1}{1 + (\omega\tau)^2}$

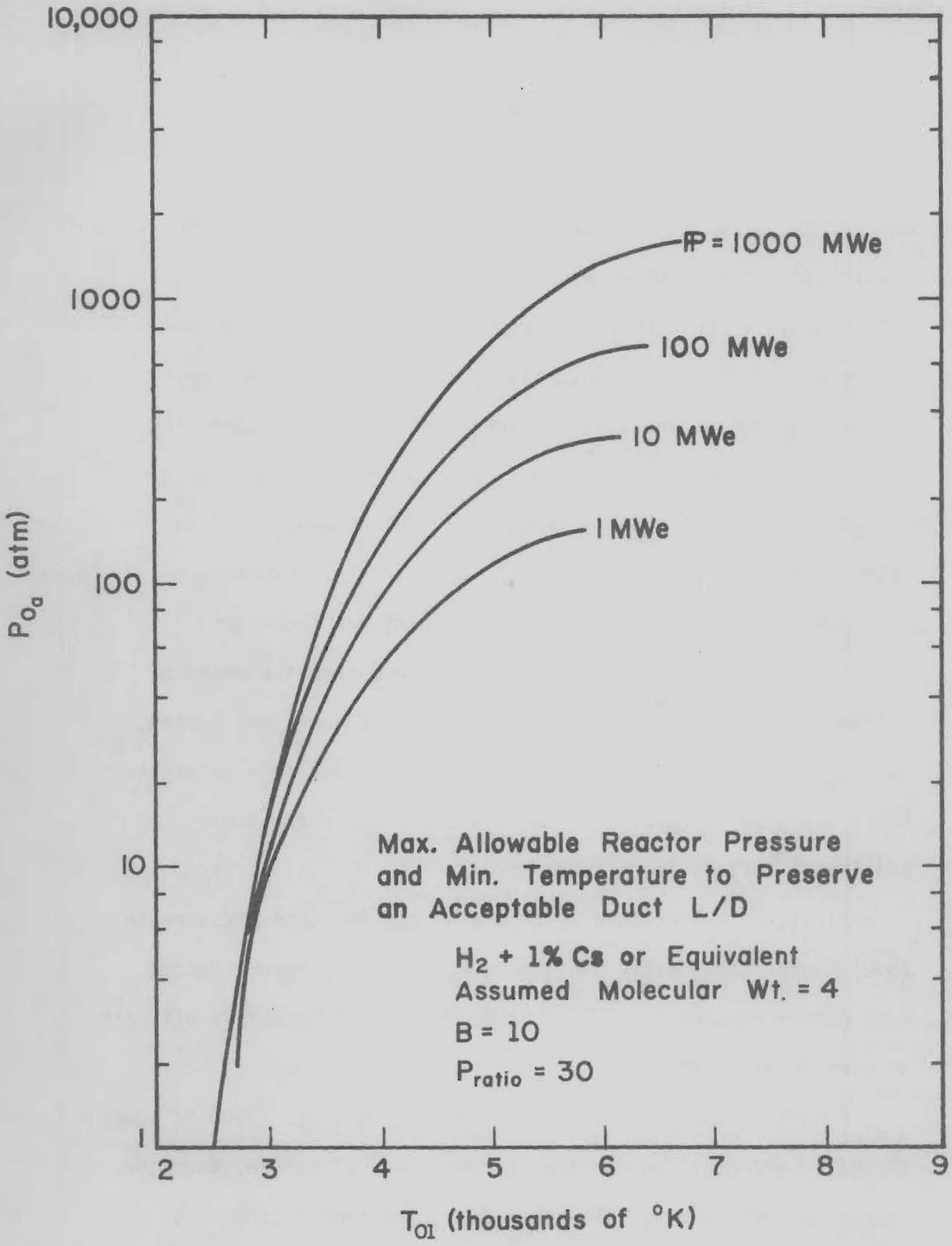

Figure 8. Maximum Allowable Reactor Pressure and Minimum Temperature to Preserve an Acceptable Duct L/D for a Pressure Ratio of 30.

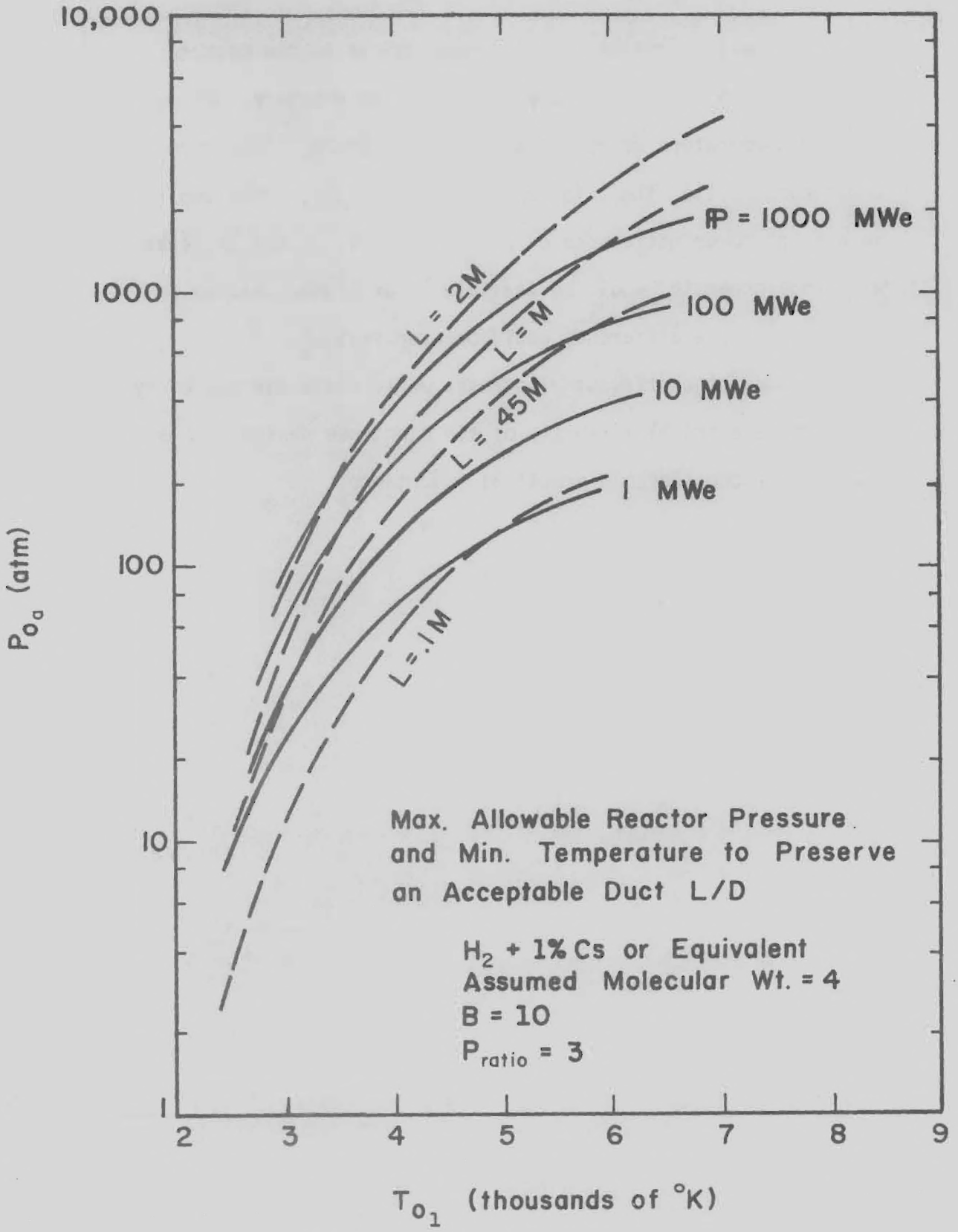

Figure 9. Maximum Allowable Reactor Pressure and Minimum Temperature to Preserve an Acceptable Duct L/D for a Pressure Ratio of 3.

where the Hall parameter, $\omega\tau$, is proportional to the magnetic field strength and inversely proportional to pressure. For a reactor temperature of 3500°K and pressure of 200 atmospheres, $\omega\tau$ is about 0.1 at the inlet and 0.8 at the exit. This implies an average power differance of only about 10%, so the continuous electrode generator would be feasible. For higher reactor temperatures the difference would be even smaller.

The use of continuous electrodes would eliminate the worry about the electrical integrity of the electrode design. This would be of considerable practical importance.

NUCLEAR ANALYSIS

J. D. Clement and K. D. Kirby

SUMMARY OF NUCLEAR CALCULATIONS

Exploratory calculations have been performed for several gas core breeder reactor configurations. The computational method involved the use of the MACH-1 one-dimensional diffusion theory code and the THERMOS integral transport theory code for thermal cross sections. Computations have been performed to analyze thermal breeder concepts and non-breeder concepts.

Analysis of breeders has been restricted to the U^{233}-Th breeding cycle, and computations have been performed to examine a range of parameters. These parameters include U^{233} to hydrogen atom ratio in the gaseous cavity, carbon to thorium atom ratio in the breeding blanket, cavity size, and blanket size. Results of a parametric survey show that breeding ratios in the range of 1.06-1.12 could be obtained with critical masses of 300 to 850 kilograms U^{233} for various material compositions in a 5 meter diameter cavity with a 0.5 meter thick blanket. The effect of fissile material in the blanket, cavity temperature, and structural material in the blanket has been estimated. The breeding ratio can be increased to 1.13 by utilizing fissionable material in the blanket without a large increase in total U^{233} mass. A decrease in average cavity temperature from 4000°K to 3000°K increases the breeding ratio from 1.10 to 1.12 with a significant reduction in cavity pressure. Cavity pressure at 3000°K is about 400 atmospheres. Structural material decreases the breeding ratio by approximately 2% for 0.2 atom percent natural molybdenum or 4% enriched molybdenum in the blanket.

Gaseous core reactors, non-breeding in nature, were also analyzed with different fuels and for varying sizes. Cavity diameters ranging from 1.2 to 3.0 meters with BeO reflectors 0.3 and 0.5 meters thick were examined with U^{233} fuel and U^{235} fuel of various enrichments. Results show U^{233} critical masses significantly lower than U^{235} critical masses due to the low energy fission resonances in U^{233}. However, for high enrichment ($\geq$93%) the U^{235} requirements are less than 15 kilograms. Pressure for the larger cavity sizes is generally below 300 atmospheres for U^{233} or highly enriched U^{235}.

COMPUTATIONAL METHODS

Nuclear analysis of the gaseous core nuclear reactor is a very difficult task requiring highly sophisticated techniques. Several analyses [24-26] have been performed which have used very sophisticated techniques and pointed out the areas of difficulties. For examining a broad range of designs however one may utilize less sophisticated techniques to observe trends and perform parametric studies in order to identify concepts for further study.

The first phase in performing exploratory nuclear analysis for the gaseous core nuclear reactor involved implementing the necessary computational tools and formalizing a computational method. The major portion of the effort early in the study was devoted to this area. In order to expedite this phase the MACH-1 code[27] was used as the primary computational tool in the nuclear analysis. To allow a more realistic model of thermal neutron processes in the high temperature gaseous core reactor concept, the THERMOS code[28] was implemented to supply thermal neutron parameters to MACH-1.

The computation method used in the nuclear analysis relies on these two codes. MACH-1 is a one-dimensional diffusion theory code with one thermal group (no upscatter) and THERMOS is a one-dimensional integral transport theory code in the thermal range with complete upscattering. All reactor configurations are assumed to be spherical and hence amenable to

one-dimensional analysis. For the MACH-1 code the 26-group "ABBN" cross section set of Bondarenko, et al.[29] was used. The thermal group of the ABBN set is for 2200 m/s (0.0253 eV) neutrons and hence is not realistic for the high temperatures of a gaseous core reactor (5000°K, kT=0.43 eV). The THERMOS code was thus used to determine thermal cross sections to be inserted into the MACH-1 computation along with the ABBN set. For a given configuration the computational method was as follows:

1. Run MACH-1 with 26-group ABBN to estimate critical concentrations and preliminary results.
2. Run THERMOS with 50 groups (up to 2.15 eV) using above concentrations and calculate spatial and spectrum averaged cross sections.
3. Run MACH-1 with 22 fast groups from ABBN (>2.15 eV) and thermal cross sections from THERMOS run.

Thus the final results of a computation may be thought of as a 23-group calculation with one thermal group using a thermal cutoff of 2.15 eV. A schematic of the computational method is shown in Figure 10. Steps 2 and 3 could be repeated if final concentrations vary markedly from the estimates; steps 1 and 2 could possibly be omitted for very similar configurations. The high thermal cutoff value is required because of the possibility of a large increase in neutron energy due to upscatter from the high temperature hydrogen moderator/coolant.

Explicit in all calculations are the assumptions associated with the two computer codes. Diffusion theory does not seem to be very restrictive based on previous comparisons to transport

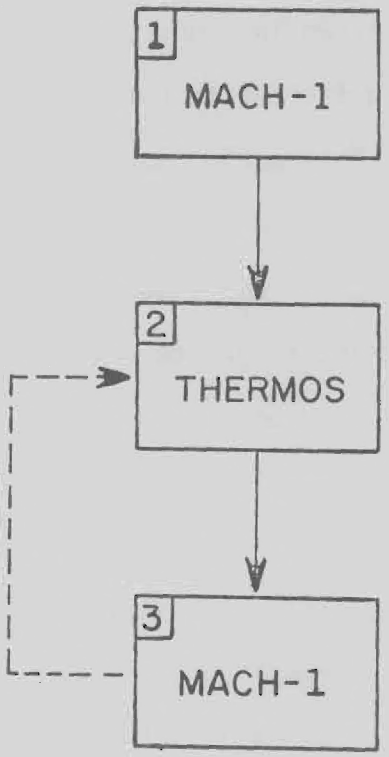

Step 1. Run MACH-1 with 26 group ABBN cross section set to estimate critical concentrations and get preliminary results.

Step 2. Run THERMOS with 50 groups (up to 2.15 eV) using above concentrations and calculate spatial and spectrum averaged cross sections.

Step 3. Run MACH-1 with 22 fast groups from ABBN (>2.15 eV) and thermal cross sections from the THERMOS calculations.

Figure 10. Computational Method for Nuclear Analysis

theory for a fast reactor configuration (k correction=+.009). THERMOS contains the assumption of isotropic scattering but this is felt to be quite sufficient at the energies involved (<2.15 eV). More restrictive assumptions for the THERMOS runs are probably the slowing-down source and the U^{233} resonance below 2.15 eV.

The slowing-down source for THERMOS is assumed to be spatially independent, MACH estimates as shown in Figure 11 show that the epithermal flux is rather flat in the cavity but decreases rapidly in the blanket region. This would imply then that the flat source assumption is rather good for the cavity and perhaps not as good in the blanket. But since the temperature is not as high in the blanket and resonance capture is important in thorium, results should not be as sensitive to thermal cross sections for blanket materials as for the cavity material.

The THERMOS Code must also handle the U^{233} resonances at 1.78 and 1.55 eV since they lie below the thermal cutoff. No Doppler broadening capabilities exist with the code so these resonances are included at room temperature only. These indirect assumptions of no Doppler broadening of these resonances should not be too severe since the resonances are very broad even at room temperature. Since only eight of the fifty THERMOS groups are used to span these resonances, results are probably less sensitive to Doppler broadening than to the low number of groups in that interval.

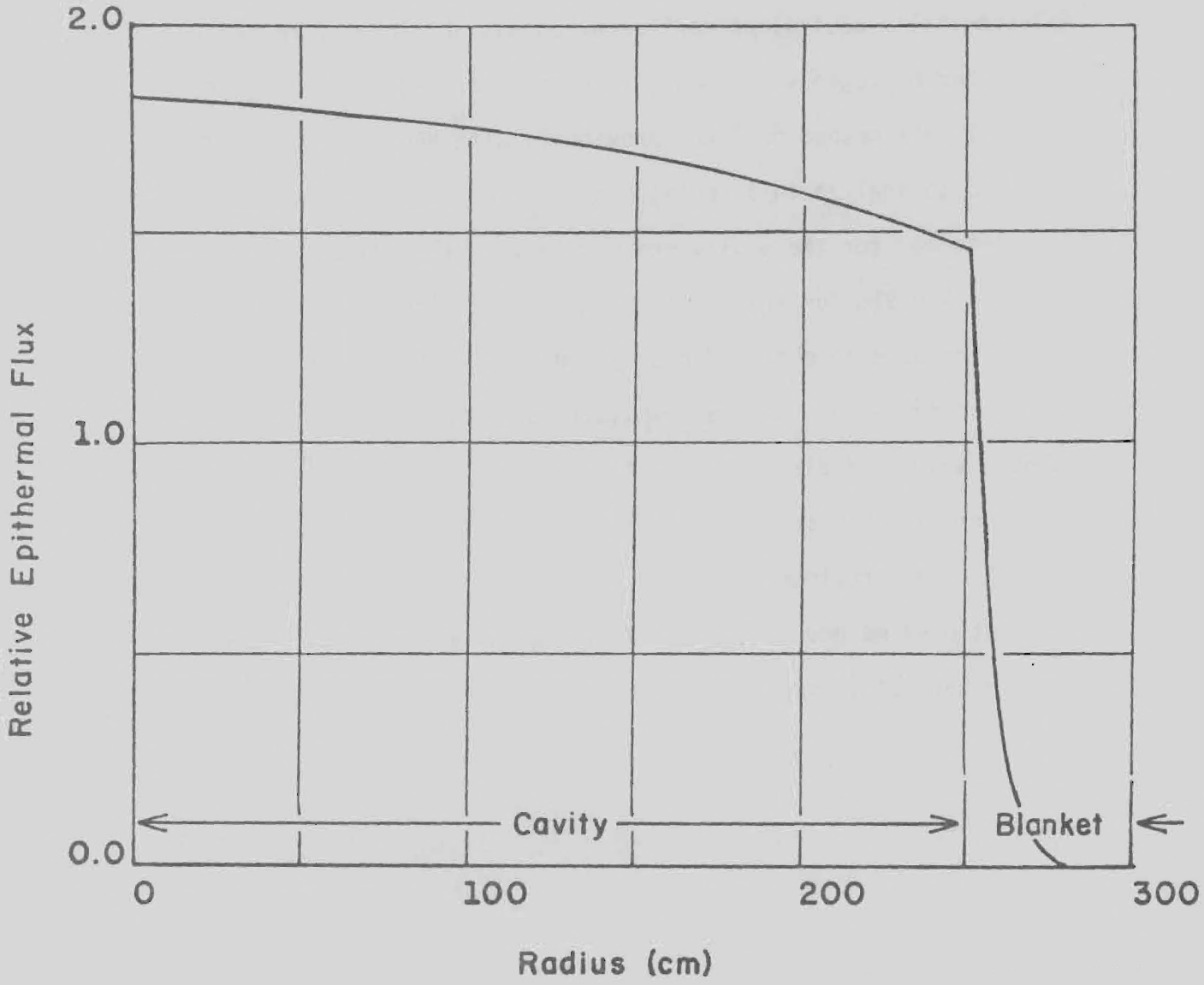

Figure 11. Spatial Distribution of Epithermal Flux (E>2.15 eV) for a Typical Gaseous Core Breeder Confuguration

A general assessment of the computational method and its assumptions was provided by a check calculation on a configuration analyzed by Whitmarsh.[24] This case is the 10 ft. cavity diameter, 2 ft. reflector region configuration described in Reference 24. An essentially equivalent configuration was obtained by reducing the number of regions by homogenizing similar regions. Then the computational method outlined previously with MACH-1 and THERMOS was used to analyze this configuration. The THERMOS computation was performed for the cavity regions only. Final results gave a value of k=0.986 for this configuration. In light of the homogenization used to obtain a nearly equivalent configuration, the agreement tends to show the computational model to be valid. The largest source of discrepancy was attributed to the sensitivity to U^{235} thermal cross sections. This points out the need for a multi-thermal group treatment. The agreement does show that this computational method should be sufficient to identify trends and perform parametric studies for various gaseous core nuclear reactors.

GAS CORE BREEDER CALCULATIONS

In this section results of the nuclear analysis of several concepts of a gaseous core breeder reactor are given. The primary objective of this portion of the nuclear analysis has been to perform nuclear calculations on various reactor configurations to determine a feasible gaseous core, thermal breeder, reactor power plant. Only thermal breeder configurations based on the Th^{232}-U^{233} breeding cycle have been examined. Although a fast breeder reactor may yield a higher breeding ratio, as found from a preliminary survey, the thermal breeder has the advantage of a much lower critical mass, simpler control, and in general, lower cavity pressure. If one uses the reactor doubling time (time necessary for the excess fuel bred to equal a new critical loading) as the figure of merit, the thermal breeder can compete favorably with the fast breeder. (The doubling time is directly preportional to the critical mass and inversely proportional to the breeding ratio minus one). For an extraterrestrial plant where excess fuel is desired a low doubling time is desired, but if all that is desired is to keep the original plant operating, then a larger doubling time (lower breeding ratio) merely compensating for process losses would be sufficient.

Since the thermal breeder does appear to be able to compete with the fast breeder and has advantages which could allow easier adaptation for extra-terrestrial use, nuclear analysis of several

configurations was carried out.

As noted previously, all the configurations examined were spherical in geometry. These cases were described as two or three region spheres in the MACH runs and as slabs in the THERMOS calculations. The configurations examined are basically as that depicted in Figure 12. The cavity region contains hydrogen as moderator/coolant, U^{233} as fuel, and sometimes thorium as fertile material. The blanket consists of graphite and thorium. The relative concentrations of the materials as well as the size of the regions were varied parametrically to examine a matrix of cases in an attempt to obtain the most feasible gaseous core, thermal breeder comcept.

The first two parameters examined were the hydrogen to uranium atom ratio in the cavity (H/U) and the carbon to thorium atom ratio in the blanket (C/Th). Initially cases were to be examined with H/U ratios ranging from 40/1 to 140/1 and C/Th ratios ranging from 2/1 to 50/1. Carbon atom density was kept constant in all calculations. Step 1 in the computational method (MACH-1 estimates) suggested that C/Th ratios greater than 10/1 yield very low breeding ratios, and that H/U ratios below 60/1 were undermoderated, hence the combined calculation (MACH-1/THERMOS) was performed for H/U from 60/1 to 140/1 and C/Th from 2/1 to 10/1. For all cases the cavity radius is 250 cm and blanket thickness is 50 cm. Results of these calculations are shown in Table 4 and Figures 13-15 for the important parameters of reactor

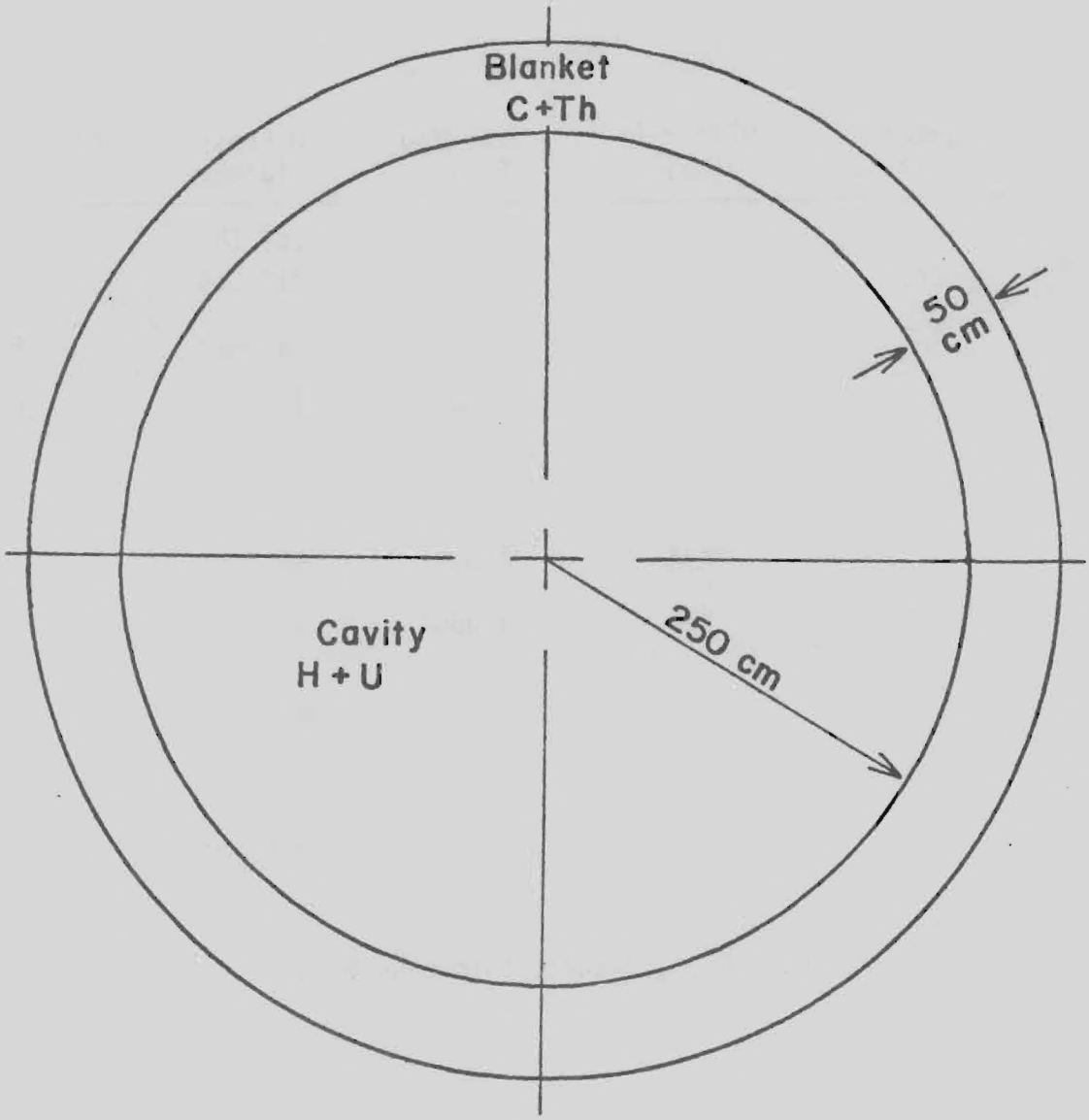

Figure 12. Typical Reactor Configuration for Nuclear Analysis

Table 4 Parametric Study of Relative Material Concentrations in a Gaseous Core Breeder Reactor

Cavity H/U Ratio	Blanket C/Th Ratio	U^{233} Mass (Kg)	Breeding Ratio	H Press (atm) (a)	H Press (atm) (b)	Doubling Time (yr) (c)
140/1	2/1	452	1.1026	710	514	9.6
	4/1	390	1.0962	612	443	8.9
	10/1	301	1.0636	472	342	10.3
100/1	2/1	576	1.1056	646	468	11.9
	4/1	494	1.0997	553	401	10.8
	10/1	375	1.0662	420	304	12.4
60/1	2/1	847	1.1029	569	413	17.8
	4/1	721	1.0966	485	351	16.2
	10/1	537	1.0635	361	261	18.4

(Cavity radius 250 cm, Blanket thickness 50 cm)

(a) Hydrogen partial pressure at 4000°K, H_2 mole fraction 0.92.
(b) Hydrogen partial pressure at 3000°K, H_2 mole fraction 0.99.
(c) For 1000 Mw(t), preportionally lower per higher average power.

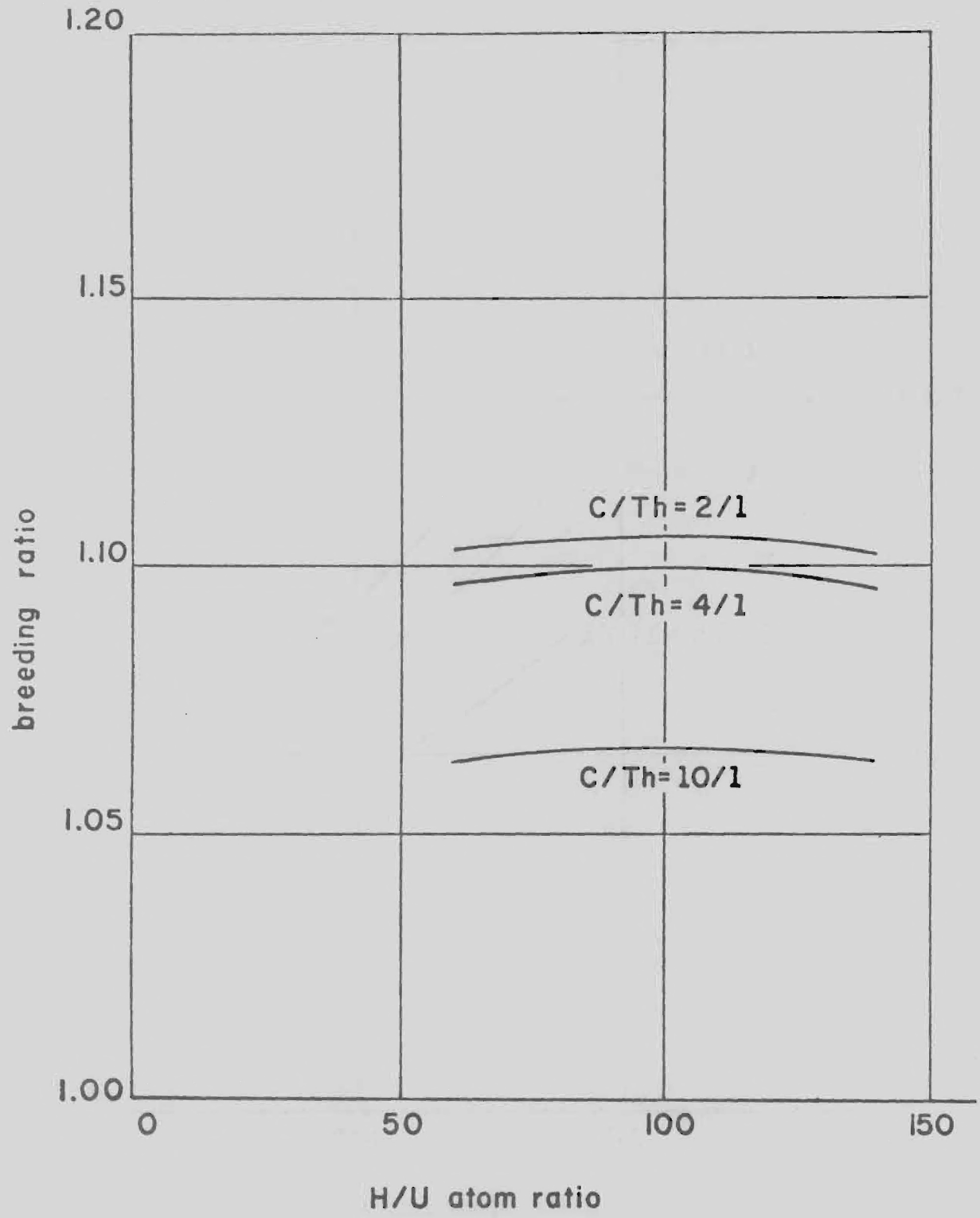

Figure 13. Effect of Thorium Concentration in the Blanket on Breeding Ratio

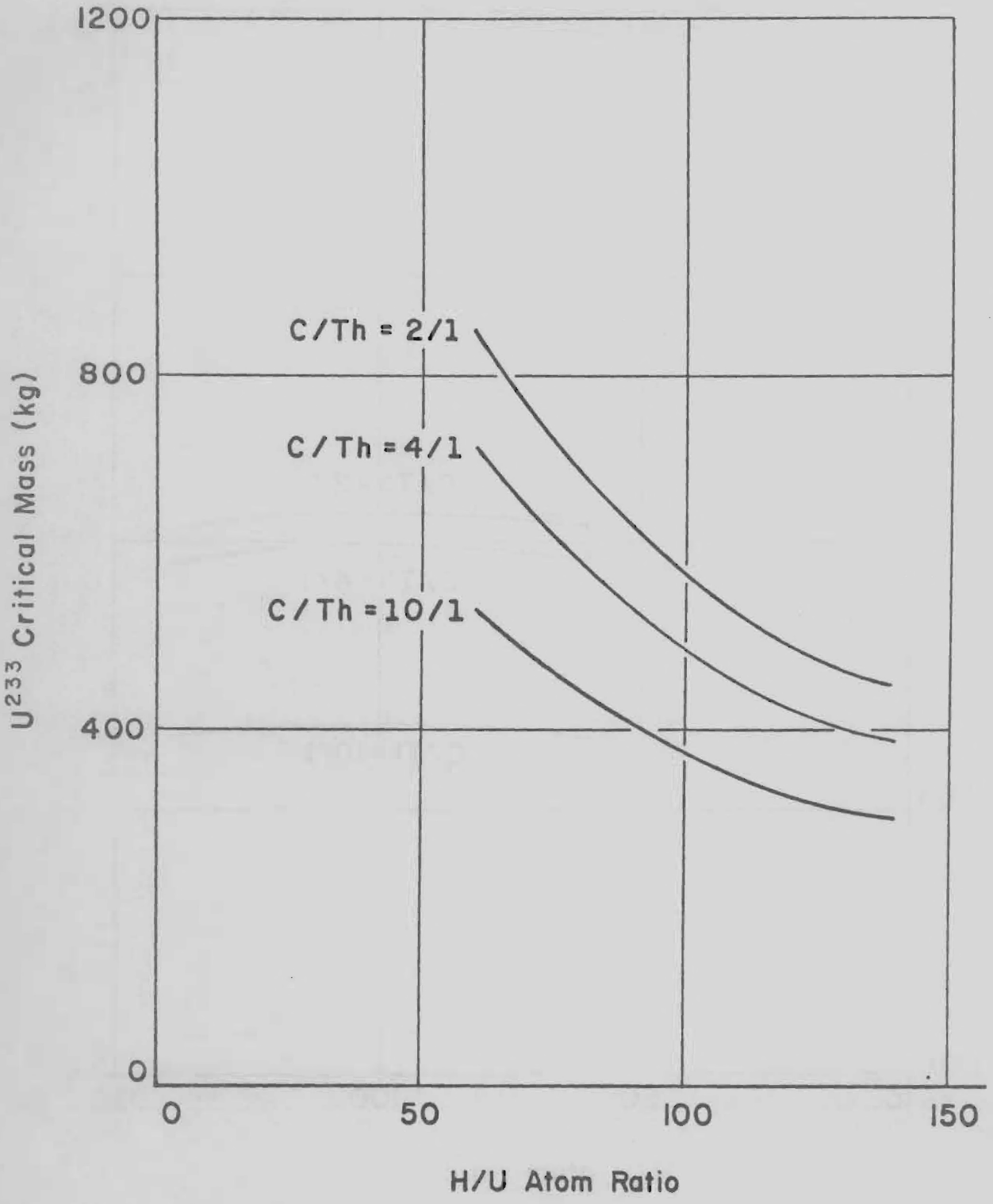

Figure 14. Effect of Hydrogen/Uranium Ratio on Critical Mass

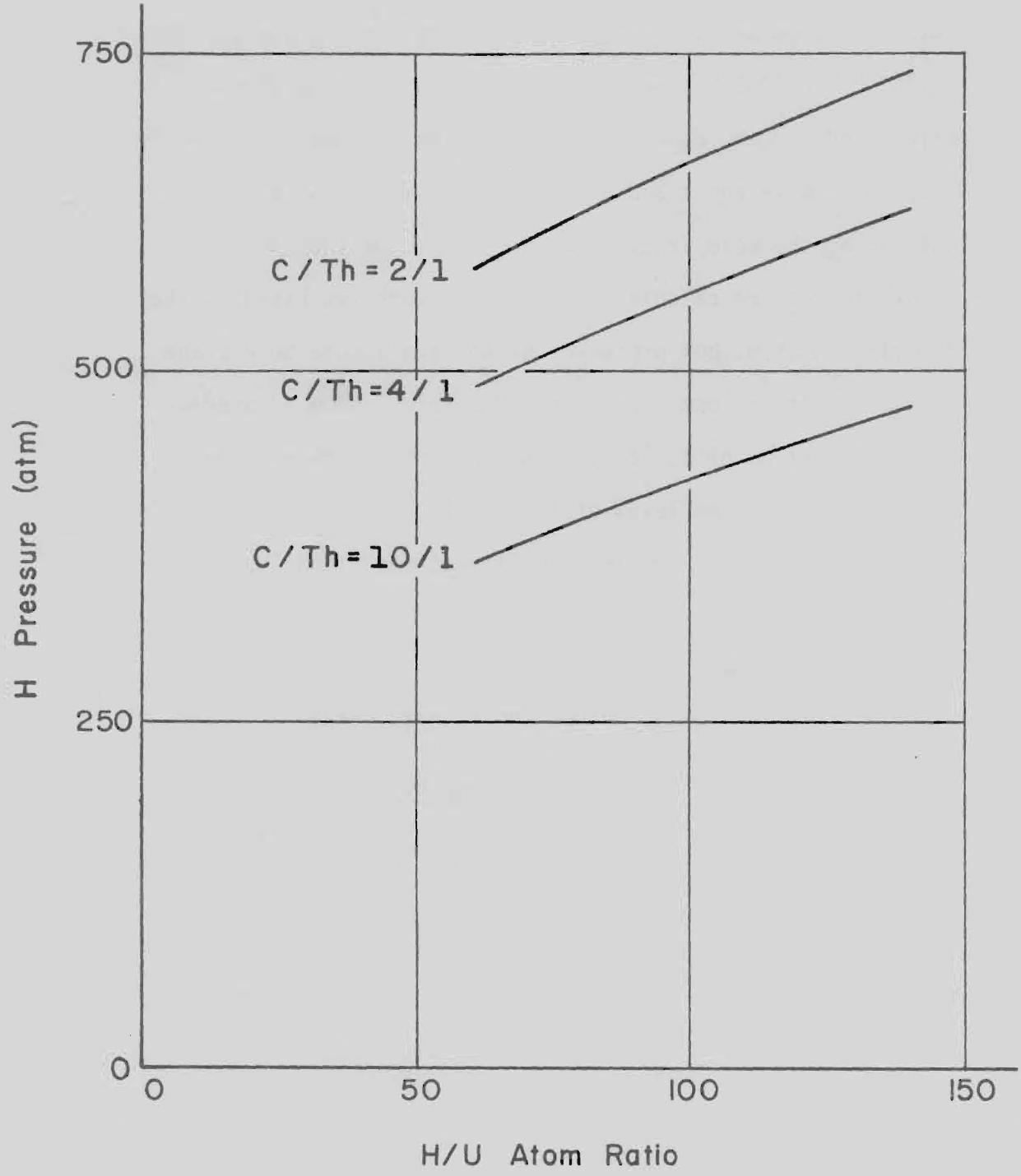

Figure 15. Effect of Hydrogen/Uranium Atom Ratio on Core Pressure

breeding ratio, U^{233} critical mass, hydrogen pressure, and doubling time. Heat transfer and system analysis studies estimated the bulk average cavity temperature for the reactor to be 3000°K to 4000°K; thermal cross sections and pressures were calculated for the case of 4000°K. At this temperature and for pressures above about 300 atmospheres dissociation of H_2 is not large; the mole fraction of H_2 is greater than 90%[30,31]. An exact pressure calculation would be iterative based on the H_2 mole fraction, but pressures given here assume an average H_2 mole fraction, but pressures given here assume an average H_2 mole fraction of 92% at 4000°K. For the doubling time calculations a power level of 1000 MW(t) was assumed. A higher power level shortens the doubling time proportionally.

A detailed breakdown of the critical composition for one case of the parametric study is shown below:

H/U = 100/1, C/Th = 4/1

Material	Atom Density	Mass
U^{233}	$1.9499 \times 10^{19} cm^{-3}$	494 kg
H	1.9499×10^{21}	212
C	8.0×10^{22}	76236
Th	2.4×10^{21}	131030

Some of the conclusions, mostly obvious, within the range of this parametric study are noted below:

1. Breeding ratio decreases as C/Th ratio increases
2. Breeding ratio appears to be maximum at H/U=100/1.
3. Critical mass decreases as C/Th or H/U ratios increase.
4. Hydrogen pressure increases as C/Th ratio decreases and as H/U ratio increases.
5. Doubling time increases as C/Th ratio increases and as H/U ratio decreases.

The first conclusion can be explained by noting that, as C/Th ratio increases, the amount of fertile material decreases hence lowering the breeding ratio. The second conclusion is essentially an observation but one may note that below a H/U ratio of 60/1 the cavity is undermoderated. Above 140/1 the effects are much more subtle; increased hydrogen absorption or the U^{233} resonance may control here, but one desires the lowest feasible H/U ratio to yield lower pressure. The decrease in critical mass noted in the third conclusion is due to the increasing amount of light atoms which soften the spectrum toward the large thermal fission cross sections of U^{233}. Hydrogen pressure is of course expected to increase as hydrogen concentration increases, but this also occurs as the C/Th ratio decreases. This is because a higher critical mass is required as C/Th decreases and, hence, for a given H/U ratio, the hydrogen concentration also increases. Variations in the doubling time are

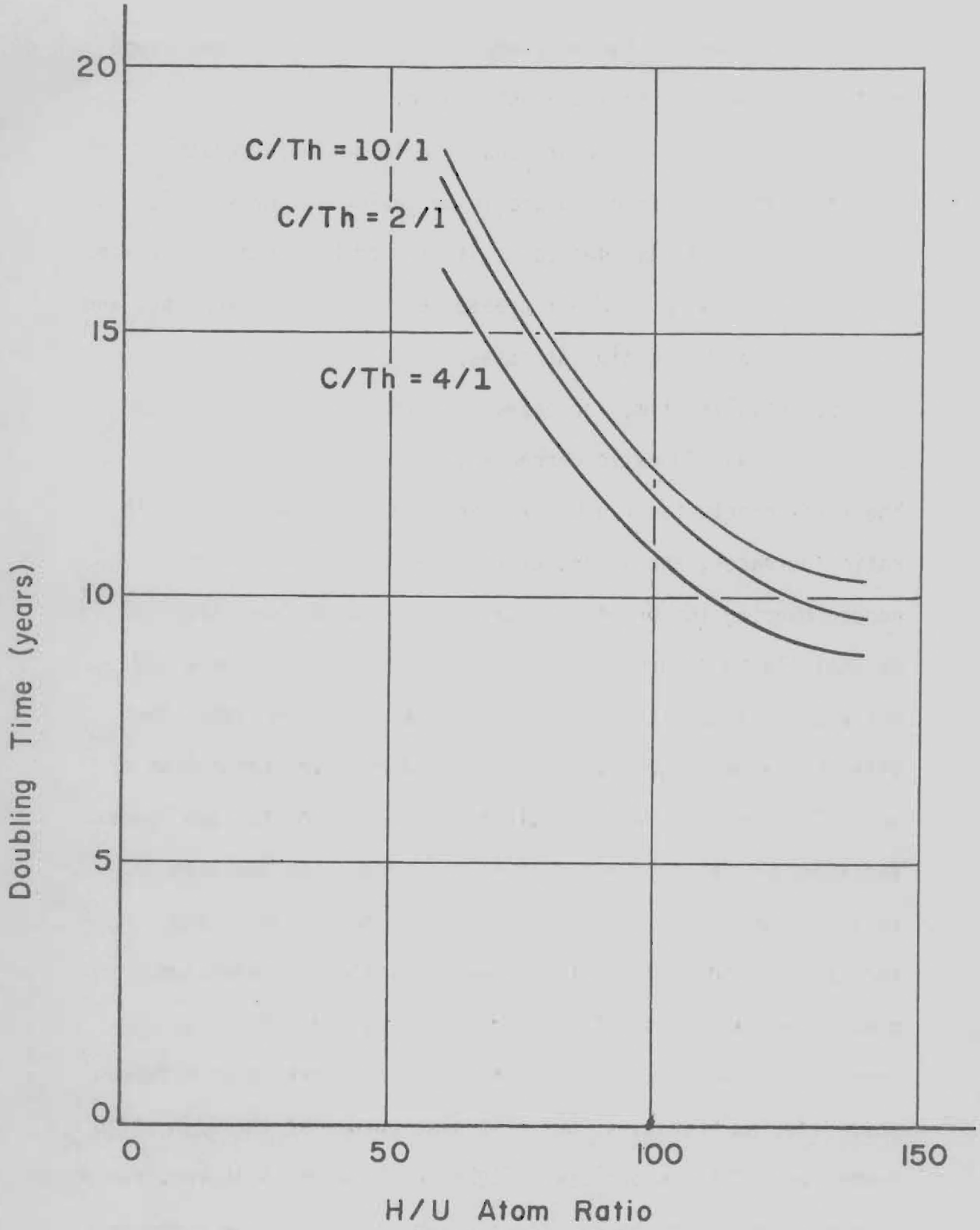

Figure 16. Effect of Hydrogen/Uranium Atom Ratio on Doubling Time

due to combined variations in breeding ratio and critical mass, with the decreasing mass as H/U increases yielding the strongest influence.

With the trends noted it is difficult to pick an optimal configuration. This is because variation in a single parameter helps one point but hinders another. For instance, one may obtain a lower critical mass by increasing the C/Th ratio but this yields a lower breeding ratio also. Or the critical mass could be lowered by increasing the H/U ratio, but this, in turn, increases the pressure. Of all the cases presented, it can be said that critical loadings are within reason; however, pressures appear high.

For the breeder concept one must assess the breeding ratios and doubling times. The breeding ratios are low compared to that for a fast breeder reactor, but they appear to be reasonable for a thermal breeder and yield some reasonable doubling times. Breeding ratios near 1.1 with attendant doubling times of about 10 years for 1000 MW operation should be quite satisfactory although engineering details and structure materials will probably affect them. In comparison to the molten salt thermal breeder with breeding ratios in the 1.05 - 1.07 range,[32] this study would show the gaseous core thermal breeder the more favorable. For the case of extraterrestrial use, if one merely wishes to compensate for process losses, a breeding ratio of 1.1 should be much more than sufficient.

In order to complement the above parametric study efforts were turned to examine areas which might improve reactor breeding ratio and decrease cavity pressure. One attempt at increasing the breeding ratio was by introducing fertile thorium into the cavity. For the case of H/U of 100/1 and C/Th of 4/1, thorium atoms were added to the cavity in amounts twice, equal and half the U^{233} atom concentration. All three cases resulted in approximately a 1% increase in breeding ratio. Additional cases with thorium in the cavity were not examined because of complications it would impose on the MHD device.

The thickness of the blanket region was also examined to see if higher breeding ratios could be obtained. Additional thicknesses of 20, 40, 75, and 200 cm were examined and the effect on breeding ratio is shown in Figure 17. One notes that the 50 cm thickness used in the study appears to be very near optimum. The smallest thickness feasible is desired here to yield lower total reactor weights.

The most obvious method of lowering cavity pressure would be to increase cavity size, so a case with a cavity radius of 350 cm was examined. For a H/U ratio of 100/1 and C/Th ratio of 4/1, the cavity pressure was reduced from 553 atmospheres to 406 atmospheres. The breeding ratio also went up 1% due to the larger blanket volume. However, the critical mass doubled (494 kg to 996 kg).

One concept which could increase the breeding ratio and also

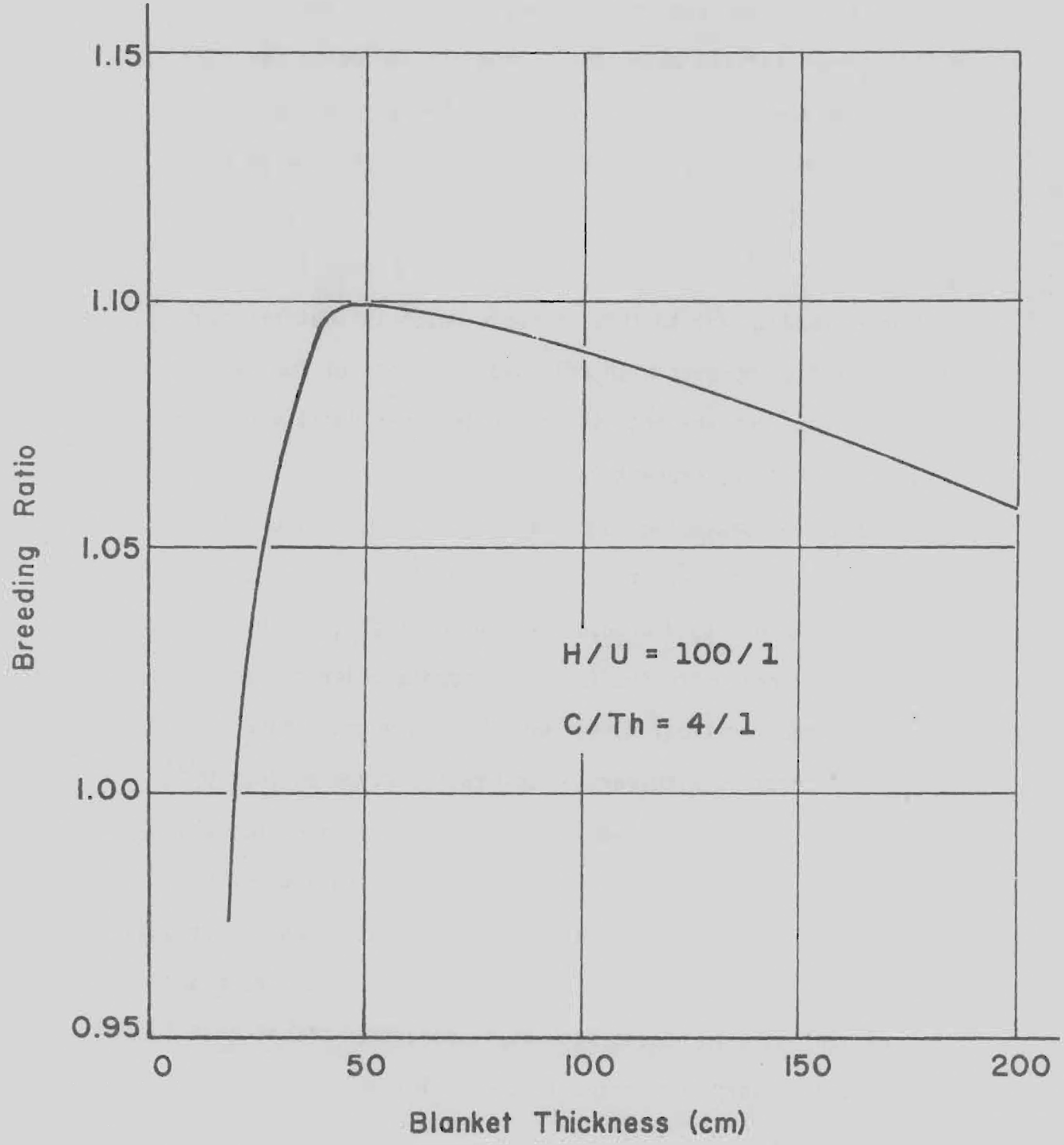

Figure 17. Effect of Blanket Thickness on Breeding Ratio

lower cavity pressure is one in which an inner annulus of the blanket contains fuel (U^{233}). By placing fissile material in the blanket the neutron flux should increase, therefore yielding more fertile absorptions, and also reducing the fuel required in the cavity for criticality, hence reducing pressure for a given H/U ratio. Results for a configuration with fuel in the inner 20 cm of a 50 cm blanket region for varying quantities of U^{233} are shown in Table 5 and Figure 18. One can note one disadvantage to this concept, which is that although breeding ratio improves with only small amounts of fuel in the blanket, pressures are not significantly lower until very large amounts of fuel are present in the blanket.

The use of deuterium as moderator/coolant in place of hydrogen could also have the potential of increasing the reactor breeding ratio due to decreased absorption (o_a^D/o_a^H = 1/660 @ 2200 m/s). Since deuterium is not as good a moderator as hydrogen higher critical masses would be expected, though. MACH estimates for cases with various D/U ratios revealed that U^{233} masses of 2500 to 5000 kg would be required yielding pressures greater than 1500 atmospheres with no case having a breeding ratio higher than a comparable hydrogen moderated case. Although with deuterium there is essentially no absorption in the moderator, the critical mass increases such as to more than offset that loss by increased absorption losses in the fuel itself.

U^{233} Atom Ratio Blanket/Cavity	U^{233} Cavity (kg)	U^{233} Tatal (kg)	Breeding Ratio	Fission Ratio Blanket/Cavity	Pressure (atm)	
					(a)	(b)
0	494	494	1.100	.02	553	401
.5	489	553	1.127	.04	552	400
1	483	608	1.126	.06	542	392
2	472	717	1.125	.09	531	384
4	468	919	1.115	.15	529	383
10	416	1496	1.114	.26	465	337

(H/U=100/1 in cavity, C/Th=4/1; 4000°K; 250 cm cavity radius; inner blanket 20 cm, C+Th+U; outer blanket 30 cm, C+Th).

(a) Hydrogen partial pressure at 4000°K, H_2 mole fraction 0.92.

(b) Hydrogen partial pressure at 3000°K, H_2 mole fraction 0.99.

Table 5 Nuclear Data for Gaseous Core Breeder with Fuel in Blanket

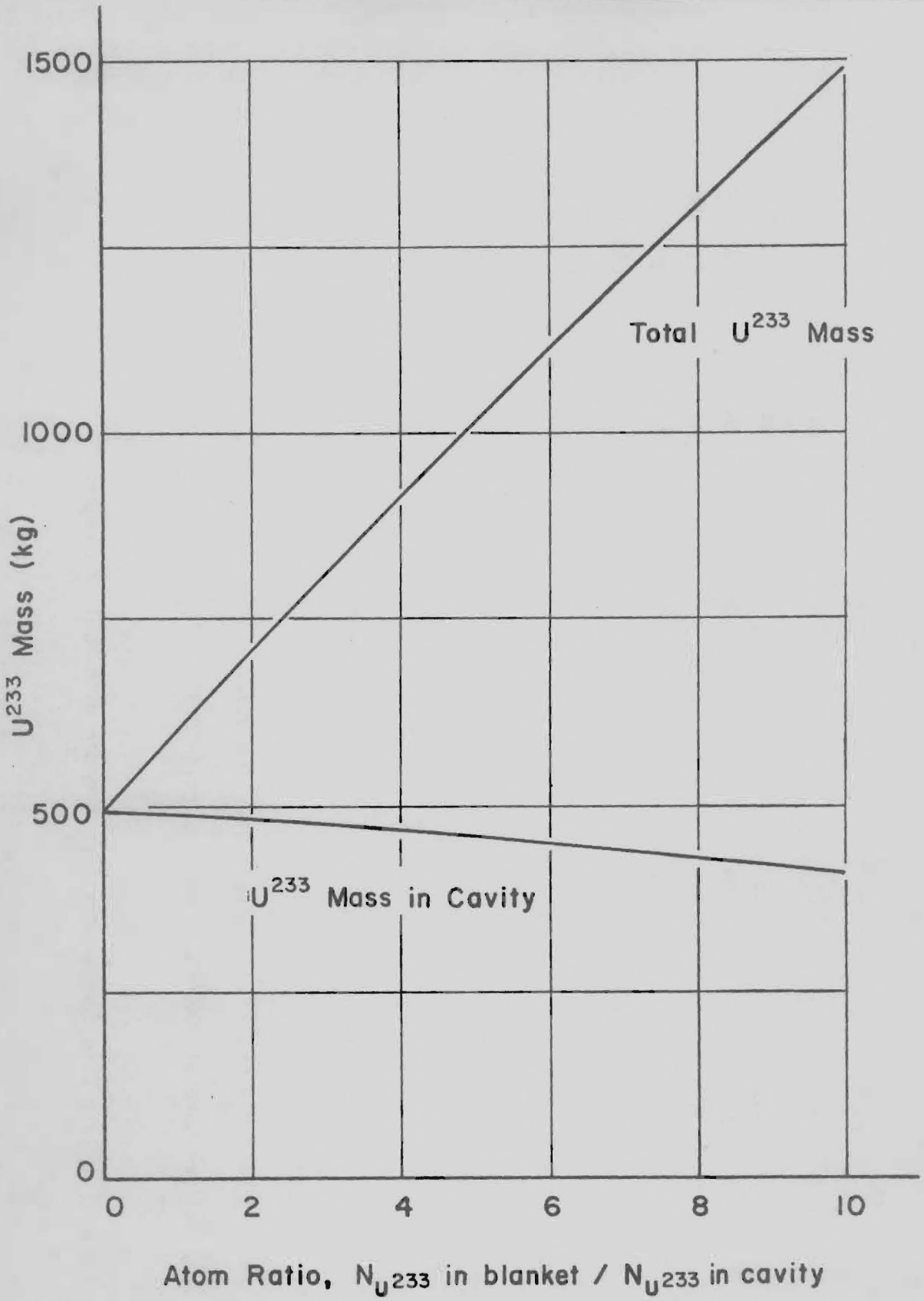

Figure 18. Effect on Critical Mass of Adding U^{233} to the Blanket Region

During the period of these studies a re-evaluation of the operating conditions of the reactor pointed out that the bulk average cavity temperature should be about 3000°K rather than 4000°K. The reasoning for this change is that MHD requirements are met with a maximum temperature of about 4000°K and hence the bulk average cavity temperature should be lower. The impact of this temperature reduction of the nuclear analysis was shown by a slight decrease in critical mass, increased breeding ratio, and, of course, lower pressure. A comparison of data for the two temperatures is shown below:

H/U=100/1, C/TH=4/1

Temperature	U^{233} Mass	Breeding Ratio	Pressure
4000°K	494 kg	1.100	553 atm.
3000°k	491 kg	1.121	399 atm.

The primary reason for the lower critical mass and higher breeding ratio is the shifting of the thermal neutron spectrum to larger cross section values in the "1/v" range. The pressure decrease is essentially linear with temperature, but the H_2 mole fraction at 3000°K also increases to 99%.

In order to obtain more realistic results additional overall systems implications must be integrated into the computations. One important aspect is the influence of structural material on the gaseous core breeder reactor. In order to estimate such an effect computations were made with molybdenum homogeneously mixed in the blanket region. The structural requirements of the gaseous core breeder have not been studied, but it is not expected that a great deal of structure in neutronically important regions is required. However, the following results for cases with structure are shown below with the data for no structure:

H/U=100/1, C/Th=4/1, 3000°K

Atom Percent Mo in Blanket	U^{233} Mass	Breeding Ratio	Pressure
0	491 kg	1.121	399 atm.
0.2 (or 4%, enriched)	493 kg	1.108	400 atm.

From the above data one sees that for these quantities of structural material the breeding ratio is still in the same range as the molten salt breeder mentioned previously. One should also note that the absorption loses in Mo structure can be reduced by isotopic enrichment in Mo^{98} and Mo^{100} as noted in Reference 24. In that case the above results could be equivalent to much larger percentages of enriched Mo.

GASEOUS CORE NON-BREEDER CALCULATIONS

This section contains the results of a parametric study of gaseous core reactor concepts where breeding of additional fuel is not the primary purpose. For extraterrestrial purposes a gaseous core reactor could be designed with a sufficiently long life to accommodate many applications. The non-breeder reactor may prove to be more favorable than the breeder for many applications due to its simplicity and lower total system weight.

Nuclear calculations have been performed for a range of cavity sizes, reflector thickness, and fuels. Cavity radii of 60,80,100, and 150 cm have been examined for both 30 cm and 50 cm thick reflectors of beryllium oxide (BeO). U^{233} fuel and U^{235} fuel of three different enrichments (.98, .93,.50) have been examined for the various geometries. The bulk average cavity temperature is assumed to be $300^{o}K$ and pressures are calculated for an H_2 mole fraction of 99%. Helium would be the more likely coolant for the non-breeder but hydrogen was used for expedience.

Table 6 gives the critical masses for the various cases. The critical masses are also depicted in Figure 19 and hydrogen pressures are shown in Figure 20. The full matrix of geometric cases was not calculated, rather the more likely combinations of cavity radius and reflector thickness were examined. Only two cases for the 150 cm radius cavity were examined.

The results of this parametric study show that the U^{233} fueled configurations are the most attractive based on critical mass and pressure. Critical masses for the U^{235} cases are not excessive, but the smaller sizes have rather high pressures. As noted above, helium would be the preferred working fluid for the gaseous core reactor in conjunction with an MHD device and helium would have less absorption than hydrogen. By performing computations

TABLE 6 GASEOUS CORE REACTOR CRITICAL MASSES (kg)

FOR VARIOUS SIZES OF A BeO REFLECTED REACTOR

Fuel	Reflector Thickness (cm)	Cavity Radius (cm)			
		60	80	100	150
.98 U^{235}	30	7.3	10.8	15.0	
	50		6.4	8.8	16.7
.93 U^{235}	30	7.7	11.3	15.8	
	50		6.7	9.3	
.50 U^{235}	30	13.8	20.9	29.4	
	50		13.1	18.2	
U^{233}	30	3.7	5.6	7.8	
	50		3.5	5.0	9.6

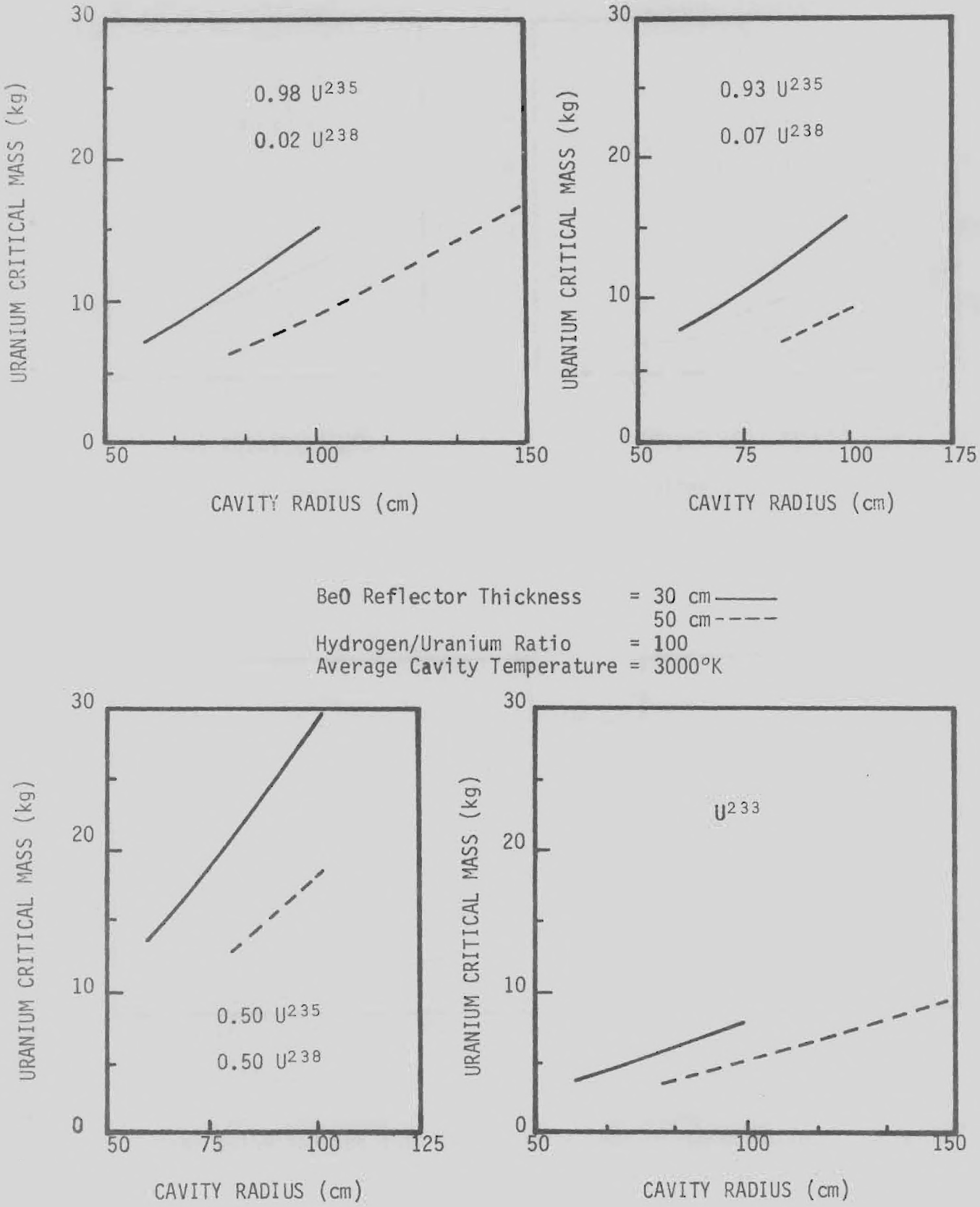

Figure 19. Gaseous Core Reactor Critical Mass for Various Sizes of a BeO Reflected Reactor

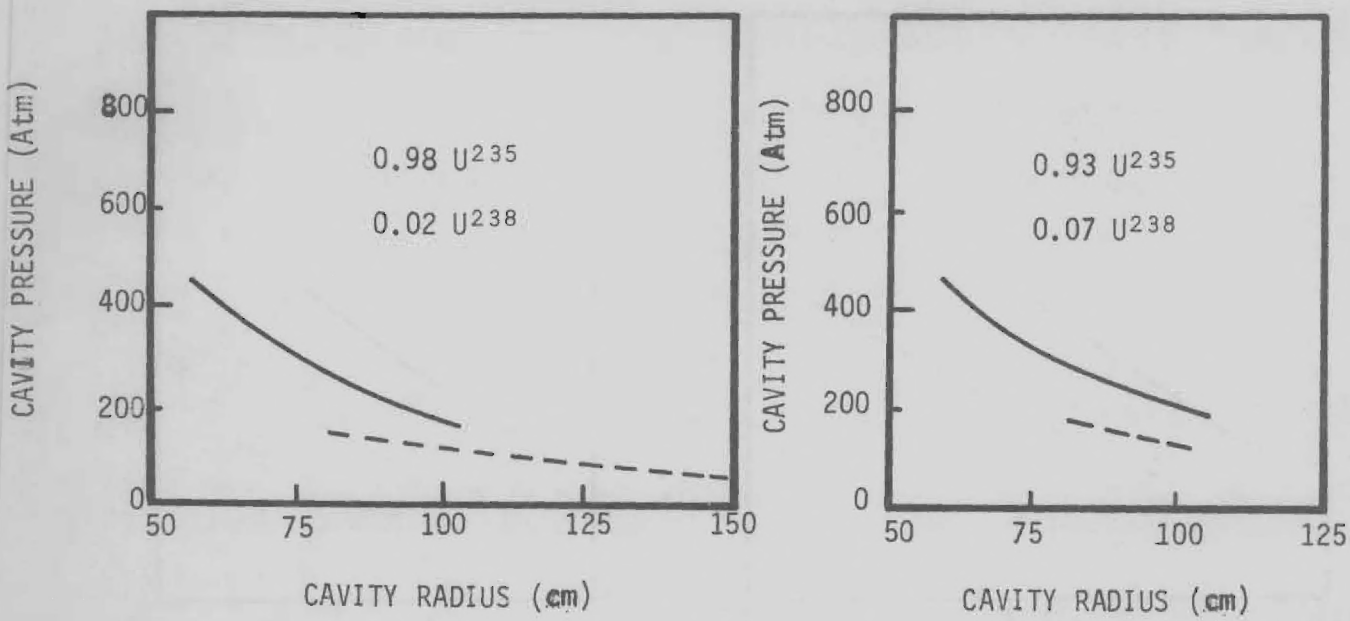

BeO Reflector Thickness = 30 cm ——
50 cm – – –
Average Cavity Temperature = 3000°K
Hydrogen/Uranium Ratio = 100

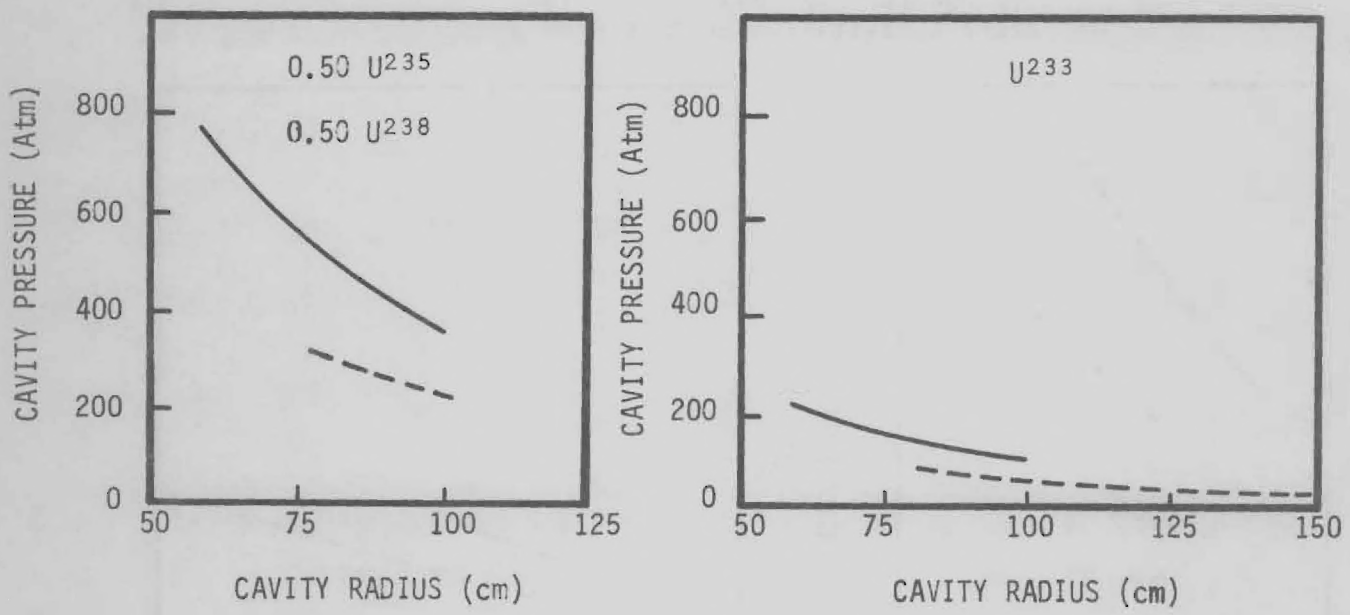

Figure 20. Reactor Pressure for Various Sizes of a BeO Reflected Reactor. Average Core Temperature 3000°K.

without hydrogen it was found that critical mass and pressure were not overly sensitive to the hydrogen as an absorber or moderator. Mass and pressure decreased about 5% for the case of no hydrogen. A helium cooled configuration should fall between the limits of hydrogen and no hydrogen.

POWER PLANT SYSTEMS ANALYSIS

J. R. Williams and Y. Y. Yang

GLOSSERY

a	Thickness of heat exchanger plate (m)
A_1	MHD duct inlet area (m^2)
A_2	Separator inlet area (m^2)
A_3	Separator exit area (m^2)
A_{E_i}	MHD duct i-th segment exit area (m^2)
A_{fr}	Frontal area of heat exchanger (m^2)
A_{ff}	Free-flow area of heat exchanger (m^2)
A_{h_1}	Heat transfer area of heat exchanger on hot side (m^2)
A_{h_2}	Heat transfer area of heat exchanger on cooler side (m^2)
A_{I_i}	MHD duct i-th segment inlet area (m^2)
A_R	Space radiator area (m^2)
b_1	Plate spacing of heat exchanger on hot side (m)
b_2	Plate spacing of heat exchanger on cooler side (m)
B	Magnetic field strength (tesla)
C_c	Capacity ratio of coolside of heat exchanger (cal/sec-^oK)
C_h	Capacity ratio of hot side of heat exchanger (cal/sec-^oK)
C_p	Heat capacity at constant presure (cal/gr-^oK)
C_i	Gas electrical conductivity in i-th segment of MHD duct (mhos/m)
D	Distance between two electrods of MHD duct (m)
E	Heat transfer effectiveness of heat exchanger
f	Friction factor
F_o	Gas flows rate at exit of reactor (kg/sec)

F_1 Gas flow rate at inlet of MHD duct (kg/sec)

F_2 Gas flow rate at exit of MHD duct (kg/sec)

F_3 Gas flow rate at exit of seperator (kg/sec)

F_4 Gas flow rate at inlet of gas turbine (kg/sec)

F_5 Gas flow rate at exit of gas turbine (kg/sec)

F_8 Gas flow rate at exit of first stage compressor which flows into mixing tank in MODE II (kg/sec)

F_g Gas flow rate in intercooler (kg/sec)

F_s Liquid sodium flow rate (kg/sec)

G_1 Flow-stream mass velocity on hot side of heat exchanger (kg/sec-m^2)

G_2 Flow-stream mass velocity on cool side of heat exchanger (kg/sec-m^2)

h_1 Convection heat transfer coefficient on hot side of heat exchanger (cal/sec-cm^2-^oK)

h_2 Convection heat transfer coefficient on cool side of heat exchanger (cal/sec-cm^2-^oK)

H Enthalpy of gas (cal/gr)

H_o Enthalpy of gas at exit of reactor (cal/gr)

H_1 Enthalpy of gas at inlet of MHD duct (cal/gr)

H_2 Enthalpy of gas at exit of MHD duct (cal/gr)

H_3 Enthalpy of gas at exit of seperator (cal/gr)

H_4 Enthalpy of gas at inlet of gas turbine (cal/gr)

H_5 Enthalpy of gas at exit of gas turbine (cal/gr)

H_6 Enthalpy of gas at inlet of first intercooler (cal/gr)

H_7 Enthalpy of gas at exit of first intercooler (cal/gr)

H_{18} Enthalpy of gas at exit of preheater on cool side (cal/gr)

H_{19} Enthalpy of gas inlet of heat regenerator on hot side (cal/gr)

H_{20} Enthalpy of gas at inlet of reactor

H_{m_i} Enthalpy of gas at exit of i-th segment of MHD duct (cal/gr)

H_t Stagnation enthalpy (cal/gr)

k Thermal conductivity (cal/sec-cm-^oK)

K MHD loading factor

KE Kinetic energy (MW)

ΔL_i Length of i-th segment of MHD duct (m)

m $= \sqrt{\frac{2h}{k\delta}}$ for thin sheet fins

M_1 Mach number at inlet of MHD duct

M_2 Mach number at exit of MHD duct

M_3 Mach number at exit of seperator

n Number of segments in MHD duct or number of passes in gas to liquid metal heat exchanger

N_{Pr} Prandtl number

N_R Reynolds number

P Pressure (atm)

P_o Reactor cavity pressure (atm)

P_1 Pressure at MHD inlet (atm)

P_2 Pressure at MHD exit (atm)

P_3 Pressure at exit of seperator (atm)

P_4 Pressure at exit of heat regenerator on hot side (atm)

P_5 Pressure at exit of gas turbine (atm)

P_6 Pressure at inlet of first intercooler (atm)

P_7 Pressure at inlet of first stage compressor (atm)

P_8 Pressure at exit of first stage compressor (atm)

P_9 Pressure at inlet of second stage compressor (atm)

P_{10} Pressure at exit of second stage compressor (atm)

P_{11} Pressure at inlet of third stage compressor (atm)

P_{12} Pressure at exit of third stage compressor (atm)

ΔP Fractional pressure drop (atm)

P_{m_i} Pressure at inlet of i-th segment of MHD duct (atm)

$\tilde{P}_{m_i}$ Average pressure in i-th segment of MHD duct (atm)

PR_1 Expansion ratio in MHD duct

PR_2 Expansion ratio in gas turbine

PR_3 Compression ratio in each compressor

PR_m Expansion ratio in each segment of MHD duct

Q Reactor power (MW)

Q_b Fraction of reactor power generated in blanket (MW)

Q_c Fraction of reactor power generated in core (MW)

Q_R Total heat rejected by each compressor unit (MW)

Q_{R_1} Heat rejected by first intercooler (MW)

Q_{R_2} Heat rejected by second intercooler (MW)

Q_{R_3} Heat rejected by third intercooler (MW)

R_1 Radius of heat regenerator (m)

R_2 Radius of preheater (m)

T Temperature ($^{\circ}K$)

T_0 Gas temperature at exit of reactor (°K)

T_1 Gas temperature at inlet of MHD duct (°K)

T_2 Gas temperature at exit of MHD duct (°K)

T_3 Gas temperature at exit of seperator (°K)

T_4 Gas temperature at exit of heat regenerator on hot side (°K)

T_5 Gas temperature at inlet of gas turbine (°K)

T_6 Gas temperature at inlet of first intercooler (°K)

T_7 Gas temperature at exit of first intercooler (°K)

T_8 Gas temperature at inlet of second intercooler (°K)

T_9 Gas temperature at exit of second intercooler (°K)

T_{10} Gas temperature at inlet of third intercooler (°K)

T_{11} Gas temperature at exit of third intercooler (°K)

T_{12} Gas temperature at exit of third compressor (°K)

T_{18} Gas temperature at inlet of mixing tank of cool gas in MODE II (°K)

T_{19} Gas temperature at inlet of heat regenerator on cool side (°K)

T_{20} Gas temperature at inlet of reactor (°K)

Tm_i Gas temperature at inlet of i-th segment of MHD duct (°K)

$\tilde{T}m_i$ Average temperature of i-th segment of MHD duct (°K)

T_R Temperature of space radiator (°K)

T_{R_i} Temperature of liquid sodium at inlet of intercooler (°K)

T_{Re_1} Temperature of liquid sodium at exit of first intercooler (°K)

T_{Re_2} Temperature of liquid sodium at exit of second intercooler (°K)

T_{Re_3} Temperature of liquid sodium at exit of third intercooler (°K)

T_u Number of heat transfer units

$T_{1,in}$ Heat exchanger hot side inlet temperature (°K)

$T_{1,out}$ Heat exchanger hot side exit temperature (°K)

$T_{2,in}$ Heat exchanger cool side inlet temperature (°K)

$T_{2,out}$ Heat exchanger cool side exit temperature (°K)

ΔT Temperature difference (°K)

U Velocity (m/sec)

U_h Overall heat transfer coefficient (Kcal/sec-m^2-°K)

V Specific volume (m^3/kg)

W_{C_1} Power required by first stage compressor (MW)

W_{C_2} Power required by second stage compressor (MW)

W_{C_3} Power required by third stage compressor (MW)

W_{MHD} Total power output of MHD duct (MW)

W_{MHD_e} MHD electrical power output (MW)

W_s Steam turbine power output (MW)

W_t Gas turbine power output (MW)

W_{ax} Power demand for auxiliary components (MW)

X Width of intercooler heat exchanger (M)

Y Height of intercooler heat exchanger (M)

Z Length of heat exchanger in direction of gas flow (M)

α Stefen-Boltzman constant = 5.67×10^{-12} (watts/cm^2-°K^4)

α_1 Ratio of free-flow to frontal area of hot side of heat exchanger

α_2 Ratio of free-flow to fontal area of cool side of heat exchanger

β_1 Ratio of total transfer area of hot side of heat exchanger to volume between plates of that side (m^2/m^3)

β_2 Ratio of total transfer area of cool side of heat exchanger to volume between plates of that side (m^2/m^3)

γ Ratio of heat capacities

γ_{h_1} Hydraulic radius of hot side of heat exchanger (cm)

γ_{h_2} Hydraulic radius of cool side of heat exchanger (cm)

λ Ratio of fin area to total area

δ Thickness of fin (cm)

η Efficiency

η_c Compressor efficiency

η_s Steam turbine efficiency

η_t Gas turbine efficiency

η_{SP_t} Cycle thermal efficiency for space power plant

η_{G_t} Cycle thermal efficiency for ground based power plant using a steam bottoming cycle

η_f Fin effectiveness

η_o Surface effectiveness

ρ Density (kg/m^3)

μ Viscosity (kg/sec-m)

DESCRIPTION OF THE THREE SYSTEMS

Three different types of advanced nuclear-MHD power plant systems were investigated. The three thermodynamic cycles which were studied are shown in Figures 1-3 and 21-23. The working fluid (hydrogen, helium, or argon) is heated in the reactor, passes through a nozzle and the MHD generator, and then through two separators. If the coaxial flow gas core or colloid core reactor is used, the uranium particles would be separated from the working fluid and returned to the reactor system. The gas exiting the separator passes into four identical heat exchanger and compressor units. One fourth of the gas flows through each unit. The three basic thermodynamic cycles are referred to as MODE I, MODE II and MODE III. These cycles are described as follows:

1) MODE I (as shown in Figures 1 and 21): The gas from the separator passes through a gas to gas regenerative heat exchanger, and into a gas turbine which is used to drive the compressor. After exiting the turbine, the gas is cooled by a gas to gas heat exchanger (preheater) and cooled further by a gas to liquid metal heat exchanger, then compressed by a three stage compressor with intercoolers between each stage. The gas exits the last stage of the compressor at a pressure slightly higher than the reactor pressure, is heated in a preheater, and heated further in the reactor blanket and regenerator, before being returned to the reactor core. Some of this high pressure gas is diverted through a cleanup system to remove gaseous fission products.

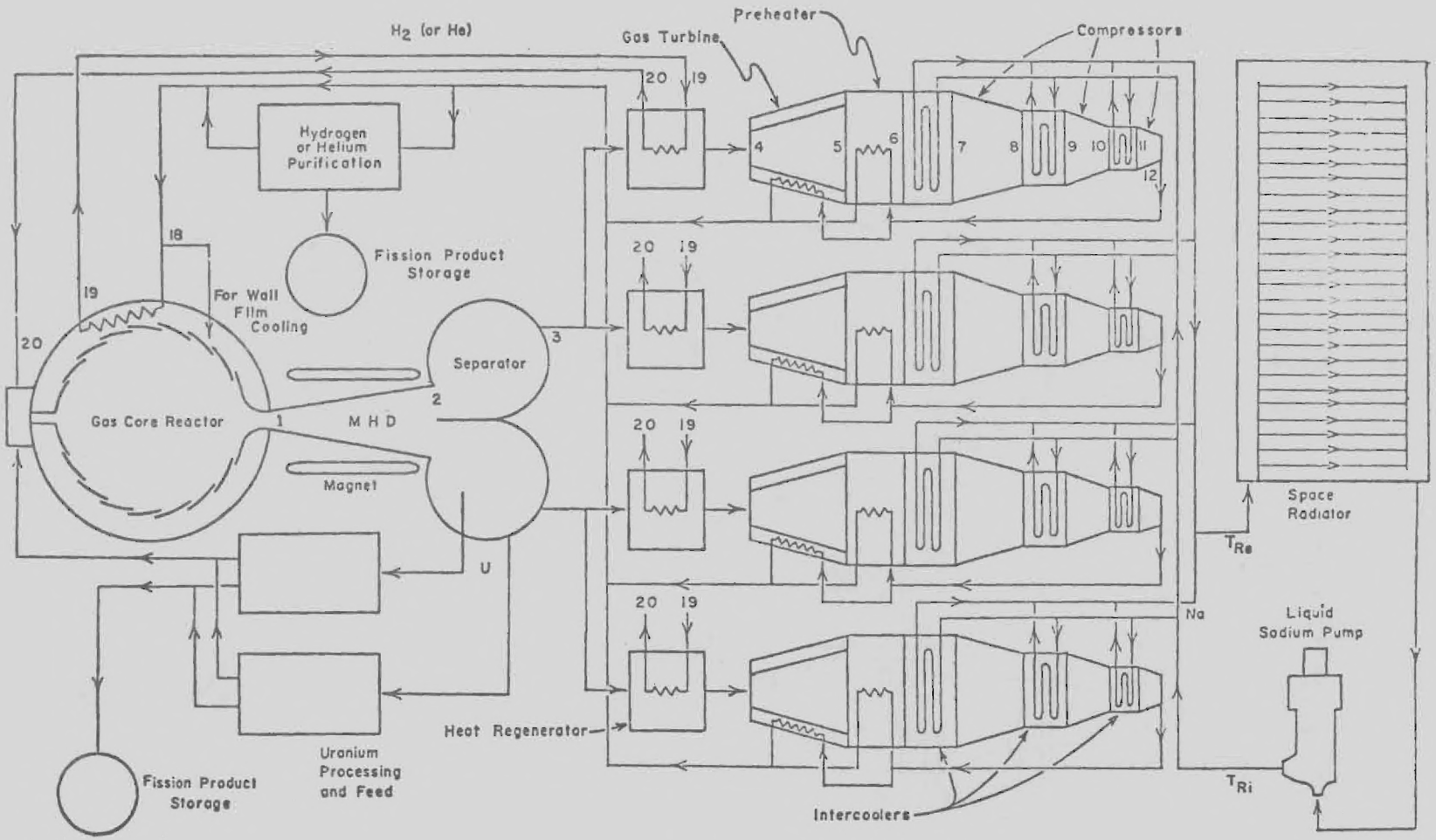

Figure 21. Turbine-Compressor Cycle with High Temperature Regenerator

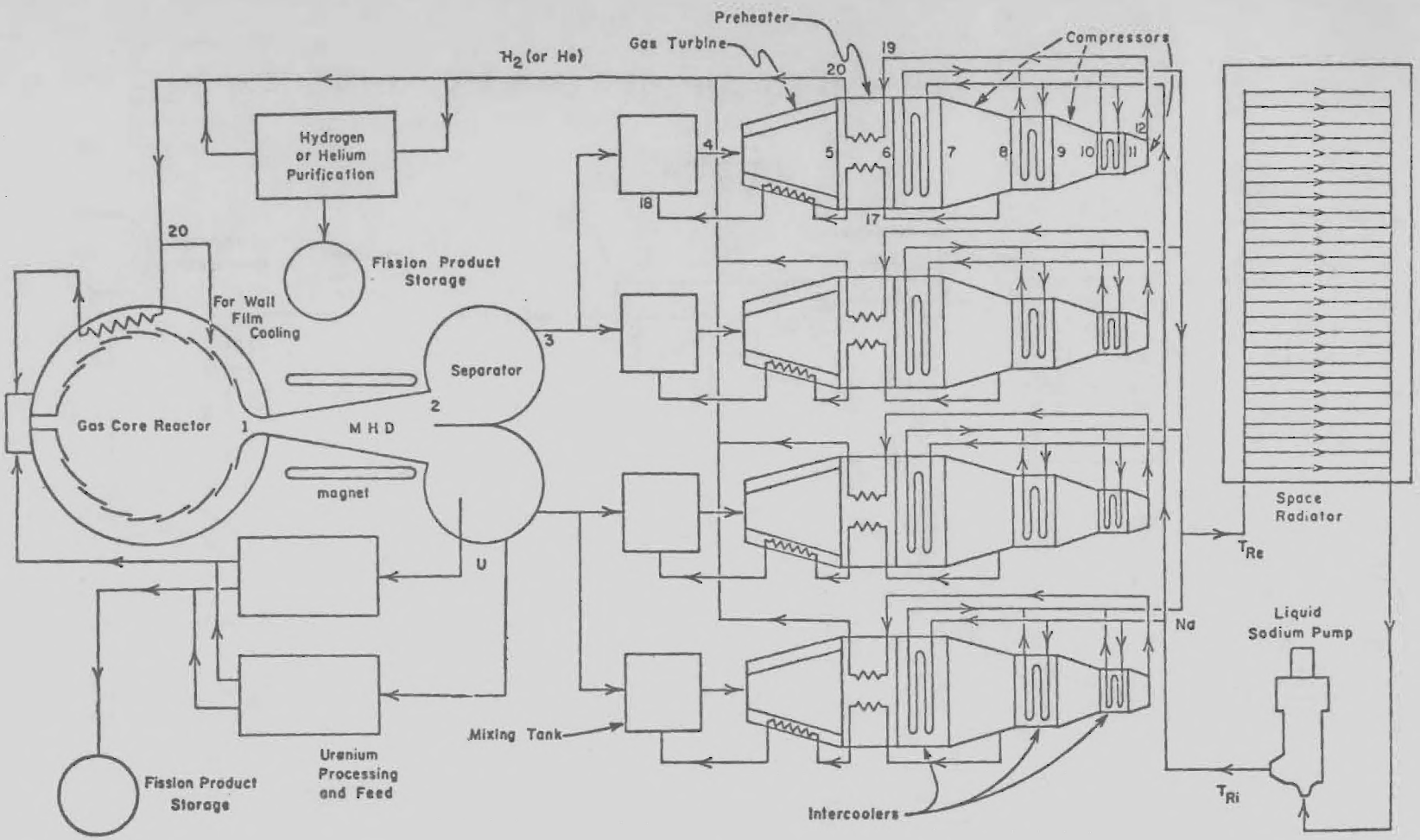

Figure 22. Turbine-Compressor Cycle Without High Temperature Regenerator.

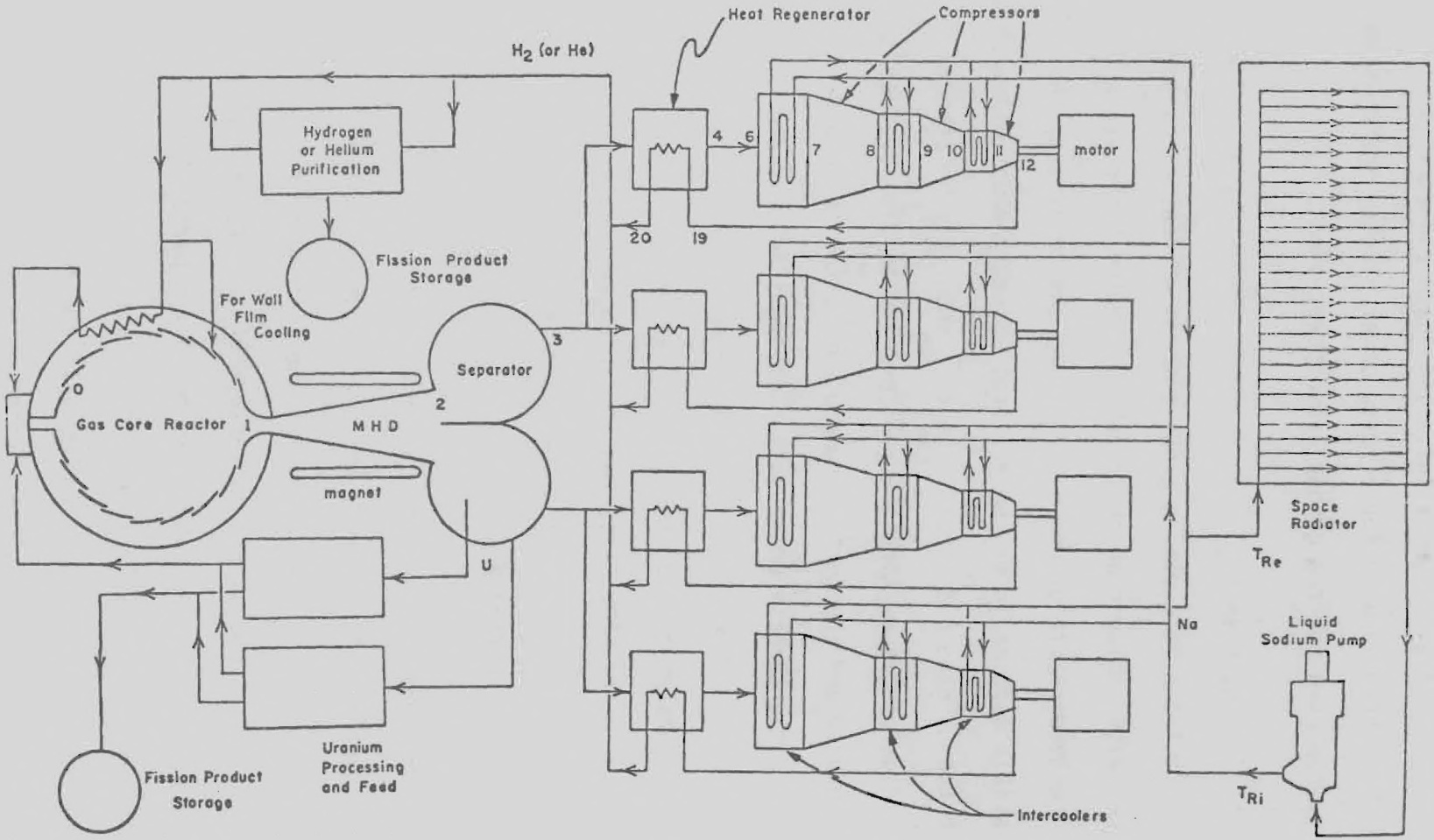

MODE III

Figure 23. Motor-Compressor Cycle With High Temperature Regenerator

The sodium coolant removes the heat from the intercooler, and is pumped to the space radiator or steam generator. The space radiator is employed when the system is used for a space power plant. Sodium-steam generators would be used for the ground based power plant.

2) MODE II (as shown in Figures 2 and 22): After the gas exits the separators, it flows into mixing tanks instead of heat exchangers. Here it is mixed with cool gas which is taken from the first stage compressor. This reduces the temperature of the gas entering the turbine to the maximum permissible turbine inlet temperature. Since the mass flow rate of gas through the turbine and first stage compressor may be several times the mass flow of gas exiting the reactor, the turbine delivers more power than in MODE I, and the turbine compressor system is considerably larger. Typically the turbine power output is significantly greater than the compressor power requirement, so the excess power is used to drive an electric generator. The rest of the system is the same as MODE I. The advantage of MODE II is that the high temperature regenerator is eliminated, so the MHD duct exit temperature can be higher without exceeding the permissible heat exchanger inlet temperature.

3) MODE III (as shown in Figures 3 and 23): This is the simplest cycle. The gas turbine and preheater are completely eliminated, and an electrical motor is used to drive the compressors. The rest of the cycle is the same as in MODE I. The advantage of this cycle is that, since the turbine is eliminated, there are no moving parts at high temperature. However, this cycle is more sensitive to any degredation of the MHD generator performance. If MODE III is used for a terrestrial power plant with steam bottoming, the electric motors can be replaced by steam turbines.

MODE I MAIN PROGRAM

The computer program MODE I calculates the parameters of the advanced nuclear MHD power plant cycle illustrated in figures 1 and 21. Imput data for hydrogen include:

1) Enthalpy data for hydrogen at pressures of 1, 3, 10, 30, 100, 300 and 1000 Atm. for temperatures of 300 to 5000 degrees Kelvin with 100 degree intervels between the data.
2) Heat capacity data for hydrogen over the same temperature and pressure range, except for 1000 Atm.
3) Values of the specific heat ratio (γ) for hydrogen over the same temperature and pressure range
4) Electrical conductivity of hydrogen seeded with 1 atom percent cesium. Helium and argon are assumed to behave as ideal gases.

General Discription

The data for the enthalpy, heat capacity and heat capacity ratio corresponding to a particular pressure and temperature are evaluated in sub-pragrams "SBH", "SBCP" and "SBGM" respectively. Given pressure P and temperature T, to find the corresponding enthalpy H, the following statements are used:

```
IAA = T/100
 AA = IAA x 100
 JJ = IAA - 2
CALL SBH (P, T, H)
```

The first two statements are used to truncate the temperature to an integral multiple of 100°K. For example,

```
If       T = 531.647
Then   IAA = T/100        = 5
        AA = IAA x 100    = 500.
        JJ = IAA -2       = 3
```

The enthalpy data are stored in an array starting with a temperature of 300°K, and data are given for each multiple of 100°K from 300°K to 5000°K. In the example, the values of AA and JJ allow the subprogram "SBH" to select the data of the enthalpy array corresponding to temperatures of 500°K and 600°K, and a linear interpolation is performed to obtian the value of the enthalpy at 531.647°K. The same approach is used to interpolate between enthalpy values given for specific pressures in the array.

Sometimes it is necessary to determine the temperature of the gas from known pressure and enthalpy values. This can also be done using the same subroutine. For example, given pressure P and enthalpy HY, to find the corresponding temperature T, the following statements are used:

```
  T = estimated value
IAA = T/100
 AA = IAA x 100
 JJ = IAA - 2
```

```
1     CALL SBH (P,T,HX)
       DH = HX -HY
      IF [ABS(DH) .LT. 10.] GO TO 3
      IF (DH .GT. 10) GO TO 2
        T = T + 1.0
      GO TO 1
2       T = T - 1.0
      GO TO 1
3     CONTINUE
```

Keeping the pressure constant, and starting with an estimated temperature T, the subprogram "SBH" is used to evaluate enthalpy HX. If HX is greater than (less than) HY, the temperature T is decreased (increased) by 1°K. This continues until HX = HY within 10 cal/gr. Then T is the temperature corresponding to pressure P and enthalpy HY.

In order to evaluate the parameters of the cycle, 5 initial values of temperature, T_4, T_6, T_{12}, T_{18}, and T_{20}, are chosen. These initial values are used in evaluating heat exchanger characteristics and gas properties. After the cycle parameters are calculated, the new values of temperature are used and the program continues to iterate until the final solution is reached.

Discription of the Model

The heat generated in reactor blanket, Q_b, is Q x 0.1, where Q is the total reactor thermal power in MWt. The heat generated in the reactor cavity, Q_c is Q - Q_b.

The flow rate of gas at the exit of the reactor cavity is

$$F_0 = \frac{Q_c \times 2.389 \times 10^2}{H_0 - H_{20}} \quad \text{kg/sec}$$

The enthalpy of the hydrogen is calculated at the inlet and exit of the reactor cavity to be H_{20} and H_0, respectively, by subroutine "SBH".

The static temperature and pressure at the exit of the nozzle for an isentropic process are

$$T_1' = \frac{T_0}{1 + \frac{\gamma - 1}{2} M_1^2} \quad {}^\circ K$$

$$P_1' = \frac{P_0}{\left[1 + \frac{\gamma - 1}{2} M_1^2\right]^{\frac{\gamma}{\gamma - 1}}} \quad \text{Atm.}$$

Where the specific heat ratio γ of hydrogen is determined by the subprogram "SBGM" at the average temperature and pressure in the nozzle. The velocity of the gas at the inlet of the MHD duct is

$$U_1 = \sqrt{\gamma R T_1'}\, M_1$$

The kinetic energy of the gas is

$$\text{K.E.} = \frac{U_1^2}{2} \times 2.389 \times 10^{-4} \quad \text{cal/gr.}$$

10 percent of cooler gas with enthalpy H_{20} enters through the walls of the nozzle for film cooling. An additional 10% is assumed to enter the MHD duct walls to provide film or transpiration cooling of the MHD duct. The total enthalpy of the mixture is

$$H_t = \frac{(H_0 + 0.1\, H_{20})}{1 + 0.1} \quad \text{cal/gr}$$

The static enthalpy at the inlet of the MHD duct is

$$H_1 = H_t - \text{K.E.} \quad \text{cal/gr}$$

Knowing the pressure $P_1 = P_t'$ and the enthalpy H_1 one can evaluate the corresponding static temperature T_1 using subroutine SBH. The density of the gas at the inlet of the MHD duct is

$$\rho_1 = \frac{P_1(1.01 \times 10^5)}{R\, T_1} \qquad Kg/m^3$$

The mass flow rate at the inlet of the MHD duct is

$$F_1 = F_0(1 + 0.1) \qquad Kg/sec$$

The MHD inlet area is

$$A_1 = \frac{F_1}{U_1\, \rho_1} \qquad m^2$$

Dividing the MHD duct into 15 segments and assuming the total expansion ratio is PR_1, the pressure ratio for each segment PR_m is taken to be

$$PR_m = PR_1^{1/n}$$

Where n is number of segments.

The pressure at the exit of each segment is

$$P_{m_{i+1}} = P_{m_i}/PR_m \qquad i = 1,2,3...15$$

$$P_{m_1} = P_1$$

The pressure drop for each segment is

$$\Delta P_i = P_{m_{i+1}} - P_{m_i} \qquad i = 1,2,3...15$$

The exit temperature of the i-th segment with expansion at constant velocity is

$$T'_{m_{i+1}} = \frac{T'_{m_i}}{PR_m^{\frac{K(\gamma - 1)}{\gamma}}} \qquad i = 1,2,3...15$$

Where K is the loading factor, and γ is the specific heat ratio corresponding to the average temperature and pressure in each segment.

The enthalpy H'_{m_i} corresponding to P_{m_i} and T'_{m_i} is calculated in subroutine SBH.

Due to the 10 percent film cooling for the MHD duct, the cooler gas with temperature T_{20} and static enthalpy H'_{20} flows into the MHD duct and the average enthalpy of the mixture is

$$Hm_i = \frac{H'_{m_i} \times F_1 \times (1 + (i - 1) \times \frac{0.1}{15}) + H'_{20} \times F_1 \times \frac{0.1}{15}}{F_1 \times (1 + i \times \frac{0.1}{15})} \quad \text{cal/gr}$$

$$i = 1,2,3...15$$

The average temperature T_{m_i} corresponding to H_{m_i} is found in the same way as before.

The average electrical conductivity of the gas, σ_i, in each segment is found in the subroutine "SBC" by giving the average temperature and pressure

$$\tilde{T}_{m_i} = \frac{T_{m_{i+1}} + T_{m_i}}{2} \quad {}^{\circ}K$$

$$\tilde{P}_{m_i} = \frac{P_{m_{i+1}} + P_{m_i}}{2} \quad \text{Atm.}$$

assuming the magnetic flux density for each segment is B. Then the length of each segment of the MHD duct is

$$\Delta L_i = \frac{\Delta P_i \times 1.01 \times 10^5}{B^2 U_1 \sigma_i (1 - K)} \qquad i = 1,2,3...15$$

The density corresponding to T_{m_i} and P_{m_i} is

$$\rho_{m_i} = \frac{P_{m_i} \times 1.01 \times 10^5}{R T_{m_i}} \qquad i = 1,2,3...15 \quad \text{Kg/m}^3$$

The inlet area (A_{I_i}) of each segment (i) is

$$A_{I_i} = \frac{F_1 + (0.1/15)F_1(i - 1)}{U_1 \rho_i} \qquad i = 1,2,3...15 \quad m^2$$

The exit area (A_{E_i}) of each segment (i) for constant velocity expansion is

$$A_{E_i} = \frac{A_{I_i}}{PR_m (K^{\frac{\gamma-1}{\gamma}} - 1)} \qquad i = 1,2,3...15 \quad m^2$$

The Mach number at the exit of the MHD duct is

$$M_2 = \frac{U_1}{\sqrt{\gamma R T_2}}$$

where $T_2 = T_{m_{16}}$ is the exit temperature of the MHD duct.

Leaving the MHD duct, the gas enters two separators, if the reactor is of the coaxial flow gas core or colloid core type. The Mach number of the hydrogen is reduced to M = 0.1 before it enters the turbine. The temperature and pressure at the exit of the separators are

$$T_3 = T_2 \frac{(1 + \frac{\gamma-1}{2} M_2^2)}{(1 + \frac{\gamma-1}{2} M_3^2)} \qquad {}^\circ K$$

$$P_3 = P_2 \frac{(1 + \frac{\gamma-1}{2} M_2^2)^{\frac{\gamma}{\gamma-1}}}{(1 + \frac{\gamma-1}{2} M_3^2)^{\frac{\gamma}{\gamma-1}}} \qquad Atm$$

Assuming no heat loss and no frictional losses in the nozzle and cyclone separators, the decrease in the enthalpy of the hydrogen passing through the MHD duct is equal to the electric power produced. The total thermal energy in the HMD duct is

$$W_{MHD} = \left[(F_0 H_0 + 0.1F_0 H_{20} + 0.1F_1 H_{20}) - (1.1F_1 H_3)\right] x(4.187 \times 10^3) \text{ MWE}$$

Where F_0 and F_1 are the gas flow rates at the inlet of the nozzle and MHD duct respectively, H_0 is the stagnation enthalpy of the gas at the nozzle inlet, H_{20} is stagnation enthalpy of the cooler gas which flows through the wall of the nozzle and the MHD duct for film cooling, H_3 is the stagnation enthalpy of the gas which exits the separators, and the numerical value 4.187×10^{3} converts Kcal/sec into MW. If two separators are used at the MHD exit, then the mass flow rate in each separator is

$$F_2 = \frac{F_1\ 1.1}{2} \qquad \text{Kg/sec}$$

The gas passes through a diffuser before entering the separator, and the velocity is reduced from M_2 to M_3.

The gas velocity at the entrance of the separator is

$$U_3 = \sqrt{\gamma\ R\ T_3} M_3 \qquad \text{m/sec}$$

The density of hydrogen at the inlet and exit of each separator is

$$\rho_3 = \frac{P_3(1.01 \times 10^5)}{T_3} \quad \text{Kg/m}^3$$

The inlet area of the separator is

$$A_2 = \frac{F_2}{U_3 \rho_3} \quad \text{m}^2$$

Each separator has two exits connected with two turbine-compressor units. The exit area is

$$A_3 = \frac{F_3}{U_3 \rho_3} \qquad \text{m}^2$$

where $F_3 = \frac{F2}{2}$ is the mass flow rate in each turbine compressor unit.

Before the gas enters the turbine it is cooled by a cylindrical counter-flow heat regenerator. The inlet temperature of the hot gas is T_3 and the inlet temperature of the cooler gas is T_{19} which is

calculated as follows:

A value T_{18} is assumed at the beginning of the program. It will be replaced by a calculated value at a later stage of the calculation. The corresponding enthalpy H_{18} is found from subprogram "SBH". Then the temperature T_{19} corresponding to H_{19} can be found.

$$H_{19} = H_{18} + \frac{Q_b(0.2398 \times 10^3)}{F_2}$$

Given the heat regenerator radius R_1 and length Z_1, the average viscosity of hydrogen in both sides μ_1 and μ_2, the average Prantl number N_{Pr_1} and N_{Pr_2}, specific heat C_{P_1} and C_{P_2} (found from subroutine SBCP), mass flow rate F_3, inlet temperature T_3 and T_{19} and inlet pressure P_3 and P_{19}, one can calculate the exit temperature T_4 and T_{20}, percentage pressure drops ΔP_3, ΔP_{19}, the overall heat transfer coefficient and heat exchanger effectiveness using subprogram SBRG .

Given the turbine exit temperature T_5, the expansion ratio of the gas turbine PR_2 for an adiabatic process is

$$PR_2 = \left(\frac{T_4}{T_5}\right)^{\frac{\gamma}{\gamma-1}}$$

and $$P_5 = \frac{P_4}{PR_2} \quad \text{Atm}$$

where $P_4 = P_3(1 - \Delta P_3)$ Atm

ΔP_3 here is the fractional pressure drop through the regenerator.

The output of each gas turbine is

$$W_t = \frac{F_4\ (H_4 - H_5)\ 4.187}{1000} \quad \text{MW}$$

Where H_4 and H_5 are found by subroutine SBH , 4.187 is the conversion factor from Kcal/sec to KW and 1000 changes the units from KW to MW.

The exit gas from the gas turbine enters a heat exchanger to preheat the hydrogen coming from the last stage compressor before it enters the blanket of the reactor. The subprogram SBRG is used as before. The input data are the size of the heat exchanger (radius R_2 and length Z_2), average viscosity of hydrogen μ_1 and μ_2 (over the temperature range of interest), average Prantl number N_{Pr_1} and N_{Pr_2}, specific heat C_{P_1} and C_{P_2}, mass flow rate F_4, inlet temperature T_5 and T_{12}, and inlet pressure P_5 and P_{12}. We can calculate the exit temperatures T_6 and T_{18} (this calculated value T_{18} is substituted for the previous estimated value T_{18} in the subsequent interation) fractional pressure drops ΔP_5 and ΔP_{12}, the overall heat transfer coefficient and the heat exchanger effectiveness.

The exit hydrogen from the hot side of this gas-gas regenerative heat exchanger is further cooled by a gas to liquid sodium heat exchanger before it enters the first stage of the compressor. It is a rectangular four-pass cross-flow heat exchanger as shown in figure 5. Another subprogram SBHE is used for this calculation. The input data are: the size of the heat exchanger X_1, Y_1, Z_1, the mass flow rate of the hydrogen F_4, the temperature T_6, the pressure P_6 where $P_6 = P_5 (1 - \Delta P_5)$ and the mass flow rate F_{s_1} and inlet temperature T_{R_i} of the liquid sodium. The output data from this subprogram are the overall heat transfer coefficient, heat exchanger effectiveness, exit temperature T_7 of the gas, and T_{Re_1} on both sides, the pressure drop ΔP_6 on the gas side and the pressure head on the liquid metal side. The heat removed from the gas side is calculated in the main program. The heat removed from the gas side is

$$Q_{R_1} = F_3 (H_6 - H_7) \quad \text{Kcal/sec}$$

The compression ratio for the first stage compressor is

$$PR_3 = \frac{P_8}{P_7}$$

where $$P_8 = \sqrt[3]{P_6^2 P_{12}} \quad \text{Atm}$$

and $$P_{12} = \frac{P_{19}}{1 - \Delta P_{12}} \quad \text{Atm}$$

The exit temperature with isentropic compression

$$T_8' = \frac{T_7}{PR_3^{\frac{\gamma-1}{\gamma}}} \quad {}^{o}K$$

The isentropic input power needed for the first stage compressor is

$$W_{c_1}' = \frac{F_3 (H_8' - H_7)\ 4.187}{1000} \quad \text{MW}$$

For a compressor overall efficiency $\eta_c = 0.87$, the actual input power needed for the compressor is

$$W_{c_1} = W_{c_1}' / \eta_c$$

The enthalpy of the hydrogen at the exit of the compressor becomes

$$H_8 = 1000\ W_{c_1} / (4.187 F_3) + H_7$$

and the corresponding temperature T_8 can be calculated by subroutine SBH.

Three sodium to gas intercoolers and compressors are used for each gas turbine unit. The calculational precedures are the same as described previously.

The total heat removed from each turbine compressor unit is

$$Q_R = Q_{R_1} + Q_{R_2} + Q_{R_3} \quad \text{Kcal/sec}$$

where Q_{R_2} and Q_{R_3} are the heat removed from the intercoolers before the second and third stage compressors. The total mass flow rate of liquid

sodium from each turbine-compressor unit is

$$F_s = F_{s_1} + F_{s_2} + F_{s_3}$$

The mixed temperature of liquid sodium at the exit of the three intercoolers is

$$T_{R_e} = \frac{F_{s_1} T_{Re_1} + F_{s_2} T_{Re_2} + F_{s_3} T_{Re_3}}{F_s} \quad {}^\circ K$$

The mixed intercooler exit temperature of the liquid sodium equals the inlet temperature of the space radiator when it is used for a space power plant divided into 10 regions with the same temperature difference ΔT_R in each region.

$$\Delta T_R = \frac{T_{R_e} - T_{R_i}}{10} \quad {}^\circ K$$

T_{R_i} is an input parameter for the program.

The average temperature in each region is

$$T_{R_j} = T_{R_e} - \Delta T_R (j - 0.5) \quad {}^\circ K \qquad j = 1,2,3...10$$

The total radiator area for each turbine compressor unit is

$$A_R = \frac{\frac{Q_R}{10} \times 4.187 \times 10^3}{\alpha E} \times \sum_{j=1}^{10} \frac{1}{T_{R_j}^4} \quad m^2$$

When this nuclear-MHD conversion cycle is used as a ground based power plant, the heat rejected from each stage of the intercooler can be used for steam generation. The steam can be used to generate additional electric power or to drive the compressor. The work output of the steam cycle is

$$W_S = Q_R \times \eta_S \quad MW$$

where Q_R is the total heat rejected from each turbine compressor unit

and η_s is the thermal efficiency of the steam power plant. η_s is a function of the steam temperature.

The cycle thermal efficiency for the space power plant is

$$\eta_{SP_t} = \left[W_{MHD} + 4 \times W_t - 4 \times (W_{c_1} + W_{c_2} + W_{c_3}) \right] / Q$$

The cycle thermal efficiency for the ground based power plant is

$$\eta_{G_t} = \left[W_{MHD} + 4 \times (W_t + W_s) - 4 \times (W_{c_1} + W_{c_2} + W_{c_3}) \right] / Q$$

THE MODE II MAIN PROGRAM

All the input data are the same as for MODE I. The heat regenerator between the cyclone separator and the gas turbines is replaced by a mixing tank.

The enthalpy at the inlet of the gas turbine is

$$H_4 = \frac{F_3H_3 + F_{18}H_{18}}{F_3 + F_8} \quad \text{cal/gr}$$

where F_3 is gas flow rate at the exit of each cyclone separator, F_{18} is the gas flow rate of cooler gas from the exit of each first stage compressor. This gas is preheated and then enters into the mixing tank to cool the hot gas before it enters the gas turbine. The total flow rate of gas passing through the gas turbine and first stage compressor is

$$F_4 = F_3 + F_{18} \quad \text{kg/sec}$$

The rest of the gas at the exit of the first stage compressor continues through the other intercooling and compression stages of the compressor. The gas exits the last stage of the compressor, passes through the preheater, and then back to the reactor.

THE MODE III MAIN PROGRAM

All the input data are the same as in MODE I. The gas turbines and preheater are eliminated. The inlet gas temperature T_6 of the first intercooler is equal to the exit gas temperature of the heat regenerator on the hot side T_4 and the inlet gas temperature on the cooler side of the regenerator T_{19} is equal to the exit temperature of the last stage compressor T_{12}. In begining the cycle evaluation, only 3 initial values of temperature T_4, T_{12} and T_{20} are chosen.

SUBROUTINES FOR GAS PROPERTIES

Subroutine SBH is used to find the enthalpy of hydrogen corresponding to given temperature and pressure conditions. Enthalpy data are read into the program and stored in a 48 x 7 array.

$$(H) = \begin{bmatrix} H_{1,1} & H_{1,2} & \cdots & H_{1,7} \\ H_{2,1} & H_{2,2} & \cdots & H_{2,7} \\ \vdots & \vdots & & \vdots \\ H_{48,1} & H_{48,2} & \cdots & H_{48,7} \end{bmatrix} \quad \text{cal/gr}$$

The first subscript represents the temperature and the second subscript represents the pressure. The range of temperature is from 300°K to 5000°K. The enthalpy data are given in each 100°K interval at 7 different pressure conditions (1, 3, 10, 30, 100, 300, 1000 Atm). For example, the element $H_{1,1}$ represents the enthalpy of hydrogen at temperature 300°K and pressure 1 Atm., the element $H_{2,3}$ represents the enthalpy at temperature 400°K and pressure 10 Atm., etc. Other values of H are found by linear interpolation. For example, to find H at T = 325°K, P = 2.5 Atm

$$H_T = T_{1,1} + \frac{H_{2,1} - H_{1,1}}{100} (325 - 300) \qquad \text{cal/gr}$$

$$H_P = H_{1,2} + \frac{H_{2,2} - H_{1,2}}{100} (325 - 300) \qquad \text{cal/gr}$$

$$H = H_T + \frac{H_P - H_T}{2} (2.5 - 1) \qquad \text{cal/gr}$$

where $H_{1,1}$ is the enthalpy at T = 300°K P = 1 Atm

$H_{2,1}$ is the enthalpy at T = 400°K P = 1 Atm

$H_{1,2}$ is the enthalpy at T = 300°K P = 3 Atm

$H_{2,2}$ is the enthalpy at T = 400°K P = 3 Atm

H_T is the enthalpy at T = 325°K P = 1 Atm

H_P is the enthalpy at T = 325°K P = 3 Atm

H is the enthalpy at T = 325°K P = 2.5 Atm

The numerical value "100" in the denominator of the first and second equations is the temperature interval between two given data at the same pressure and the numerical value "2" in the denominator of the third equation is the pressure difference between 3 Atm and 1 Atm. The numerical value "(325 - 300)" is the temperature difference, and the value "(2.5 - 1)" is the pressure difference.

The subroutines SBCP (for heat capacity), SBC (for electrical conductivity), and SBGM (for the heat capacity ratio) use the same procedure of linear interpolation as subroutine SBH. The data for the heat capacity, heat capacity ratio and enthalpy are taken from Patch[33], and the electrical conductivity data are taken from Rosa[15].

HEAT EXCHANGER SUBROUTINES

Subroutine SBRG

The subroutine SBRG is used to calculate the cylindrical gas to gas counterflow type heat exchanger performance. Input data include:

1) Size of heat exchanger = Radius R, Length Z

2) Mass flow rate F_g

3) Inlet temperature and pressure on both hot and cool sides

4) Viscosity of hydrogen gas μ_1 and μ_2 on both sides

5) Prantl number of hydrogen gas N_{Pr_1}, and N_{Pr_2}, on both sides

6) Average specific heat of hydrogen gas C_{P_1} and C_{P_2} on both sides

Output data include:

1) Overall heat transfer coefficient, U_h Kcal/sec-m^2-^oK

2) Number of heat transfer units T_u

3) Exchanger effectiveness E

4) Exit temperature on both sides

All the surface properties of the heat exchanger and the reference data used in the subprogram are taken from reference 34. The subscript "1" represents the hot side and "2" represents the cool side. The surface characteristics are listed in Table 2. The frontal area of the heat exchanger is

$$A_{fr} = \pi R^2$$

The ratio of total heat transfer area of one side to total heat exchanger volume are

$$\alpha_1 = \frac{b_1 \beta_1}{b_1 + b_2 + 2a} \qquad ft^2/ft^3$$

$$\alpha_2 = \frac{b_2 \beta_2}{b_1 + b_2 + 2a} \qquad ft^2/ft^3$$

Where b_1 and b_2 are the plate spacing of both sides, β_1 and β_2 are ratios of transfer area to volume between plates. a = 0.012 is used in this program is the thickness of the plate.

The heat transfer areas for both sides are

$$A_{h_1} = A_{fr} Z \alpha_1 \qquad ft^2$$

$$A_{h_2} = A_{fr} Z \alpha_1 \qquad ft^2$$

Where Z is the length of the heat exchanger.

The free-flow areas on both sides are

$$A_{ff_1} = \alpha_1 \gamma_{h_1} A_{fr} \qquad ft^2$$

$$A_{ff_2} = \alpha_2 \gamma_{h_2} A_{fr} \qquad ft^2$$

Exchanger flow-stream mass velocities are

$$G_1 = \frac{F_g}{A_{ff_1}} \qquad lb/\ hr\text{-}ft^2$$

$$G_2 = \frac{F_g}{A_{ff_2}} \qquad lb/hr\text{-}ft^2$$

The Reynolds numbers are

$$N_{R_1} = \frac{4 \gamma_{h_1} G_1}{\mu_1}$$

$$N_{R_2} = \frac{4\gamma_{h_2} G_2}{\mu_1}$$

where γ_h is the hydraulic radius and μ is viscosity. The relation between Reynolds number and heat transfer characteristics can be expressed in two approximate equations derived from experimental correlations given by Kays.[34]

$$\frac{h_1}{G_1 C_{p_1}} N_{Pr_1}^{2/3} = 10^{(-0.1 - 0.735 \log_{10} N_{R_1})}$$

$$\frac{h_2}{G_2 C_{p_2}} N_{Pr_2}^{2/3} = 10^{(0.0817 - 0.809 \log_{10} N_{R_2})}$$

for the range of Reynolds numbers from 300 to 1000. Both C_p and N_{Pr} are input data, the values of G and N_R are calculated from the previous equations. So the value of the unit conductance for thermal-convection heat transfer, h, on both sides is calculated.

The correlations[34] for the friction factors in the same range of Reynolds numbers as before can be expressed as

$$f_1 = 10^{(0.88 - 0.87 \log_{10} N_{R_1})}$$

$$f_2 = 10^{(0.9283 - 0.9145 \log_{10} N_{R_2})}$$

The fin effectiveness is calculated from

$$\eta_{f_1} = \frac{\tanh (m_1 \times \ell_1)}{m_1 \times \ell_1}$$

$$\eta_{f_2} = \frac{\tanh (m_2 \times \ell_2)}{m_2 \times \ell_2}$$

where $m = \frac{2h}{k\delta}$ and

k is the heat conductance of the fin

δ is the thickness of the fin

The surface effectivenesses are

$$\eta_{o_1} = 1 - \lambda_1 (1 - \eta_{f_1})$$

$$\eta_{o_2} = 1 - \lambda_2 (1 - \eta_{f_2})$$

where the λ's are the ratio of fin area to total area for both sides. The overall coefficient of heat transfer neglecting the very small wall resistance is

$$\frac{1}{U_1} = \frac{1}{\eta_{o_1} h_1} + \frac{1}{(A_{h_2}/A_{h_1})\ \eta_{o_2} h_2}$$

The capacity rate is

$$C_h = F_g C_{p_1} \qquad \text{Btu/hr°F}$$

$$C_c = F_g C_{p_2} \qquad \text{Btu/hr°F}$$

The number of heat transfer units is

$$Tu = \frac{A_{h_1} U_1}{C_c}$$

The relation between exchanger effectiveness E and number of heat transfer units can be expressed as

$$E = \sum_{i=1}^{n} \frac{E_i \prod_{j \neq i}^{n} (Tu - Tu_j)}{\prod_{j \neq i}^{n} (Tu_i - Tu_j)}$$

where the E_i's corresponding to the Tu_i's are known.

The exit temperatures of the gas for both sides are calculated by

$$T_e = \frac{C_h(T_{1,in} - T_{1,out})}{C_{min}(T_{1,in} - T_{2,in})} = \frac{C_c(T_{2,out} - T_{2,in})}{C_{min}(T_{1,in} - T_{2,in})}$$

The equation for the pressure drop (neglecting the entrance and exit loss) is given as follows

$$\Delta P = \frac{G^2 v_{in}}{2g_c}\left[2\left(\frac{v_{out}}{v_{in}} - 1\right) + \left(f\frac{Z}{\gamma_h}\frac{\bar{v}}{v_{in}}\right)\right]$$

where v_{in} and v_{out} are specific volumes of the gas at inlet and outlet and $\bar{v}$ is the mean specific volume.

Subroutine SBHE

This subroutine is used to calculate the performance of the rectangular 4-pass gas to liquid metal cross-flow type intercooler as shown in figure 5. The surface characteristics are listed in table 3. The relation between Reynolds number and friction factor on the liquid metal side is given by $f_2 = 0.46\ N_R^{-0.2}$, the relation between Reynolds number and friction factor on the gas side can be expressed by

$$f_1 = 10^{(0.23 - 0.559 \log_{10} N_{R_1})}$$

for the range of Reynolds number from 300 to 1000. The relation between Reynolds number and $\left(\frac{h_1}{G_1 C_{p_1}}\right) N_{Pr_1}^{2/3}$ also can be expressed by a correlation in the same range of Reynolds numbers.

$$\left(\frac{h_1}{G_1 C_{p_1}}\right) N_{Pr_1}^{2/3} = 10^{(-0.38 - 0.534 \log_{10} N_{R_1})}$$

These equations are taken from experimental correlations by Kays.

The calculational procedure for the overall heat transfer coefficient, the number of heat transfer units and exchanger effectiveness are as used in subprogram SBRG , except the exchanger effectiveness is modified by the number of passes

$$E' = \frac{N\,E}{1 + E\,(N - 1)}$$

where N = 4 is the number of passes.

E is the exchanger effectiveness of a single pass. The equation to calculate exit temperatures and pressure drops are the same as used in subroutine "SBRG".

RESULTS

Figure 24 illustrates the effect of reactor exit temperature and space radiator temperature on the overall thermal efficiency of a regenerative turbine-compressor (MODE I) power plant system. The upper solid curves are for a terrestrial cycle. The dotted lines represent the same cycle but with heat rejection from a space radiator. The lower solid curves are the total space radiator area.

As the radiator temperature is decreased, the efficiency of the space plant increases but so does the size and weight of the radiator. The final choice of heat rejection temperature will depend on an economic analysis of the whole system to determine the optimum compromise between radiator size and efficiency. The radiator size decreases as the reactor temperature is increased due to the increase in plant efficiency with reactor temperature. As the efficiency increases, more electric power is produced and less heat is rejected.

Figure 25 illustrates the effect of MHD pressure ratio on plant efficiency. For MODE I the efficiency appears to be insensitive to pressure ratio above a pressure ratio of about 4. However, low pressure ratios result in high regenerator inlet temperatures which adversly affect the reliability of the regenerator. Thus higher pressure ratios, of 10 or more, are desired to reduce both the regenerator temperature and the turbine inlet temperature. The high

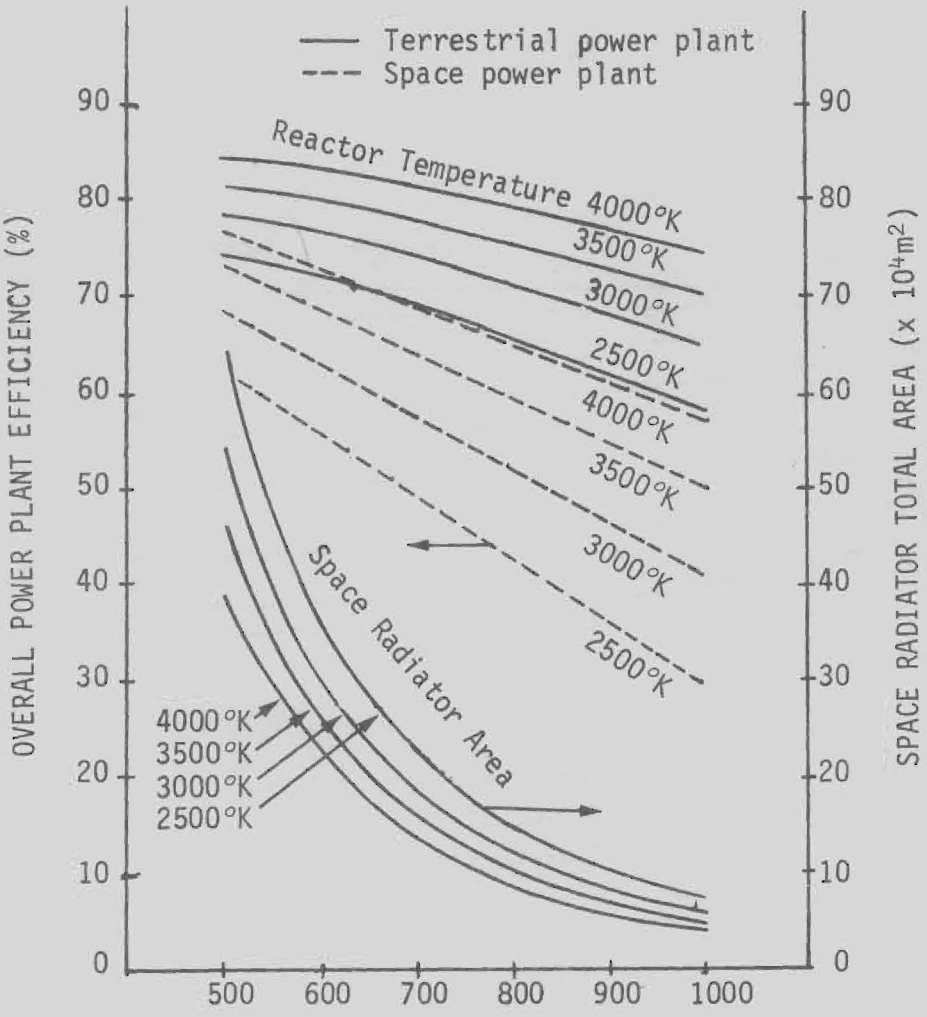

MODE I H_2 + 1% Cs (or equivalent)

Reactor Power	10,000 MW_t
Reactor Pressure	200 Atm
MHD Loading Factor	0.8
MHD Expansion Ratio	15

Figure 24. MODE I Power Plant Efficiency and Space Radiator Area vs. Reactor Exit Temperature and Average Temperature of Heat Rejection from Radiator (Space) on to Steam Generator (Terrestrial).

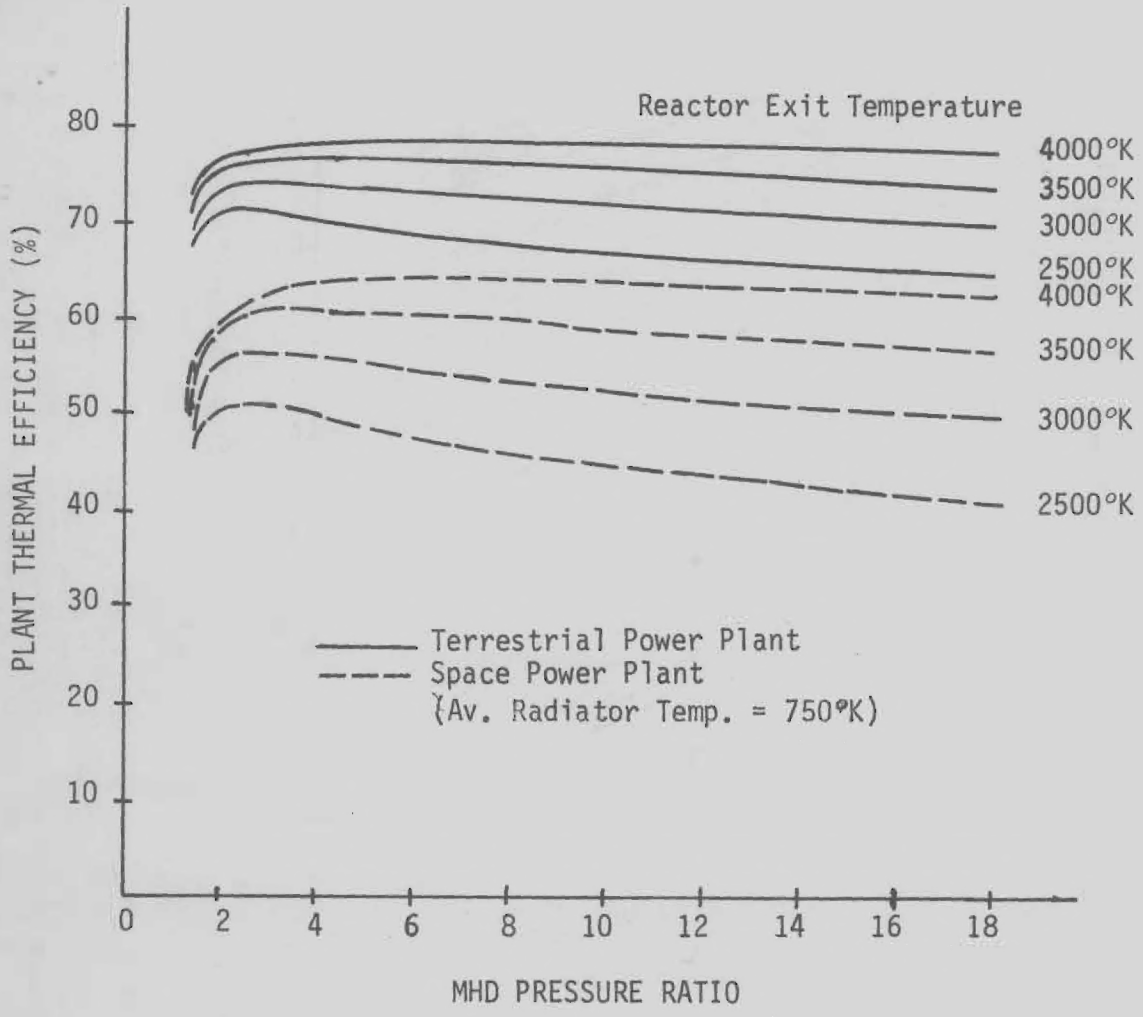

MODE I	Hydrogen
Reactor Power	10,000 MW_t
Reactor Pressure	200 Atm.
MHD Loading Factor	0.8
Av. Radiator Temp. (Space)	750°K

Figure 25. MODE I Plant Thermal Efficiency vs. MHD Pressure Ratio (Hydrogen)

space plant efficiency results from the relatively low (750°K) average radiator temperature. A radiator temperature increase of 200°K would reduce the efficiency by about 10%.

Figure 26 illustrates the dependence of MHD power output, compressor power requirement, turbine power output, mass flow rate of hydrogen and overall plant efficiency on the reactor exit temperature for a specific MODE I configuration. The mass flow rate drops by more than a factor of two as the reactor exit temperature increases from 2500 to 4000°K. This results in a corresponding decrease in the compressor work required, and an increase in turbine power.

Large MHD pressure ratios result in small turbine pressure ratios and a high ratio of MHD power to turbine power. The pressure ratios can be chosen to make the turbine power equal the compressor power required. The plant efficiency (total power output per thermal kilowatt) increases with reactor temperature even though the MHD power decreases due to the reduced mass flow rate. Lower flow rates also result in smaller compressors and turbines.

Figure 27 presents the efficiency for MODE II terrestrial and space power plants and the space radiator area as a function of the heat rejection temperature and reactor temperature. For a given set of conditions the MODE II configuration is less efficient than MODE I since the regenerator has been replaced by irreversible mixing of the hot gas from the MHD duct with cooler gas from the compressor. This recirculation increases the gas flow through the turbine and thereby increases the size and weight of the turbine and first stage compressor.

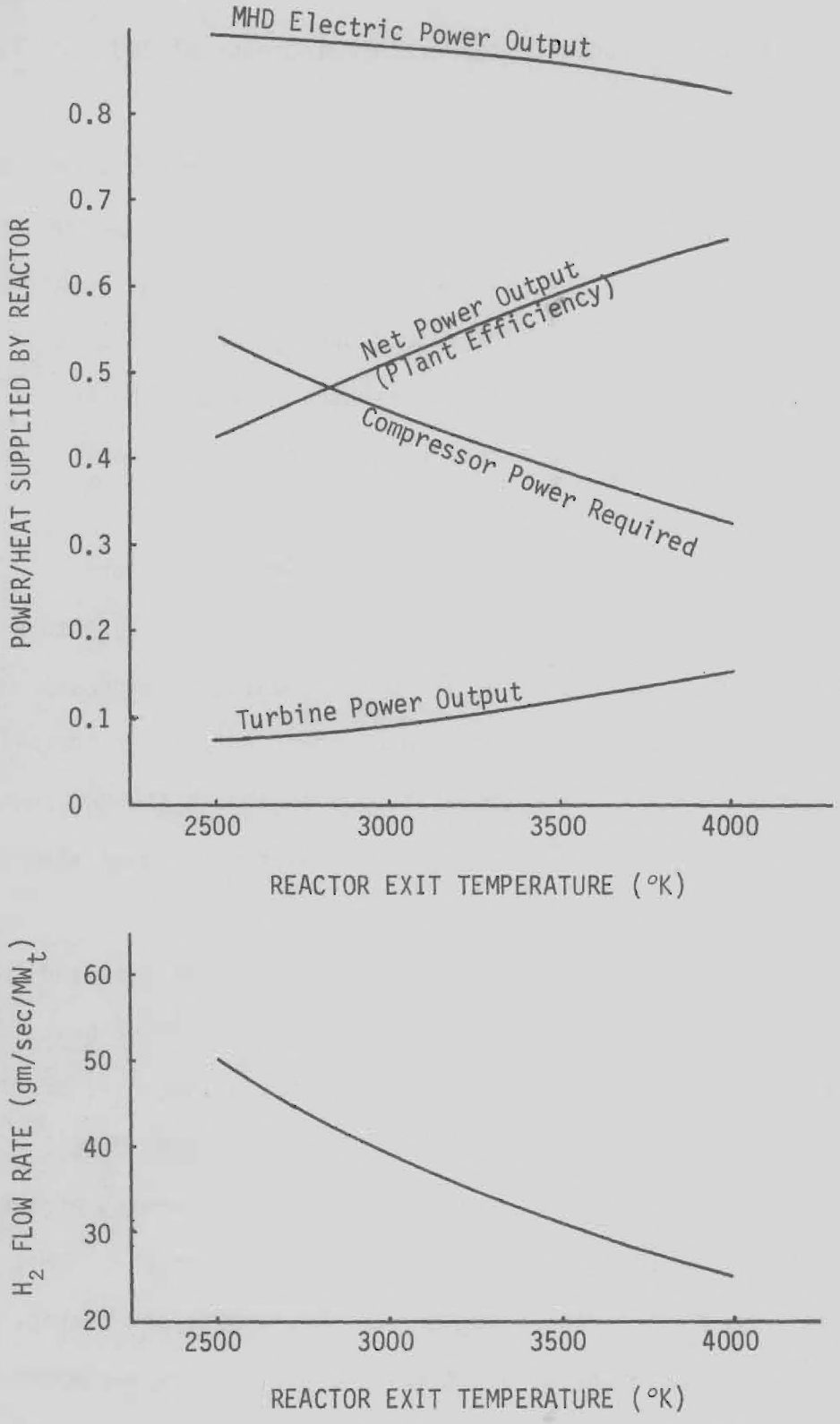

Figure 26. MHD, Turbine and Net Power Output, Compressor Power Required, and H_2 Mass Flow Rate for a specific MODE I Configuration.

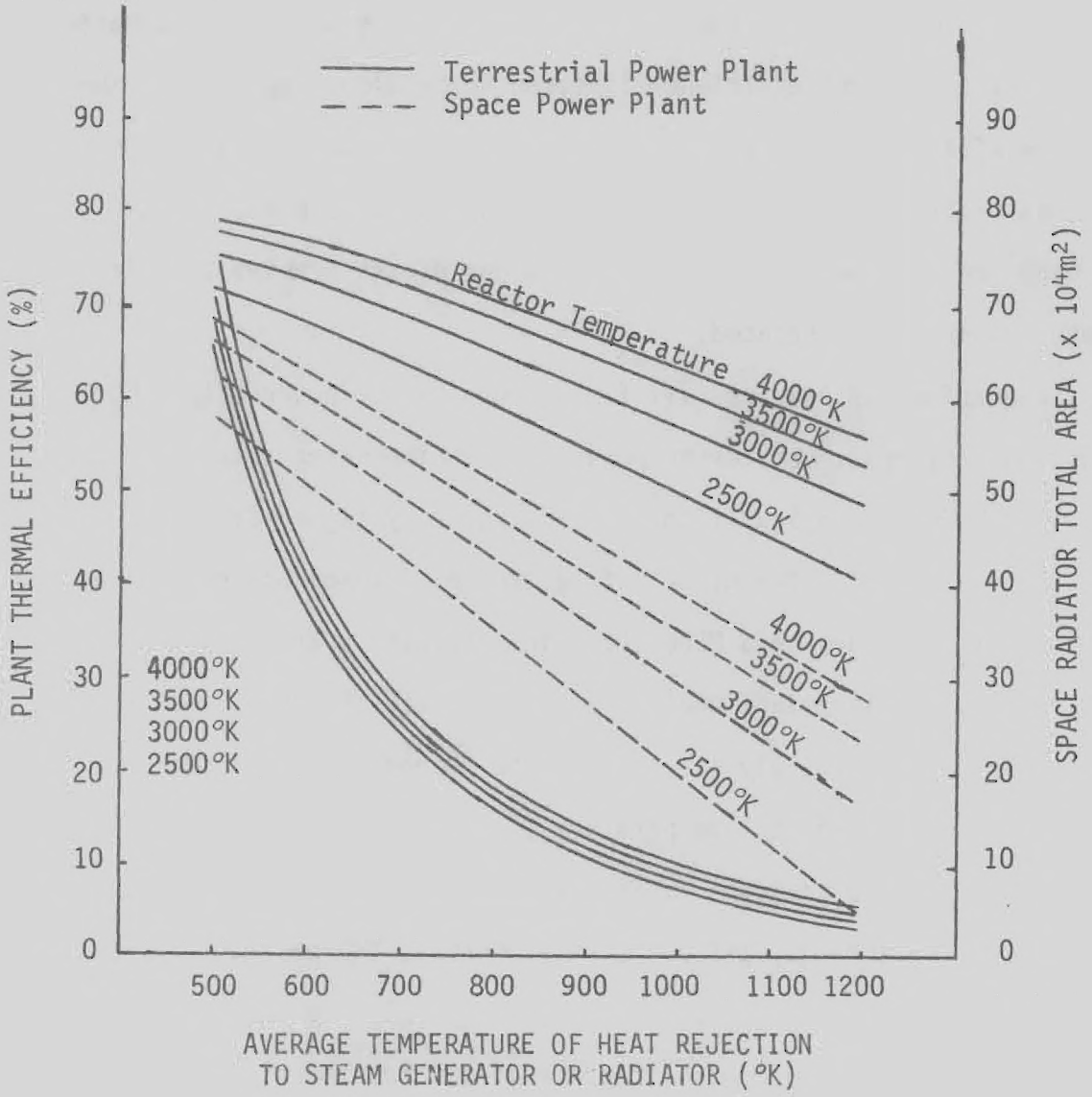

MODE II	H + 1% C_s (or equivalent)
Reactor Power	10,000 MWt
Reactor Pressure	200 Atm
MHD Loading Factor	0.8
MHD Expansion Ratio	15

Figure 27. MODE II Power Plant Efficiency and Space Radiator Area vs. Reactor Exit Temperature and Average Temperature of Heat Rejection from Radiator (Space) on to Steam Generator (Terrestrial).

The effect of MHD duct presure ratio on overall plant efficiency is illustrated by figure 28. The dependence on efficiency of an MHD-turbine cycle is insensitive to MHD pressure ratio for values greater than 5 since the MHD efficiency is taken to be almost as high as the turbine efficiency. However, larger MHD pressure ratios result in reduced recirculation of gas from the first stage compressor back through the turbine, so the size and weight of the turbine and first stage compressor is reduced.

The effect of reactor exit temperature on MHD power output, net plant power output, compressor power and turbine power output for a specific MODE II configuration is illustrated by figure 29.

Figure 30 shows the effect of reactor exit temperature and average radiator temperature on a MODE III plant efficiency and radiator area. For this particular plant configuration, the efficiency of the space power plant drops rapidly as the radiator temperature is increased. For a relatively low radiator temperature (750°K), plant efficiency is insensitive to MHD pressure ratio (figure 31). The effect of reactor temperature on the MODE III plant power output, MHD power, compressor power and flow rate are illustrated by figure 32. As expected, the major reason for the decrease in power output for the higher radiator temperature is the large increase in compressor power required. Increasing the reactor temperature decreases the compressor power requirement because of the corresponding decrease in mass flow rate.

The magnetic field strength is held constant over the length of the MHD duct. The duct length is calculated by considering the duct to

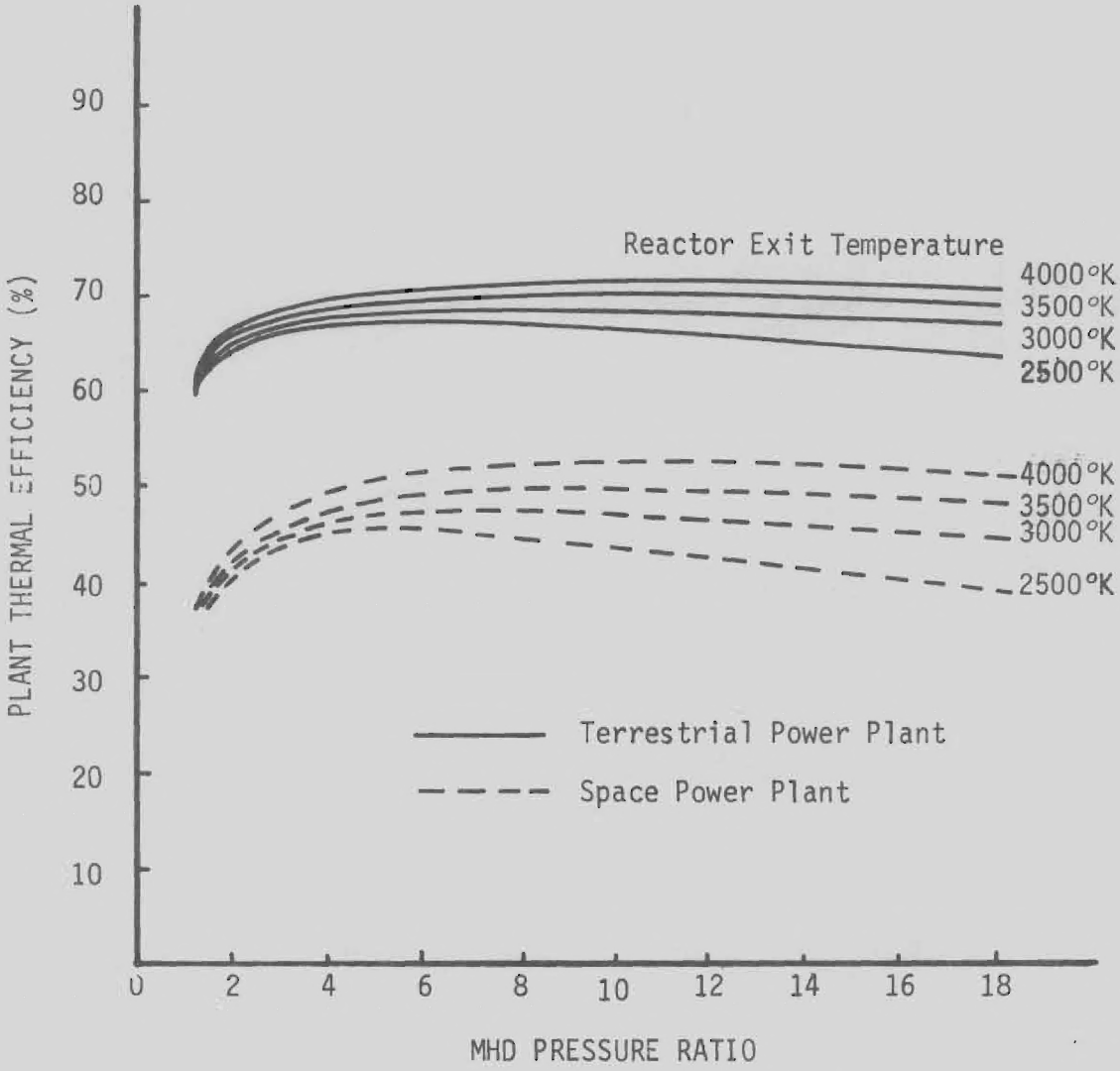

MODE II	Hydrogen
Reactor Power	10,000 MWt
Reactor Pressure	200 Atm
MHD Loading Factor	0.8
Av. Radiator Temp. (Space)	750°K

Figure 28. MODE II Plant Thermal Efficiency vs. MHD Pressure Ratio (Hydrogen).

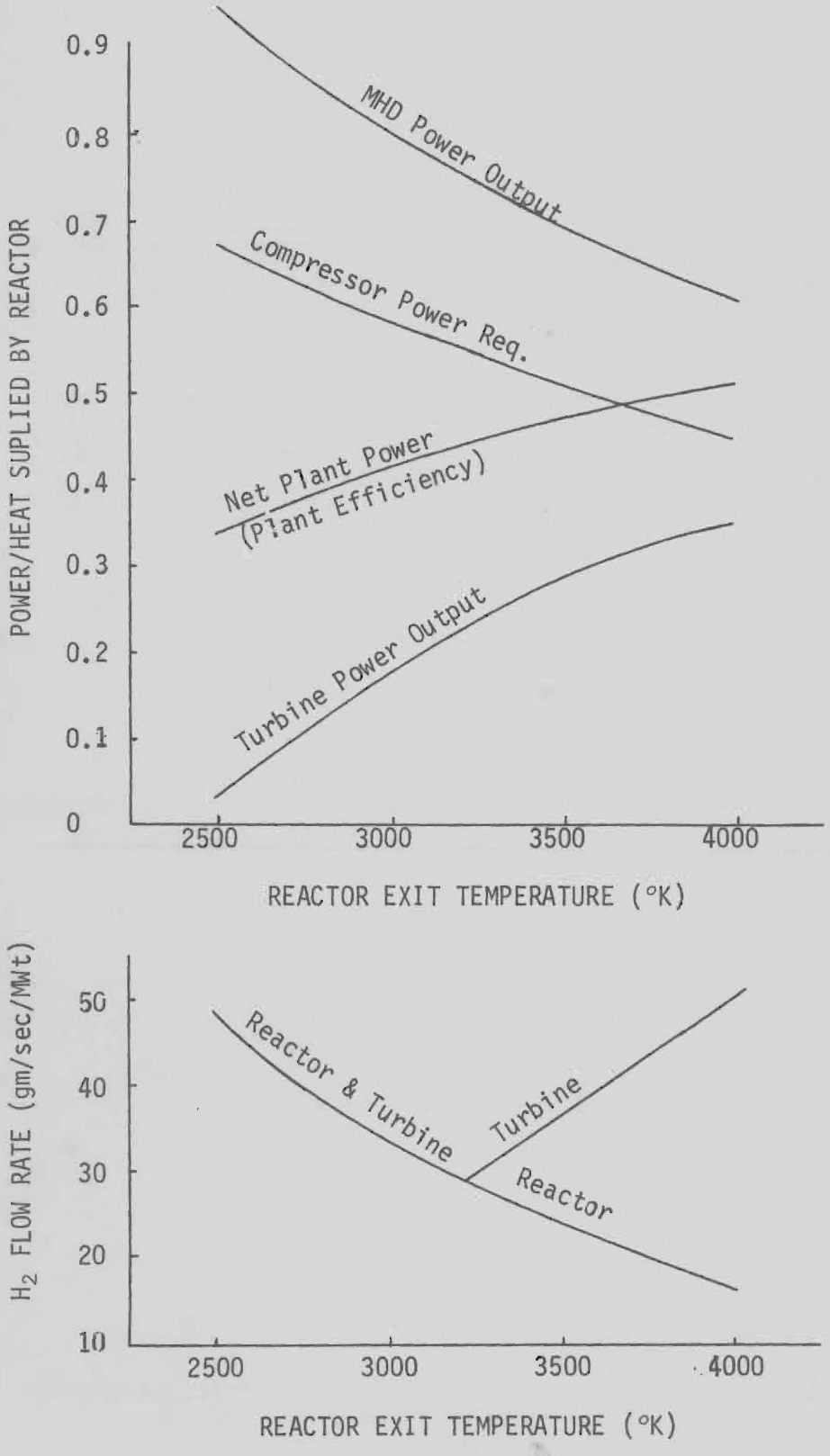

Figure 29. MHD, Turbine and Net Power Output, Compressor Power Required and H_2 Mass Flow Rate vs. Reactor Exit Temperature for 800°K Radiator Temperature, for a Specific MODE II Configuration.

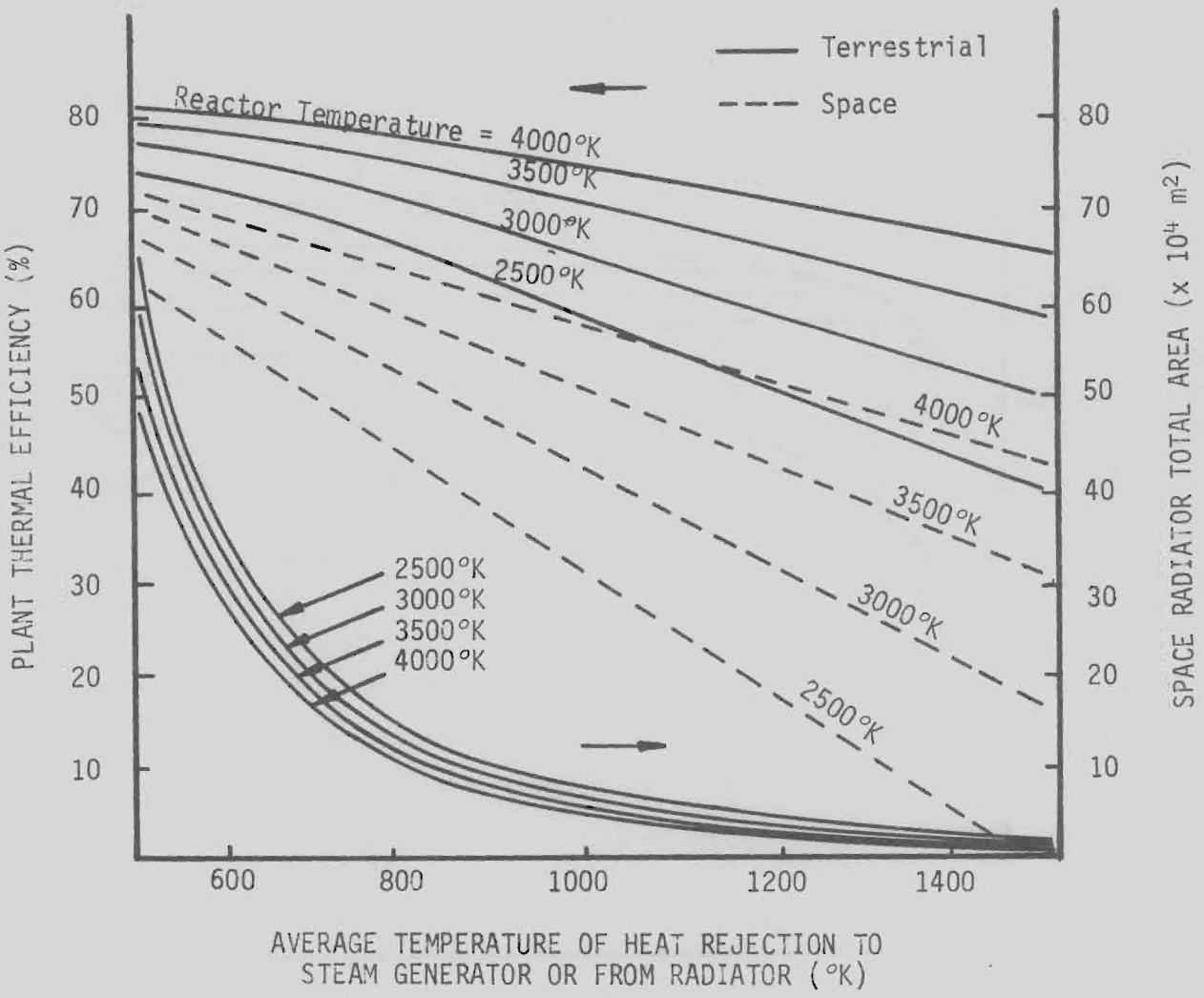

MODE III	H_2 + 1% C_s (or equivalent)
Reactor Power	10,000 MWt
Reactor Pressure	200 Atm
MHD Loading Factor	0.8
MHD Expansion Ratio	15

Figure 30. MODE III Power Plant Efficiency and Space Radiator Area vs. Reactor Exit Temperature and Average Temperature of Heat Rejection from Radiator (Space) on to Steam Generator (Terrestrial)

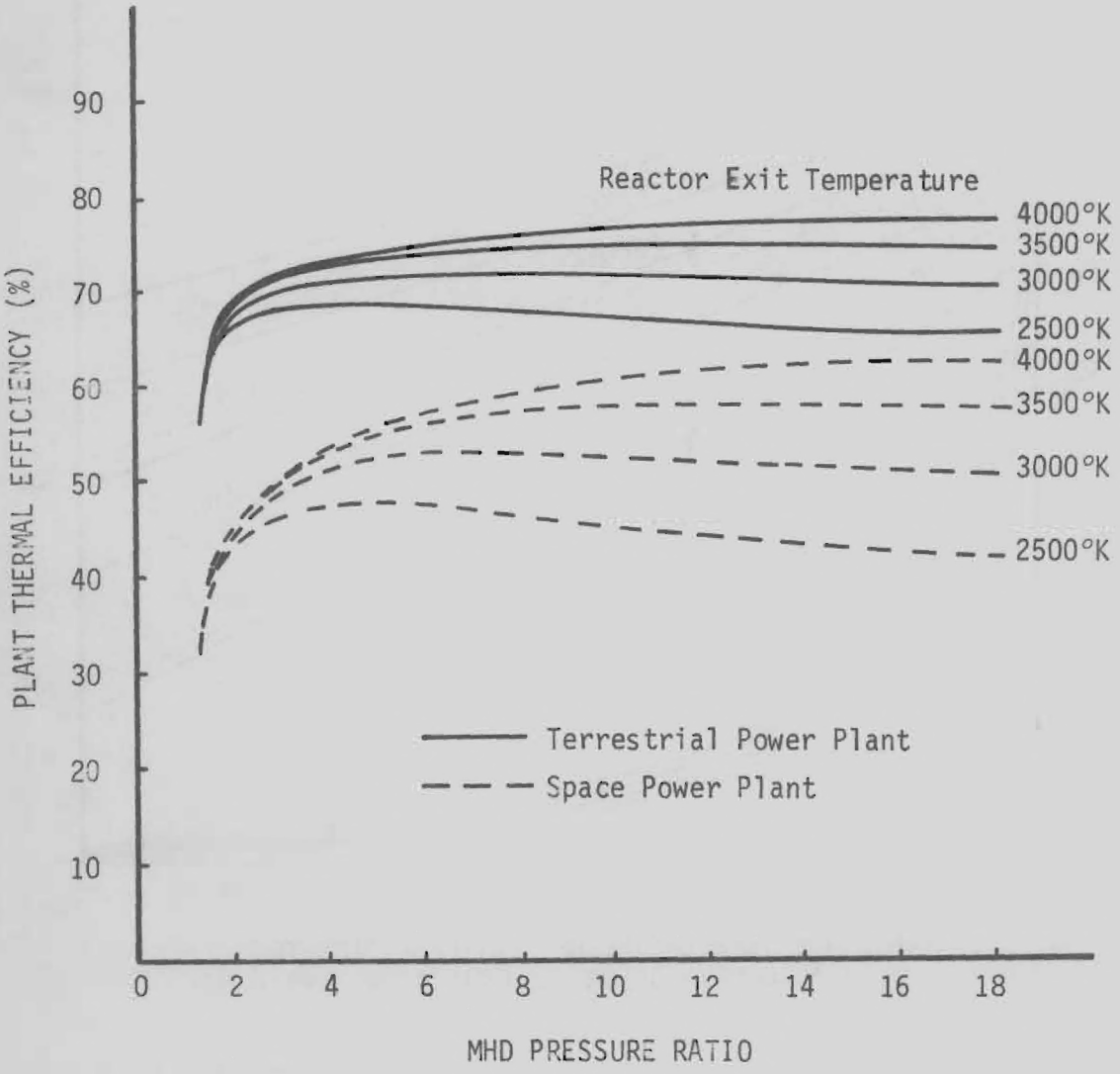

MODE III	Hydrogen
Reactor Power	10,000 MWt
Reactor Pressure	200 Atm
MHD Loading Factor	0.8
Av. Radiator Temp. (Space)	750°K

Figure 31. MODE III Plant Thermal Efficiency vs. MHD Pressure Ratio (Hydrogen)

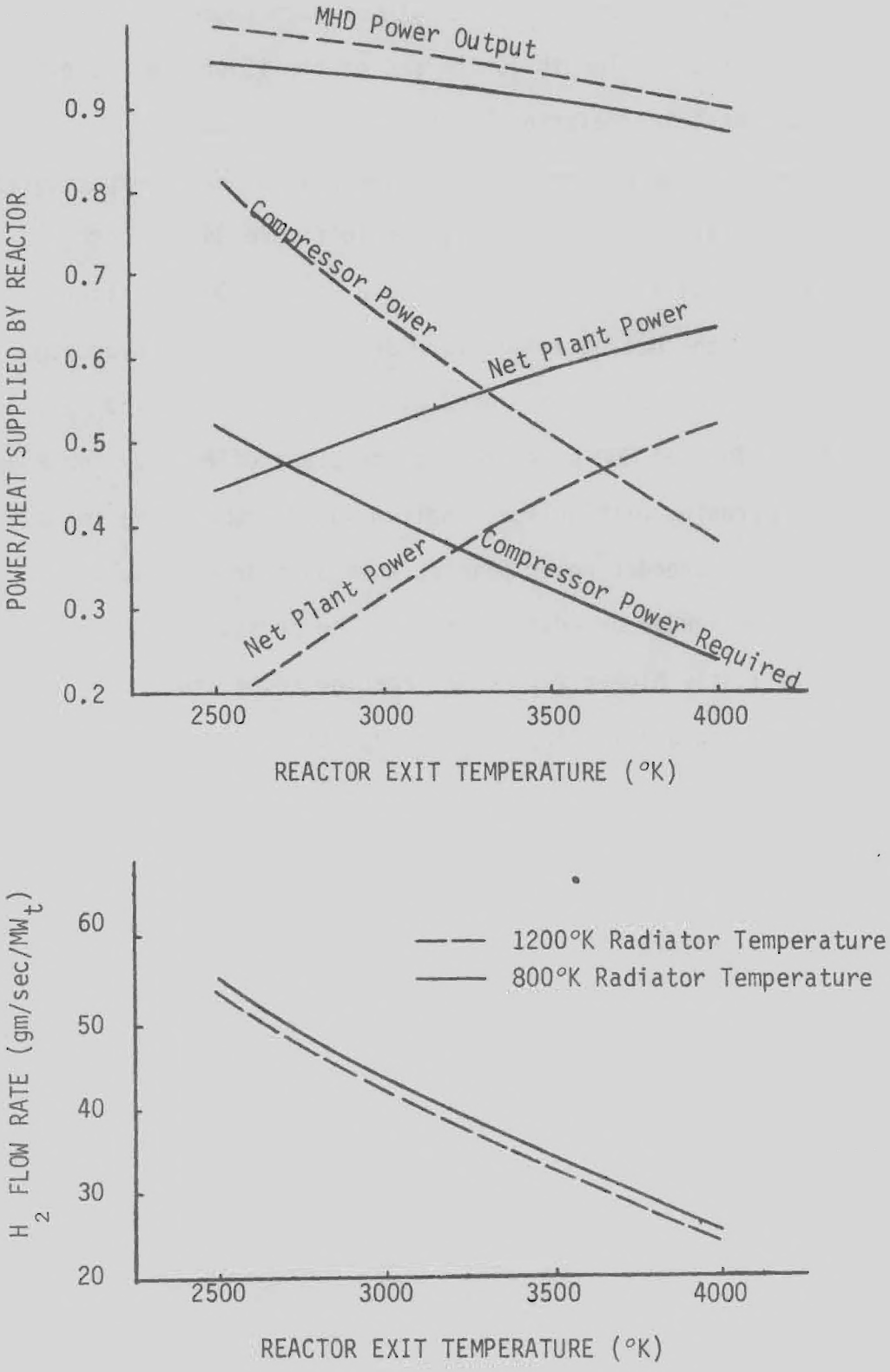

Figure 32. MHD and Net Power Output, Compressor Power Required and H_2 Mass Flow Rate vs. Reactor Exit Temperature for 1200°K and 800°K Radiator Temperatures, for a Specific MODE III Configuration.

be devided into 15 segments, each with a pressure ratio equal to the total raised to the 1/15 power. The length of each segment is calculated, and the total length is the sum of the 15 segment lengths. Figure 33 illustrates the relationship between length to exit diameter ratio and magnetic field strength for various reactor exit temperatures.

The MHD duct exit temperature is shown in figure 34 for both helium and hydrogen as a function of pressure ratio. Due to its higher value of γ, the helium temperature drops faster than hydrogen, so smaller MHD pressure ratios are used with helium. Figures 35-37 illustrate the effect of MHD pressure drop on plant efficiency for Modes I, II and III operating with helium. Helium would probably be the gas used in smaller non-breeder power plants, whereas hydrogen would most likely be used for larger breeder reactors. The pressure ratio for maximum efficiency is slightly higher for higher reactor temperatures. Figure 38 presents approximate relations between magnetic field strength and L/D ratio.

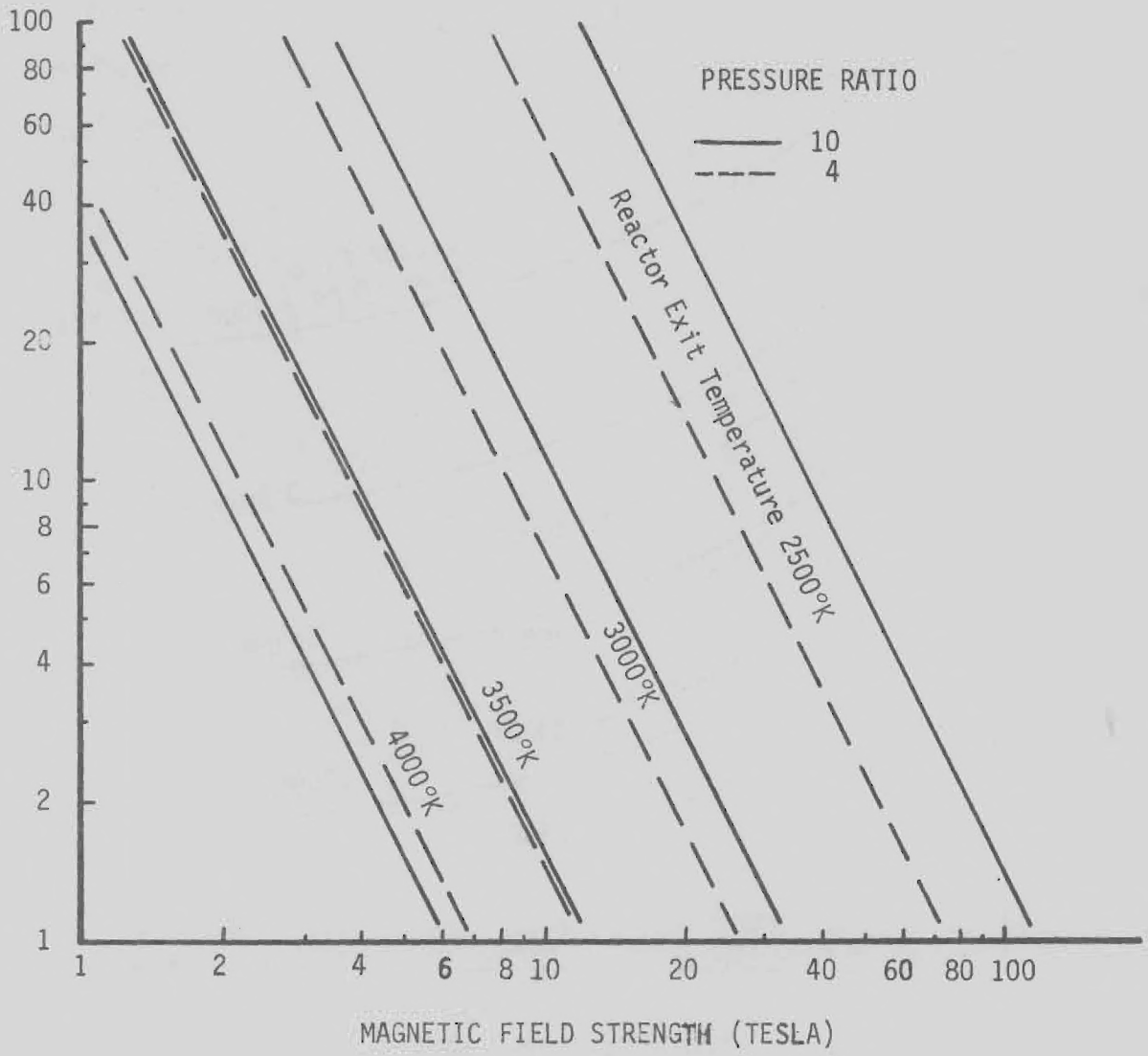

MODE III	Hydrogen
Reactor Power	10,000 MW$_t$
Reactor Pressure	200 Atm
MHD Loading Factor	0.8

Figure 33. MHD Duct L/D Ratio vs. Magnetic Field Strength for Hydrogen + 1% Cesium (or Equivalent) and 200°K Nonequillibrium Ionization.

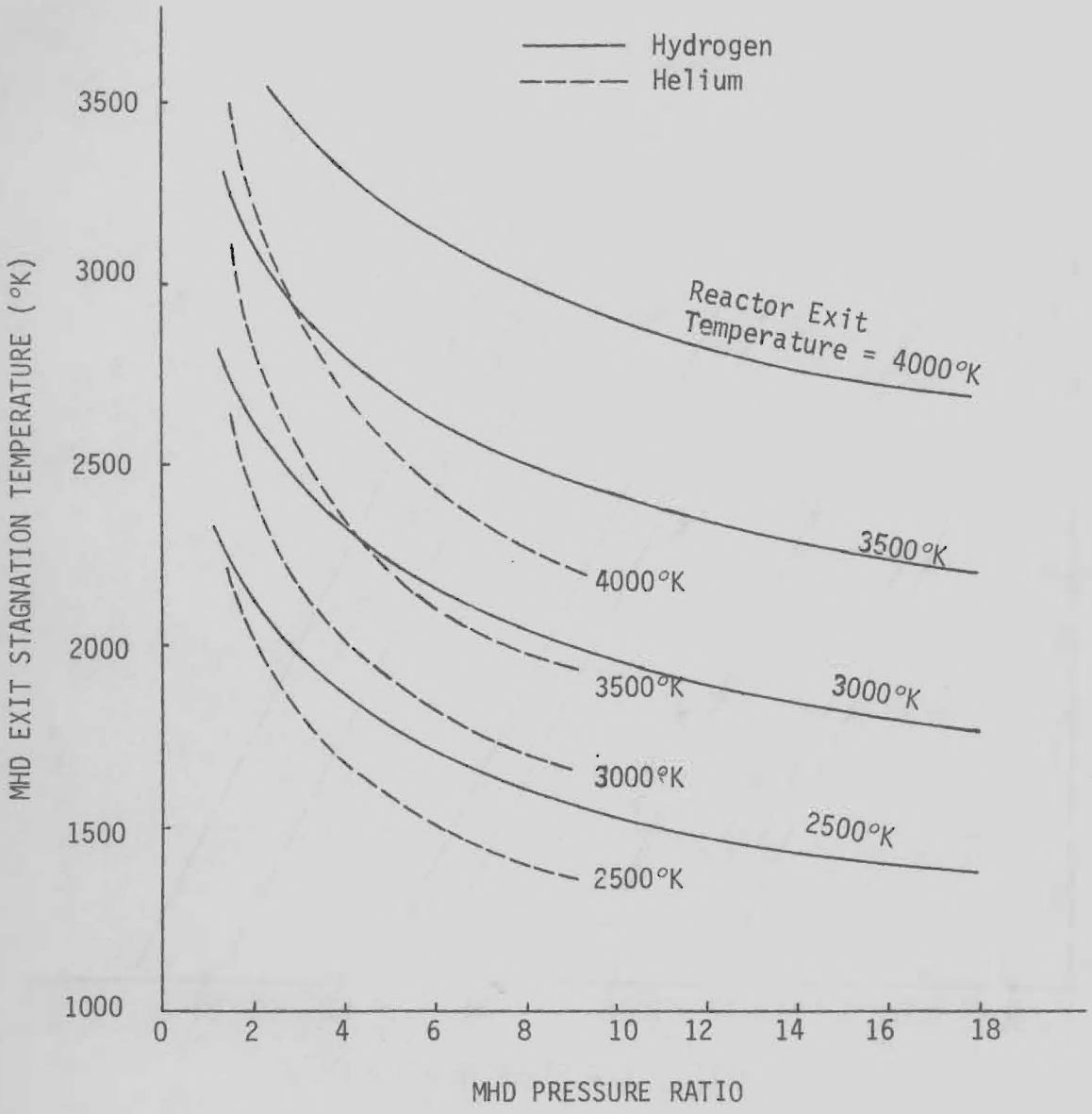

Figure 34. MHD Duct Exit Temperature vs. Pressure Ratio and Reactor Exit Temperature.

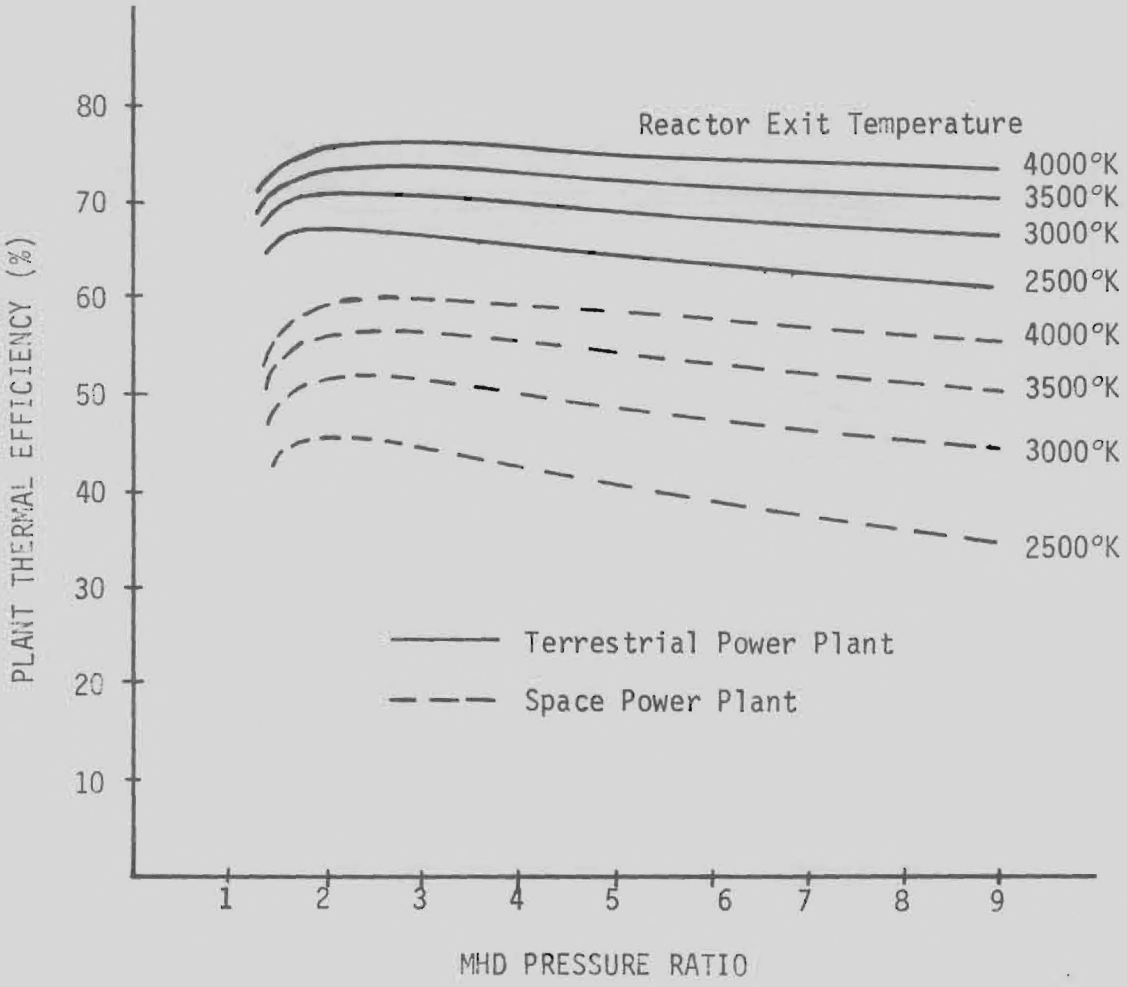

MODE I	Helium
Reactor Power	10,000 MWt
Reactor Pressure	50 Atm
MHD Loading Factor	0.8
Av. Radiator Temp. (Space Plant)	750°K

Figure 35. MODE I Plant Thermal Efficiency vs. MHD Pressure Ratio (Helium)

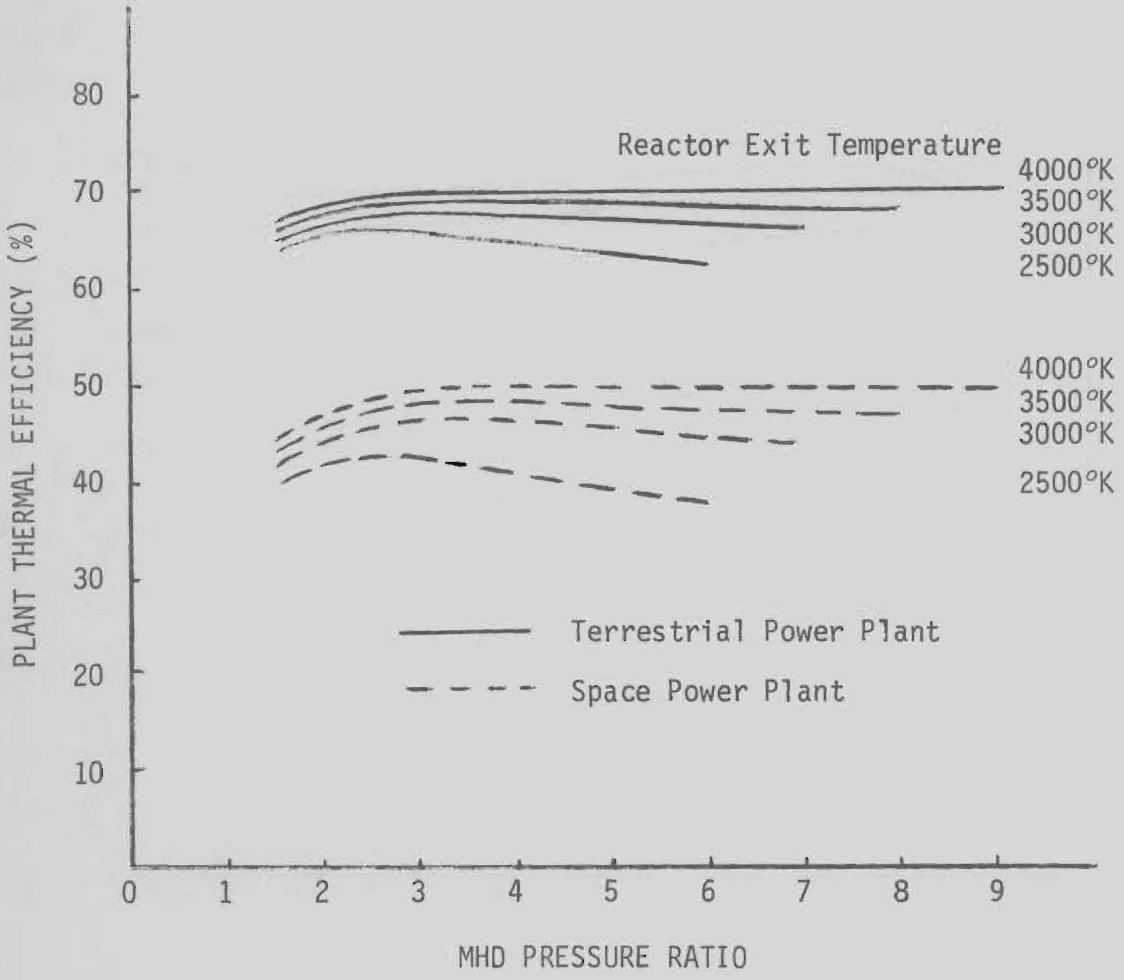

MODE II	Helium
Reactor Power	10,000 MWt
Reactor Pressure	50 Atm
MHD Loading Factor	0.8
Av. Radiator Temp. (Space)	750°K

Figure 36. MODE II Thermal Efficiency vs. MHD Pressure Ratio (Helium)

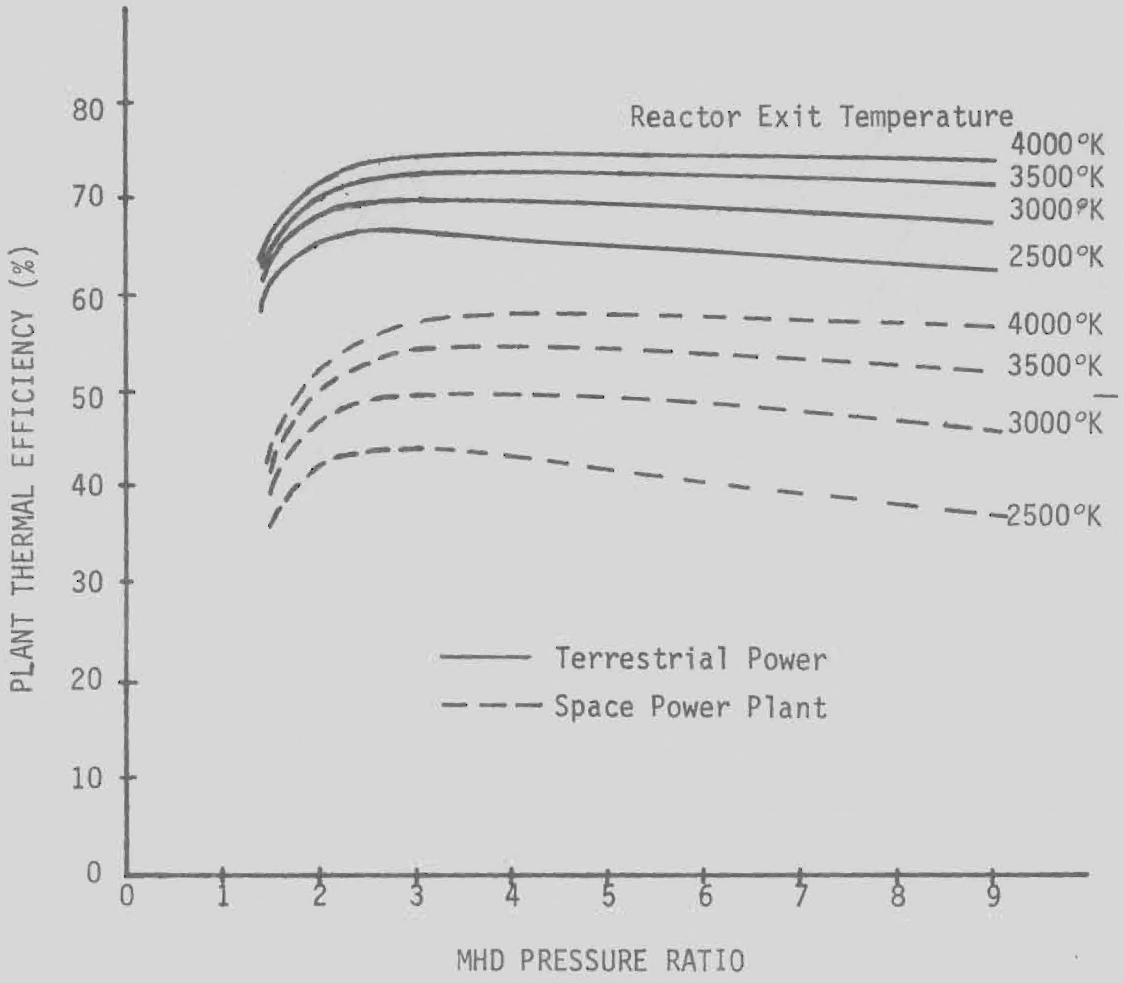

MODE III	Helium
Reactor Power	10,000 MWt
Reactor Pressure	50 Atm
MHD Loading Factor	0.8
Av. Radiator Temp. (Space Plant)	750°K

Figure 37. MODE III Plant Thermal Efficiency vs. MHD Pressure Ratio (Helium).

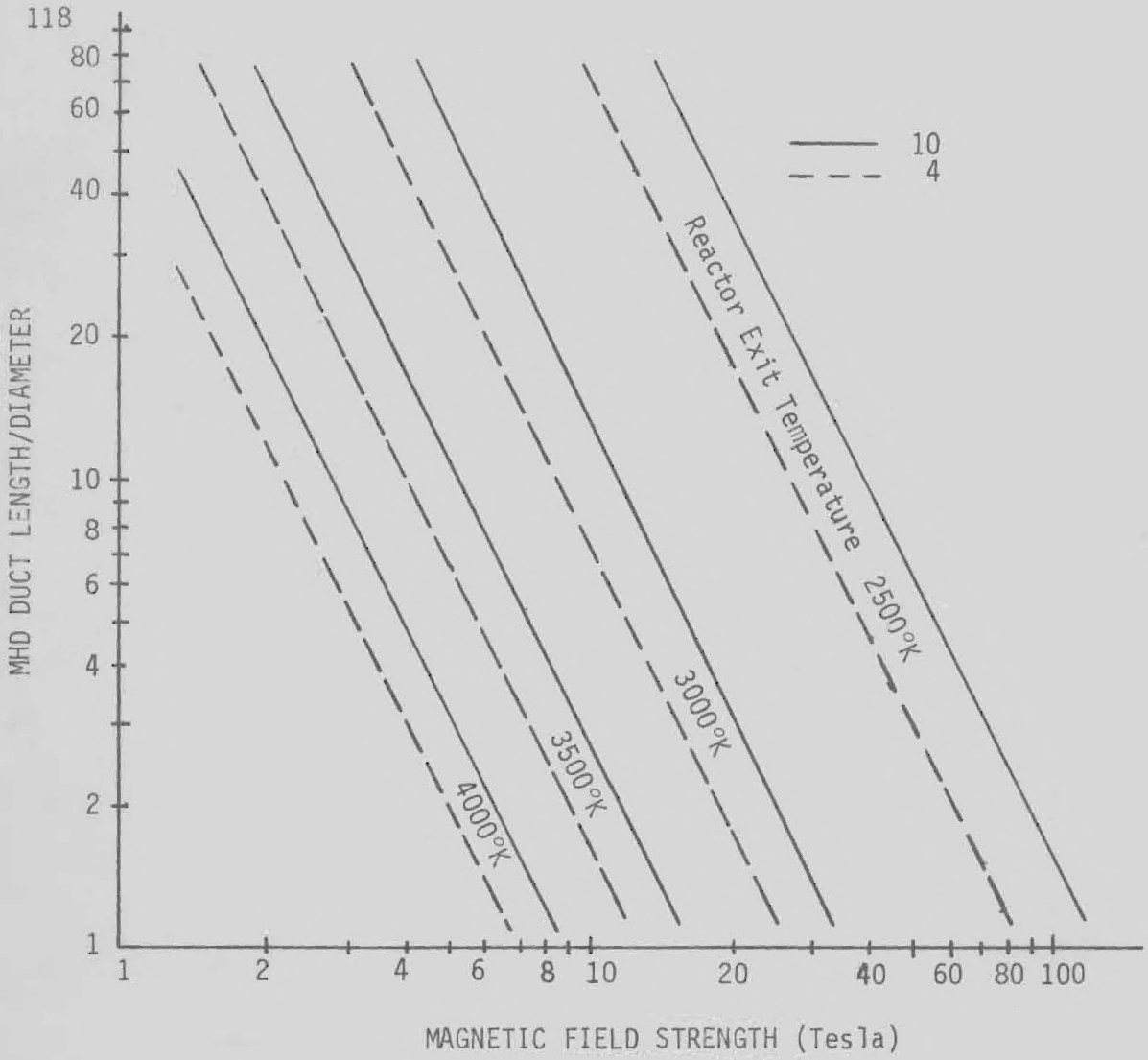

MODE III	Helium
Reactor Power	10,000 MWt
Reactor Pressure	50 Atm
MHD Loading Factor	0.8

Figure 38. MHD Duct L/D Ratio vs. Magnetic Field Strength for Helium + 0.45% Cesium (or equivalent) and 200°K Nonequillibrium Ionization.

COSTS AND APPLICATIONS

J. R. Williams

SPACE APPLICATIONS

The nuclear-MHD power plant system which has been described may have a number of applications in space. Such plants using compact non-breeder reactors could produce power in the multimegawatt range for a variety of missions. Figure 39 illustrates a MODE I plant in use for electric propulsion. Figure 40 shows a MODE II plant in space.

An artist's concept of MODE III Satellite Nuclear Power Station (SNPS) is illustrated by figure 41. Figure 42 depicts this power plant in synchronous orbit with microwave transmission to a receiving antenna on earth. Studies at Reytheon[22] and the Grumman Aerospace Corporation[23] have shown that safe microwave transmission of electric power from synchronous orbit is feasible with efficiencies of 70 to 80%. These studies have been performed in connection with a Satellite Solar Power Station (SSPS) study currently underway. The SNPS would have the advantage of SSPS in providing power without pollution. Since the SNPS would appear to be the major application for large breeder reactor-MHD power plants, this possible space application is discussed further.

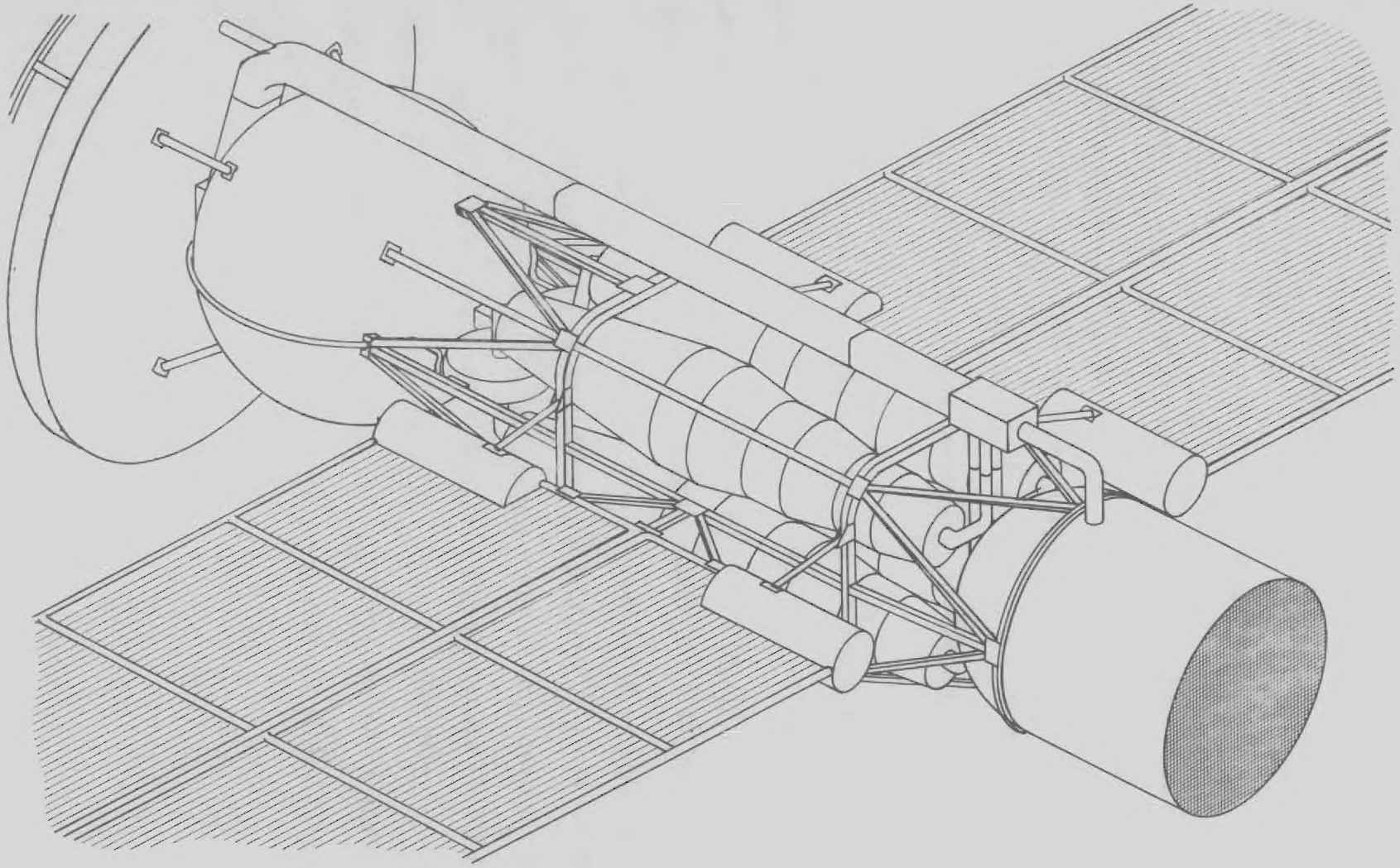

Figure 39. MODE I Power Plant for Electric Propulsion.

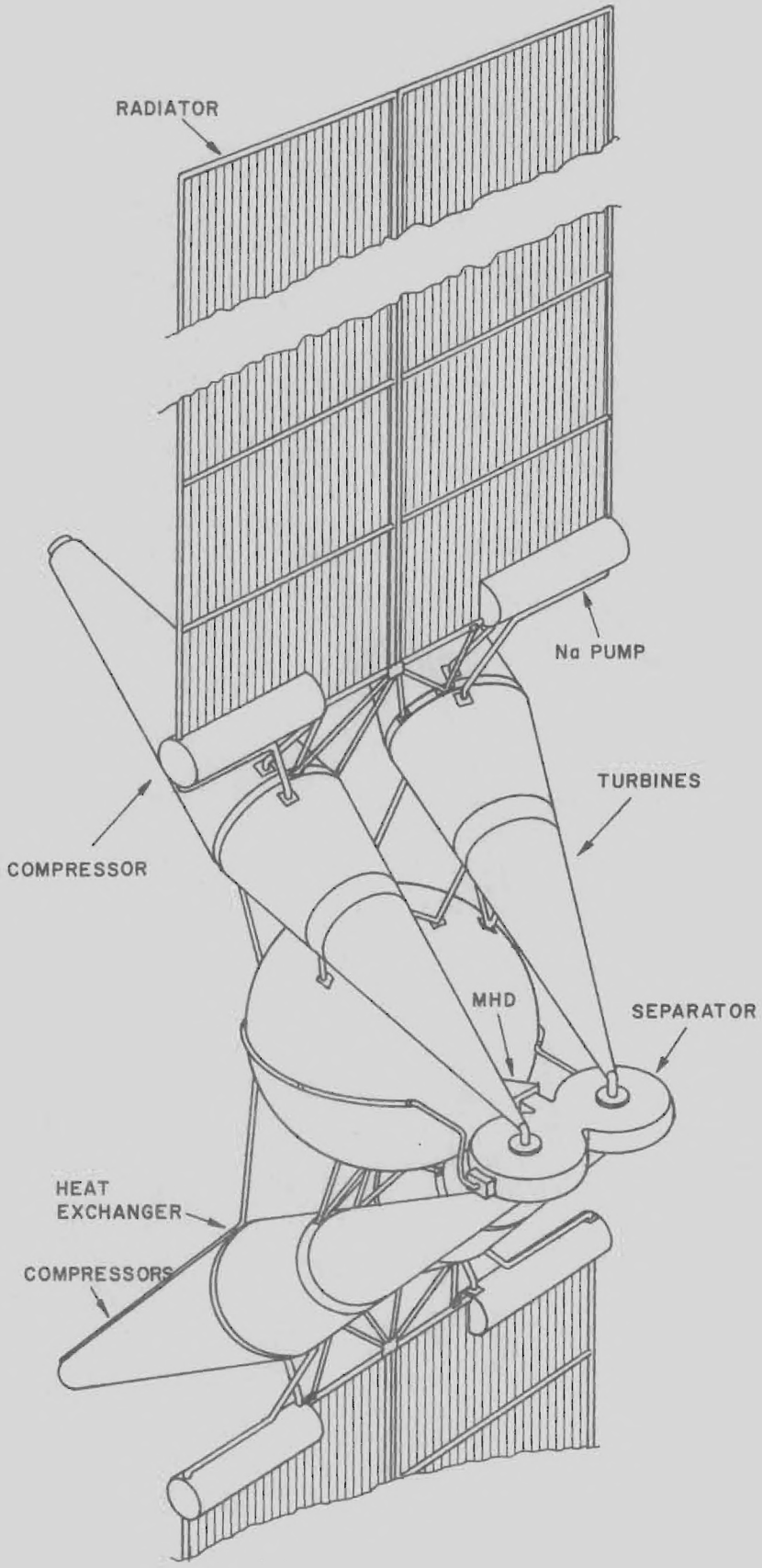

Figure 40. MODE II Space Power Plant.

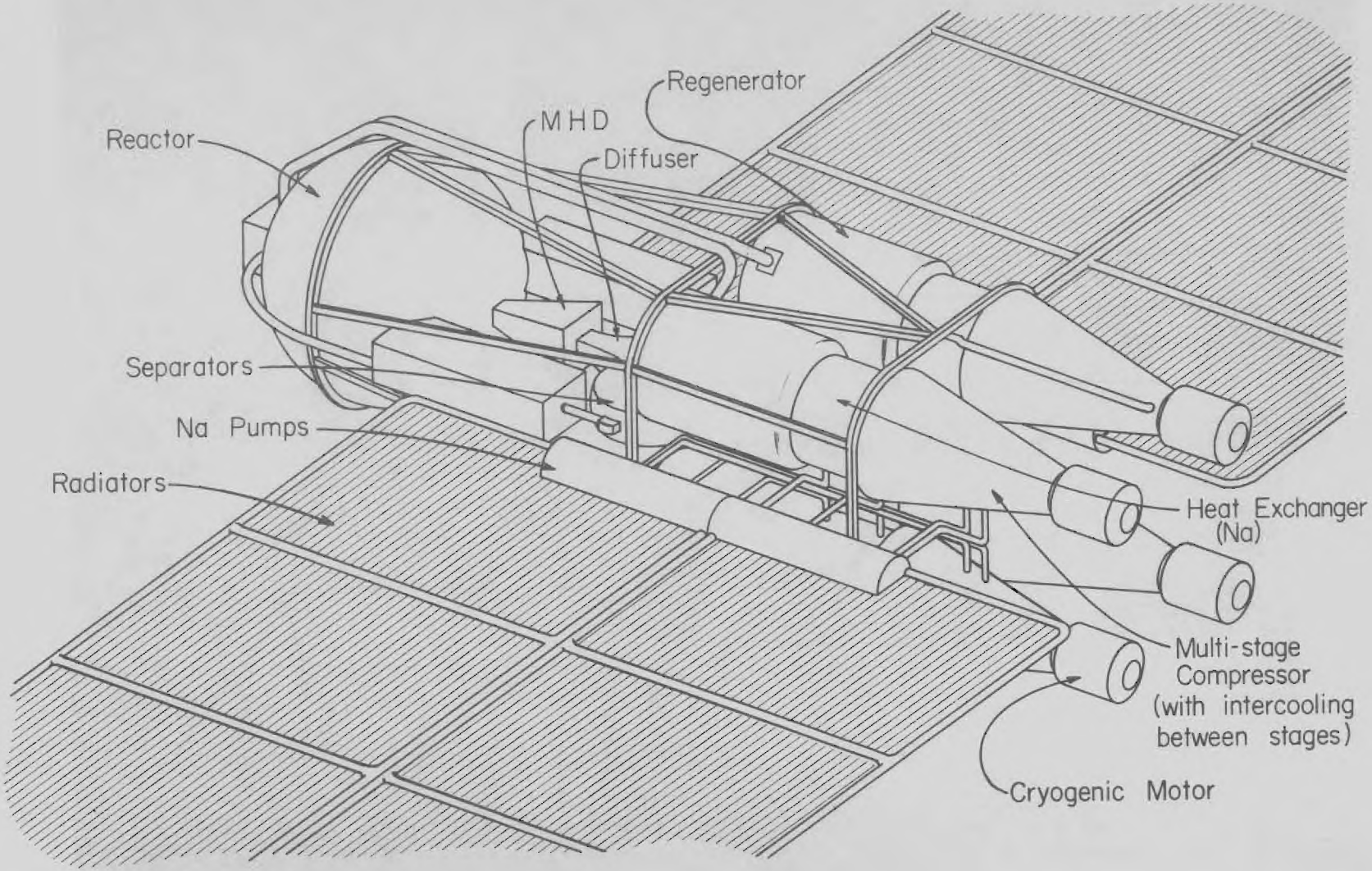

Figure 41. Mode III SNPS Power Plant

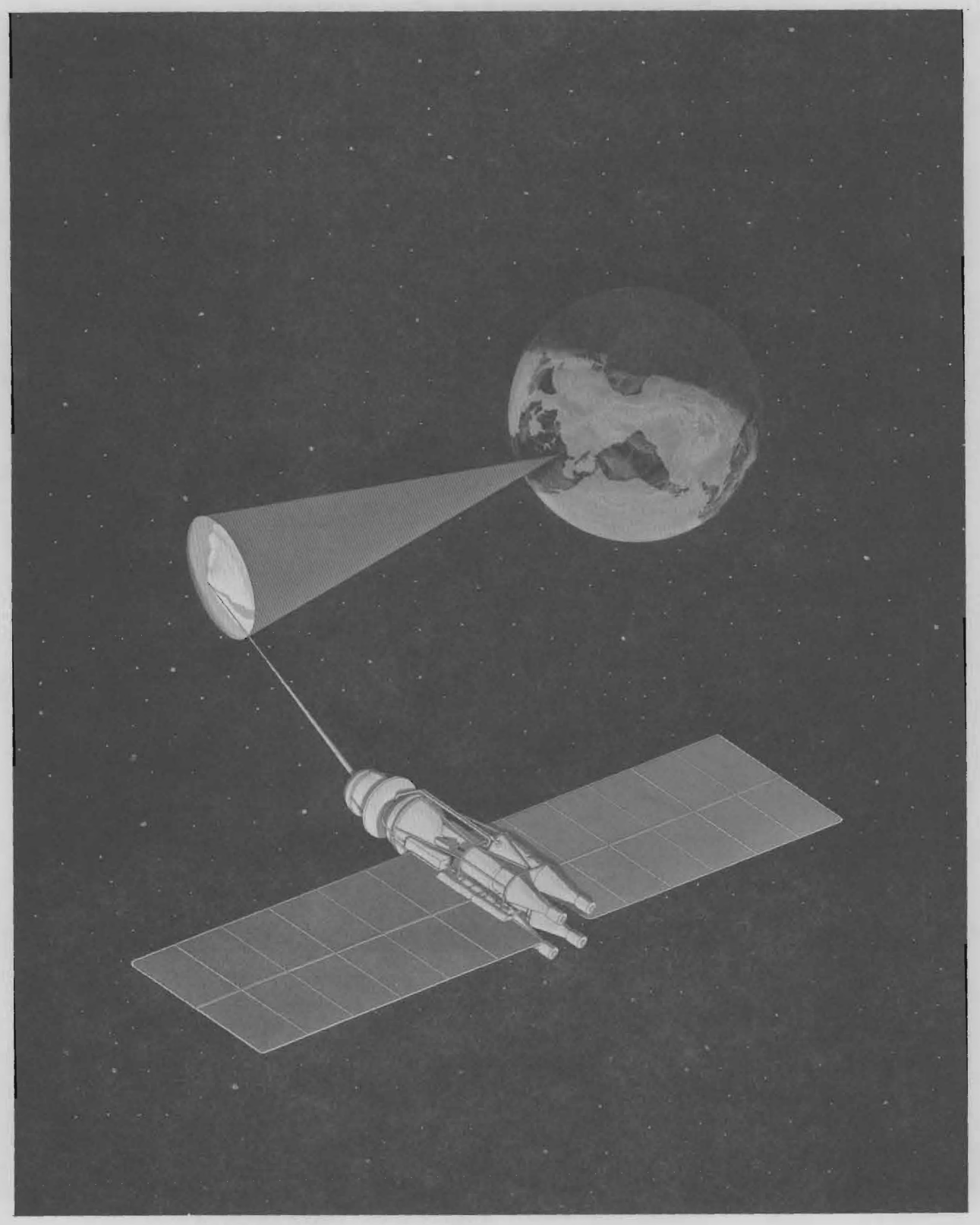

Figure 42. Satellite Nuclear Power Station in Synchronous Orbit.

THE SATELLITE NUCLEAR POWER STATION

Power Transmission to Earth

A detailed study of the microwave transmission of power from an orbiting power station to earth has recently been reported by the Grumman Aerospace Corporation[35] and Raytheon[22]. The Grumman-Raytheon study considered a system which would transmit 13,000 MW from synchronous orbit to provide 10,000 MW of electrical power from the receiving antenna on the ground. The transmitting antenna is proposed to be 1 km in diameter, and converts high voltage d.c. electric power into a 3,000 MHz microwave beam with an efficiency of about 90%. Heat produced by dissipative power losses in the antenna is radiated to space by cooling fins. Atmospheric attenuation of the beam would vary from less than 2% on a clear day to about 7% under worst weather conditions.

This beam would be intercepted at the ground by a rectifying antenna, called a rectenna. Schottky barrier diodes uniformly distributed throughout the antenna structure provide rectification so that the output from the antenna is high voltage direct current. On the basis of experiments performed to date, the projected conversion efficiency of the receiving antenna would lie in the range of 85 to 90%. Thus, depending on weather conditions and the rectenna efficiency, the overall transmission efficiency could vary from 70% to 80%. The diameter proposed for the receiving antenna to intercept 90% of the power in the beam is 6.8 km (4.3 miles) if the rectenna is located at the equator.

At higher latitudes the rectenna could be ellipsoidal with a minor axis of 6.9 km and a major axis of $6.9/\cos\theta$ km where θ is the latitude in degrees. For example, at a latitude of 40 degrees, the major axis of the elliptical rectenna would be 9 km.

The power density of the microwave beam arriving at the rectenna has a gaussian profile, dropping from a maximum intensity of 81 mW/cm^2 at the center to 8.1 mW/cm^2 at the edge. At a distance of twice the antenna radius the power density is 0.009 mW/cm^2, and at three times the radius the intensity is 8×10^{-8} mW/m^2. The radiation protection guide for humans, as set in 1966 by the American National Standards Institute (USAIC95.1-1966) is 10 mW/cm^2 for continuous exposure, and this standard also applies in western Europe. The limits are higher for short term exposure. Studies have shown[35] that occupants of aircraft which might accidently fly through the beam would not be harmed.

An exclusion area surrounding the rectenna could prevent humans or animals from receiving any significant exposure. Also, since the microwave intensity reaching the ground around and beneath the antenna is tolorable, this area could be farmed productively. Although the rectenna absorbs 99% of the microwave energy striking it, it stops very little sunlight, so the land beneath the antenna can be used for the production of food. The heat release due to beam attenation in the atmosphere, antenna losses, and microwave heating of the land around and beneath the antenna is about 10% of the thermal discharge from today's most efficient thermal power plants.

Weight Estimates

Ragsdale[36,37] has estimated the weight of a gaseous core reactor for rocket propulsion, and for a 22,000 MWt reactor with a 3 meter cavity diameter and a 76 cm moderator-reflecter, he arrived at a moderator weight of 120,000 lbs. and a pressure ressel weight of 140,000 lbs., based on a reactor pressure of 1000 Atm., which is an upper limit of pressures which might be encountered in gas core power reactors. Weight estimates for the hydrogen turbopump range from a low of 5000 lbs. to a high of 24,000 lbs. Nuclear calculations for the gaseous core breeder reactor, given earlier in this report, resulted in a moderator weight of 168,000 pounds and a weight of thorium fertile material of 288,000 pounds. The weights of hydrogen and fissle uranium are almost negligible by comparison: 466 pounds for the hydrogen and 1086 pounds for the uranium. If the total hydrogen and uranium weight in the plant is four times that in the reactor core (two times would probably be more realistic), then the total uranium weight would be about 4000 pounds and the total hydrogen weight about 2000 pounds. Thus, an upper limit on the reactor weight can be arrived at:

Moderator	170,000 lbs	(77,000 Kg)
Pressure Vessel	140,000 lbs	(64,000 Kg)
Thorium	288,000 lbs	(130,000 Kg)
Uranium	4,000 lbs	(-2,000 Kg)
Hydrogen	2,000 lbs	(-1,000 Kg)
Other Components	75,000 lbs	(34,000 Kg)
TOTAL WEIGHT	679,000 lbs	(308,000 Kg)

If the SNPS power plant is to produce 13,000 MW of electrical power at an efficiency of 50%, the reactor must have a thermal power output of 26,000 MWt. The weight of a nuclear reactor is not proportional to power output; the percentage increase in weight is much less than the percentage increase in power output. However, adapting the conservative position that the weight is proportional to power output, the projected weight of the 26,000 MWt reactor would be 800,000 lbs. (363,000 Kg).

As a comparison, the 1100 MWt NERVA XE-Prime Engine weighs 40,000 lbs.[38] (18,000 Kg). Based on this power to weight ratio at a power of 1100 MWt, any reasonable extrapolation of NERVA technology to 26,000 MWt will yield a reactor weight of less than 800,000 pounds, even when allowance is made for breeding. Westinghouse[39] conducted an engineering study of the colloid core reactor and arrived at a weight of 41,000 lbs. (19,000 Kg) for a 2000 MWt reactor. No attempt was made to optimize the weight of the reactor. Thus, this reactor with twice the power level would have the same weight as the NERVA. A linear projection, using this power to weight ratio, to 26,000 MWt would yield a total reactor weight of 533,000 lbs. (242,000 Kg). This is a very conservative estimate, even when allowance is made for breeding.

Thus it is seen that, regardless of the type of reactor used (solid core, colloid core or gas core), a conservative estimate of the total reactor weight is 800,000 lbs. (363,000 Kg)

Most of the weight of the MHD generator is the weight of the superconducting magnet. Rosa[15] has developed techniques for projecting superconducting magnet weights for MHD generators of up to 10,000 MWe output. For a field strength of 10 Tesla and a flow velocity of 1000 m/sec, the magnet weight would be 11,000 lbs. (5000 Kg) for an average electrical conductivity of 100 mho/m, which is typical for the SNPS system, or 25,000 lbs. (11000 Kg) for a 20 mho/m average conductiviy. Stekly[40], et al, have projected the specific weight of a magnet for a 100 MWe generator to be 106 Kg/MW, which is about a factor of four higher than predicted by Rosa's correlations. If Rosa's correlations are indeed low by a factor of four, then the magnet for a 13,000 MWt SNPS would weigh about 100,000 lbs. Since most of the MHD generator weight is associated with the magnet, the total weight of the MHD energy conversion system would be less than 200,000 lbs. Thus, 200,000 lbs. is taken to be a conservative estimate of the MHD generator.

Projections of turbine-compressor weights to thousand megawatt power levels are difficult to make since large turbines have only been built for terrestrial power generation and weight minimization was not a major factor. Based on the mass flow rate, temperature, pressure and velocity of the hydrogen passing through the turbines, the turbine volume is calculated to be about 100m^3. Similarly, the

compressor volume is about 100 m^3, and the heat exchangers total about 200 m^3. Using an average material density within the turbine compressor and heat exchanger, of 0.1 gm/cm^3, the total weight of each turbine-compressor-heat exchanger unit would be 88,000 lbs. (40,000 Kg). There are four such units with a total weight of 352,000 lbs. (160,000 Kg). Thus, including structure and piping, the total weight of the turbine-heat-exchanger-compressor system is taken to be 400,000 lbs. (180,000 Kg).

Ragsdale[36] made use of a study by Haller[41] to arrive at a specific radiator weight of 140 Kg/MW for a large size radiator operating at 1100°K. The use of advanced heat-pipe radiators should reduce this specific weight considerably, but using the values of 140 Kg/MW, the weight of the radiator required to reject 13,000 MW of heat is 1,820,000 Kg, or 4,000,000 lbs.

Other system components include the uranium and thorium reprocessing system, the radiactive waste storage and ejection system, electric motors (MODE III), various pumps, the control system, and a shield to protect delicate electronic components from nuclear radiation damage.

Based on the weight of the NERVA shield, Ragsdale[35] determined that a disk shadow shield for a 22,000 MWt gas core reactor would range from 180 to 225 gms/cm^2. Taking the weight to be 225 gm/cm^2, the total weight of a 10 m diameter disk shadow shield for the SNPS reactor would be 177,000 Kg (390,000 lbs.). With supporting structure, this becomes 400,000 lbs. (182,000 Kg). The total weight of the fuel and thorium reprocessing system is difficult to project, and

any comparison with today's reprocessing plants is unwarrented, since in the case of the colloid and gas core reactor there are no fuel elements to fabricate and disassemble. It is believed that such a facility for the SNPS would probably have a total weight in the range of 1,000,000 to 2,000,000 pounds. The value of 2,000,000 pounds for the reprocessing system is used in estimating the total system weight. Similarly, a value of one million pounds is assumed for the waste deposal system, and the total weight of all other plant components including pumps, the control system, and electronics, but not including the microwave system, is taken to be 1,200,000 lbs.

Based on these estimates, the weights of the SNPS components and total power plant weight are detailed below:

SNPS 13,000 MW_e WEIGHT ESTIMATES

	x 10^3 pounds	x 10^3 Kg
Nuclear Reactor	800	363
MHD Systems	200	91
Turbine-Compressor-Heat Exc.	400	182
Radiator	4000	1820
Shield	400	182
Reprocessing System	2000	910
Waste Disposal	1000	450
Other	1200	545
TOTAL POWER PLANT	10,000	4,535
Microwave Antenna	9000	4082
Additional Thorium*	1000	453
TOTAL SYSTEM WEIGHT	20,000	9,070

*Additional thorium is provided here to permit up to 40 years of reactor operation at 26,000 MWt.

Cost Factors

The major cost difference between the SNPS and similar types of terrestrial power plants is the fact that it must be assembled and operated in orbit. Grumman[35] did an extensive study of propulsion requirements for the SSPS and arrived at a "most likely" cost of $100/lb for transporting the system components to synchronous orbit. This cost was based on making use of a reusable space shuttle to deliver components to low earth orbit and an ion propulsion system for transportation from low earth orbit to synchronous orbit.

The Grumman study noted that a considerable savings in propulsion costs could be effected if the SSPS could be assembled in low earth orbit and then, when completed, boosted into synchronous orbit. However, it was considered impractical to assemble an SSPS in low earth orbit because of various factors relating to the size of the solar arrays and the effects of the Van-allen radiation on solar cells. These factors would not be important for an SNPS, so the SNPS would certainly be assembled in low earth orbit and then be transported to synchronous orbit after completion. This should reduce space transportation costs below the $100/lb projected for the solar power plant. Since the projected total weight for the SNPS power plant system, including microwave antenna, is 20 million pounds for a 10,000 MWe plant, even if the space transportation cost per pound is taken to be

$100, the increase in capital cost of the plant due to space transportation is $200/KWe.

The SSPS study[35] also arrived at a total cost of the microwave transmission system of $120 per KWe delivered to the ground, and a total cost of the receiving antenna and rectification system of $50 per KWe. These systems would be identical for the SNPS, so the costs should be the same.

The cost of the nuclear power plant is difficult to project, but should be comparible to present nuclear plants. Colloid core and gaseous core reactors require no fabrication of fuel elements. The simplified fuel cycle for these reactors offers the potential of considerable cost savings in this area. The high power level (about 25,000 MWt) of the proposed SNPS improves further the economics of on-site fuel reprocessing. On the other hand, the requirement for remote operation and maintenance will increase operating costs in comparison with similar terrestrial power plants. Thus, with the costs of conventional nuclear power plants running $300/KW, the projected cost of the SNPS nuclear power plant (exclusive of transportation) is taken to be $500/KW, or 5 billion dollars for a single SNPS power plant. For a system of this size, however, the final cost per plant may be considerably less than 5 billion, especially if a number of these plants are built. The total capital cost of the SNPS may be broken down as follows:

Nuclear-MHD Power Plant	$500/KWe
Microwave Transmission System	120/KWe
Power Receiving System	50/KWe
Space Transportation	200/KWe
TOTAL SNPS CAPITAL COST	$870/KWe

These data indicate that the capital cost of an SNPS may be well under $1000/KWe, assuming that a reusable space shuttle is available to place plant components in low earth orbit and an advanced nuclear-MHD power plant is developed. These cost projections do not include any research or development costs, such as shuttle development.

An important aspect of SNPS economics is that all societal costs are internalized to the power plant system. There are no "hidden" costs to society associated with pollution or depletion of non-renewable resources. Since the reactor would breed its own fuel from fertile thorium, plentiful supplies of fuel would be available for the next thousand years or more, which provides plenty of time for the development of more exotic energy sources, such as fusion with direct conversion.

THE SPACE RADIATOR

Assuming an emissivity of 0.9, the total area required for SNPS radiators was calculated. An SNPS producing 13,000 MW of electrical power at an overall thermal efficiency of 56% would reject about 10,000 MW of heat, as shown by the upper curve on figure 39. If the radiator, as shown in figures 6 and 7, has a length three times its width, then the width of the radiator base may be calculated as a function of radiator temperature. There are two such radiators used with the power plant. As seen in figure 40, the base of a 750°K radiator for a 13,000 MWe SNPS would measure 200 meters, and its length would be 600 meters. At 1000°K, these dimensions are cut almost in half.

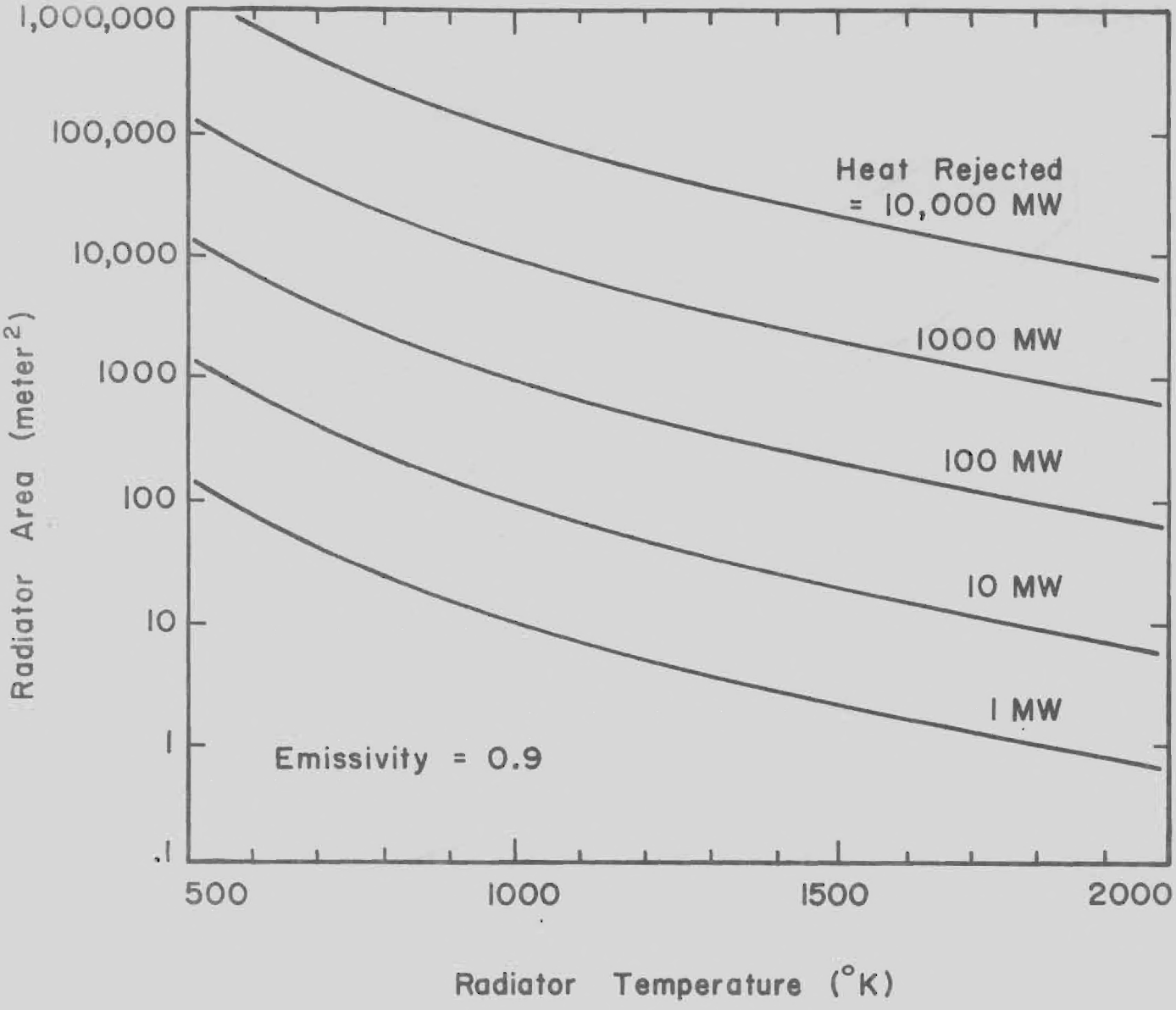

Figure 43. Radiator Area Required vs. Average Heat Rejection Temperature.

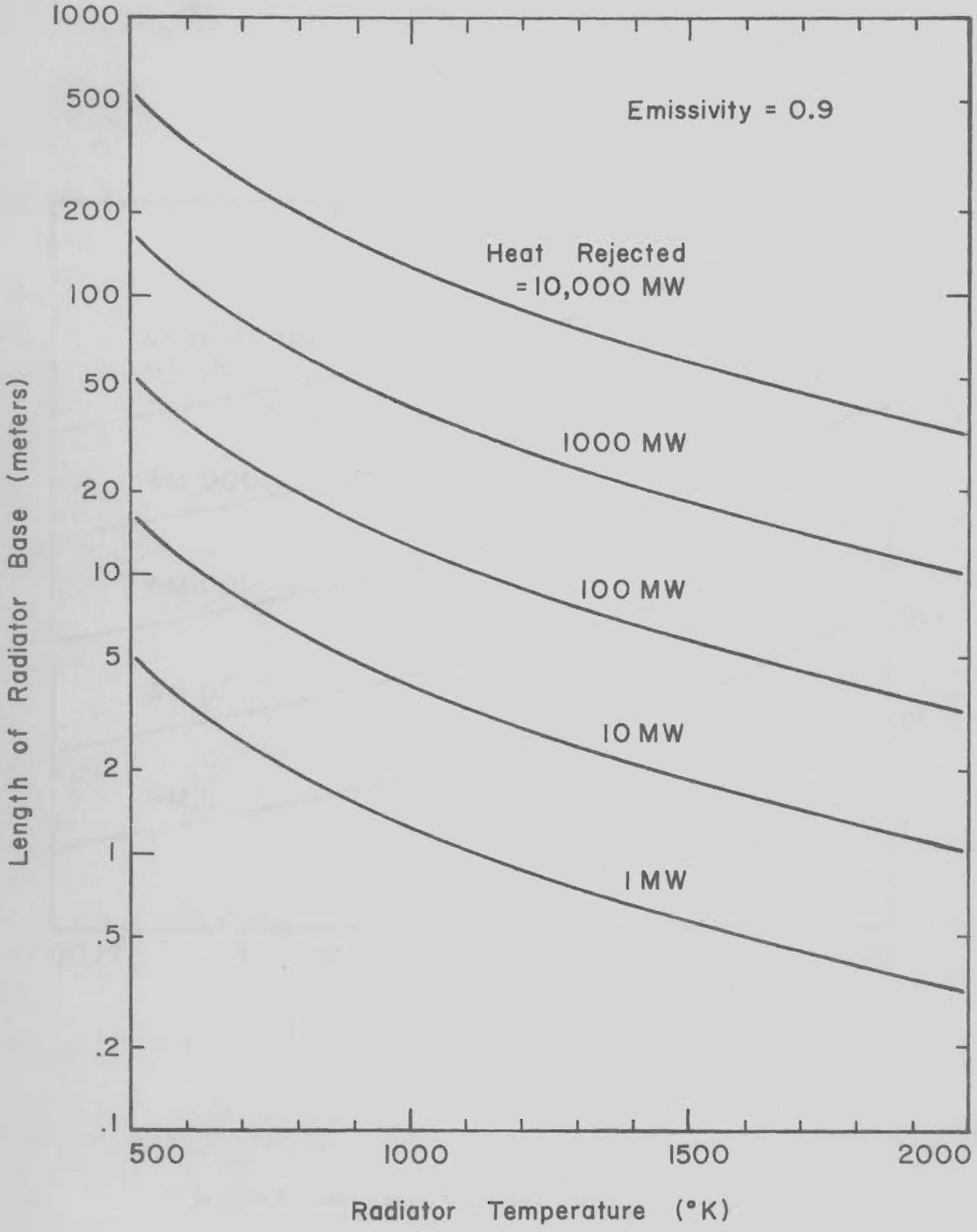

Figure 44. Width of Radiator Base vs. Average Temperature (Length of Radiator = 3 x Width, 2 Radiators used).

HEAT TRANSFER IN GAS CORE POWER REACTORS

James H. Rust and Rogers Farr

GLOSSARY

e_g	Gas emissive power
K	Absorption coefficient (m^{-1})
q	Heat flux (watts/m^2)
q_e	Edge heat flux (watts/m^2)
q_R	Radiated heat flux (watts/m^2)
Q	Volumetric heat generation rate (watts/m^3)
Q_i	Coefficients in polynomial expression of Q
r	Radial distance inside U-H_2 gaseous core (m)
r_o	Cavity radius (m)
r_e	Core radius (m)
r'	Dimensionless radius, r/r_e
T	Temperature (°R)
T_e	Edge temperature (°R)
T_b	Brightness temperature (°R)
T_w	Containment wall temperature (°R)
ε_w	Containment wall emissivity
σ	Stefan-Boltzmann constant (watts/m^2 - $°R^4$)
τ	Optical thickness

HEAT TRANSFER IN GAS CORE POWER REACTORS

Practically all of the work up to the present time dealing with heat transfer in gaseous core reactors has been concerned with the type of reactor considered for rocket propulsion in which the fuel region was pure uranium. In breeder power reactors the fuel region would probably contain only a small percent uranium mixed in hydrogen gas, so the heat transfer problems are different. For this reason, a study was undertaken to evaluate the temperature profile in a spherical gaseous core power reactor.

The simplest case to evaluate, illustrated in figure 45, is a reactor in which the stagnent uranium-hydrogen gaseous core is perfectly contained, that is, there is no mixing with the surrounding hydrogen flow. This would be the case for infinite separation ratio, which is the ratio of the mass flow rate of hydrogen to mass flow rate of uranium. In reality, there would be mixing; in fact there may be a great deal of mixing. Thus, the following analysis is for a limiting case which would probably not be approached in a power reactor. The more realistic case of strong mixing between the two regions would be much more difficult to solve.

This study concerns the determination of steady-state temperature profiles as a function of radius in a sperical gaseous core nuclear reactor with complete separation between the U-H_2 core and surrounding hydrogen. The reactor shown in figure 45 has a core

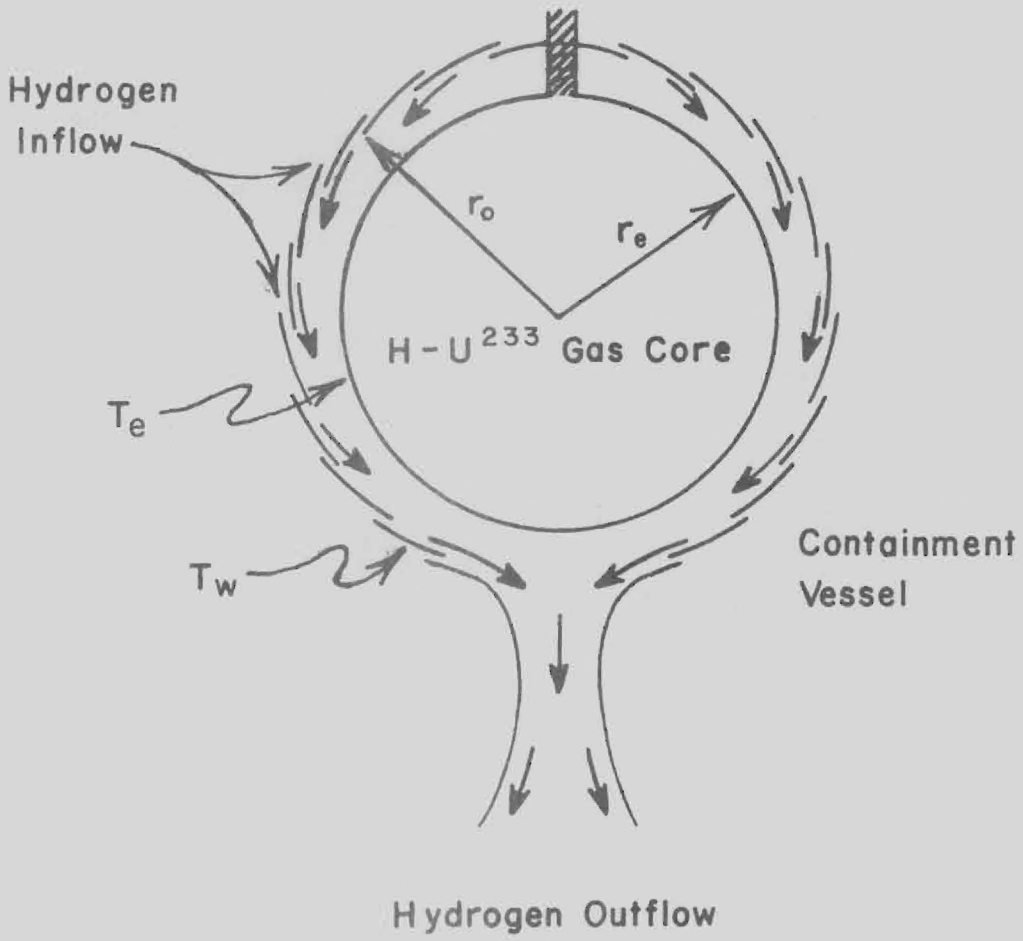

Figure 45. Gas Core Power Reactor with Perfect Containment of the Fuel Region (Infinite Separation Ratio)

which is a hydrogen and uranium-233 plasma. The core is separated form its containment vessel by flowing hydrogen. The hydrogen and uranium gases are assumed gray gases, which means the radiation absorption coefficient is independent of wavelength. The containment wall is also assumed gray so that the wall emissivity and reflectivity are independent of wavelength.

The basic approach used for solving temperature profiles is the same as that proposed by Ragsdale and Kascak[42]. The radiation absorption coefficient is assumed temperature dependent and the volumetric heat generation rate may be radically dependent.

Assuming that the heat flow is basically a diffusion process, the heat flux may be related to the temperature gradient by

$$q = \frac{-4}{3K} \frac{\partial e_g}{\partial r} \qquad (1)$$

where $e_g = \sigma T^4$ is the gas emissive power

K = temperature dependent absorption coefficient

q = heat flux

The temperature T must be expressed in absolute units and σ is the Stefan-Boltzmann constant.

The heat flux q can be easily related to the volumetric heat generation rate Q. Let us assume that Q may be expressed as an n^{th} degree polynomial in r

$$Q(r) = \sum_{i=0}^{n} Q_i r^i \qquad (2)$$

The heat flux q for a sphere is given by

$$q(r) = \frac{\int_0^r Q(r) 4\pi r^2 dr}{4\pi r^2} = \frac{\int_0^r \sum_{i=0}^{n} Q_i r^i \; 4\pi r^2 dr}{4\pi r^2} \tag{3}$$

Integration gives

$$q(r) = \sum_{i=0}^{n} \frac{Q_i r^{i+1}}{i+3} \tag{4}$$

Equation (1) may now be expressed as

$$\frac{\partial e_g}{\partial r} = \frac{-3K}{4} \sum_{i=0}^{n} \frac{Q_i r^{i+1}}{i+3} \tag{5}$$

which relates the volumetric heat generation rate and absorption coefficient to the gas emissive power. Introducing the relation for e_g defined previously, Eq. (5) becomes

$$4\sigma T^3 \frac{\partial T}{\partial r} = \frac{\partial(\sigma T^4)}{\partial r} = \frac{-3K}{4} \sum_{i=0}^{n} \frac{Q_i r^{i+1}}{i+3} \tag{6}$$

which, if T is considered as a function of r only, can be written as a first order, first degree differential equation

$$T'(r) = \frac{dT}{dr} = \frac{-3K(T)}{16\,\sigma T^3} \sum_{i=0}^{n} \frac{Q_i r^{i+1}}{i+3} \; i \tag{7}$$

Equation (7) may be solved numerically for the core temperature profile by use of Runga-Kutta methods. However, the edge temperature, T_e, at the core boundary is not a known quantity.

Because of materials limitations, the containment wall temperature T_w is constrained. This in turn affects the core edge temperature

T_e. The edge temperature can be evaluated from the brightness temperature.

Let a brightness temperature T_b be so defined that σT_b^4 gives the radiated heat flux q_R

$$q_R = \sigma T_b^4 \tag{8}$$

The brightness temperature can be determined from the net heat flux from the core edge by

$$q_e = \sigma F(T_b^4 - T_w^4) \tag{9}$$

F is the geometric configuration factor given by

$$F = \left\{1 + \left(\frac{r_e}{r_o}\right)^2 \left(\frac{1 - \varepsilon_w}{\varepsilon_w}\right)\right\}^1 \tag{10}$$

where r_o is the containment wall radius and ε_w is the emissivity of the wall; the emissivity of the core edge is assumed to be 1. If the reactor core were radiating heat to a black environment at zero temperature $q_e = \sigma T_b^4$.

The brightness temperature is obtained by substituting Eq. (10) into Eq. (9) yielding

$$T_b = \left\{\frac{q_e}{\sigma}\left[1 + \left(\frac{r_e}{r_o}\right)^2 \left(\frac{1 - \varepsilon_w}{\varepsilon_w}\right)\right] + T_w^4\right\}^{1/4} \tag{11}$$

where q_e is obtained form Eq. (4).

$$q_e = \sum_{i=0}^{n} \frac{a_i r_e^{i+1}}{i + 3} \tag{4}$$

Ragsdale and Kascak propose the following relationship between the edge temperature T_e and the brightness temperature T_b,

$$\frac{T_e}{T_b} = \left[\frac{1}{2}\left(1 + \frac{a}{\tau}\right)\right]^{1/4} \qquad (12)$$

where τ is the optical thickness KD for a sphere of diameter D. The constant a is equal to 3 for a sphere. Therefore, Eq. 12 becomes

$$\frac{T_e}{T_b} = \left[\frac{1}{2}\left(1 + \frac{3}{2Kr_e}\right)\right]^{1/4} \qquad (13)$$

Equation 12 was obtained by writing a heat balance on the outermost "layer of gas in the radiating volume. The layer was considered to be optically thin ($\Delta\tau << 1$) and all gas in the layer was assumed to be at temperature T_e.

Equation 13 may not be directly evaluated because K is a function of T and, therefore, must be evaluated at T_e. Rewriting Eq. 13 as

$$T_e = T_b\left[\frac{1}{2}\left(1 + \frac{3}{2r_e K(T_e)}\right)\right]^{1/4} \qquad (14)$$

indicates that T_e must be determined by iterative methods. This is accomplished by the use of Newton's method which is essentially a difference halving process.

Once Eq. 14 is solved for the edge temperature, Eq. 7 may be solved numerically for the temperature profile across the core.

The data used for temperature dependent absorption coefficients for hydrogen and uranium-233 are tables prepared by Patch and Parks, et al., respectively. The data for uranium-233 and hydrogen are shown in Figs. 46 and 47, respectively. Their data are actually Rosseland Mean Opacities which are approximated in this analysis as absorption coefficients. Since the opacities are functions of temperature and pressure, the data are presented in tables of opacity versus temperature for several pressures. The data could

be used in tabular form for determining temperature distributions by Eq. 7; however, excessive run times would be involved due to the necessary interpolations. Consequently, it was decided to fit the data by polynomials. For a given element and pressure, the data were divided into three regions based on temperature and the curve in each region approximated by an appropriate n^{th} degree polynomial. Different regions were necessary to get an adequate fit over the entire temperature range because of sharp slopes apparent in the data.

The polynomials were determined by polynomial regression analysis. This analysis indicates the degree of polynomial necessary to give a reasonably good fit to a set of data points, in this case (T,K). The technique employs a least squares fit of the data by successive polynomials and examines the standard deviation about the regression line in each case. The smaller the deviation, the better the fit.

Polynomials for absorption coefficient as a function of temperature were calcualted using the method of polynomial regression in a computer program listed by Carnahan, Luther, and Wilkes. Table 1 gives the resulting data for uranium-233 and Table 2 gives the data for hydrogen. The bi are listed across the page as b1, b2, b3,...

In finding the core temperature distribution by Eq. 7, the absorption coefficient for mixtures of uranium and hydrogen must be known. This is calculated form the respective mole fractions of each constituent. The total absorption coefficient can be expressed as the sum of the mole fraction of each constituent times its respective absorption coefficient.

TABLE 7. CURVE FITTING COEFFICIENTS FOR ROSSELAND MEAN OPACITIES FOR URANIUM

	n	Bo	Bi (i = 1,2,...,n)		
Pressure 100 atm					
Region I	2	78.411241	0.07142237	-0.19510212-05	
9,000°R < T < 18,000°R					
Region II	3	-2464.3373	0.43378078	-0.18453261-04	0.23436684-09
18,000°R < T < 36,000°R					
Region III	5	517.46978	-0.01780635	0.25569865-06	-0.18418945-11
36,000°R < T < 162,000°R			0.65434720-17	-0.9119177-23	
Pressure 200 atm					
Region I	2	343.5128	0.12325828	-0.31180460-05	
9,000°R < T < 18,000°R					
Region II	3	-142.48971	0.27006503	-0.12279980-04	0.14357437-09
18,000°R < T < 37,800°R					
Region III	5	1065.3079	-0.0338455.8	0.14255469-05	-0.30166070-11
37,800°R < T < 162,000°R			0.99109368-17	-0.12707349-22	
Pressure 500 atm					
Region I	1	2247.821	0.10923947		
9,000°R < T < 18,000°R					
Region II	3	6319.1810	1.3405559	-0.52168067-04	0.57485233-09
18,000°R < T < 36,900°R					
Region III	5	3577.0967	-0.11527248	0.15726356-05	0.10863165-10
36,900°R < T < 162,000°R			0.37289915-16	-0.50554460-22	
Pressure 1000 atm					
Region I	2	3101.4171	0.48893969	-0.10624812-04	
9,000°R < T < 23,400°R					
Region II	2	28278.333	-1.107116	0.11528397-04	
23,400°R < T < 47,700°R					
Region III	4	4683.364	-0.111246172	0.107141709-05	-0.47221869-11
47,700°R < T < 162,000°R			0.782717345-17		

TABLE 8. CURVE FITTING COEFFICIENTS FOR ROSSELAND MEAN OPACITIES FOR HYDROGEN

	n	Bo	Bi (i = 1,n)	
Pressure 100 atm				
Region I	1	-0.9232474-03	0.18465474-06	
5,000°R < T < 10,000°R				
Region II	3	0.27430530	-0.55909157-04	0.33266415-08
10,000°R < T < 40,000°R			-0.45863002-13	
Region III	4	0.51056687	0.27215882-04	-0.12613882-08
40,000°R < T < 90,000°R			0.15771435-13	0.64104167-19
Pressure 250 atm				
Region I	1	-0.33938046-02	0.67878046-06	
5,000°R < T < 10,000°R				
Region II	4	1.6636352	-0.35634726-03	0.24367824-07
10,000°R < T < 40,000°R			-0.57673215-12	0.46082694-17
Region III	4	-7.6287698	0.66147455-03	-0.16297889-07
40,000°R < T < 90,000°R			0.16267037-12	-0.58333333-18
Pressure 500 atm				
Region I	1	-0.90829947-02	0.18165995-05	
5,000°R < T < 10,000°R				
Region II	4	3.6883812	-0.80889054-03	0.56031524-07
10,000°R < T < 50,000°R			-0.12914091-11	0.10263729-16
Region III	3	65.812377	-0.23385567	0.28980714-07
50,000°R < T < 90,000°R			0.12253333-12	
Pressure 1000 atm				
Region I	1	-0.23708567-01	0.47418567-05	
5,000°R < T < 10,000°R				
Region II	3	3.7094896	-0.83737335-03	0.52732395-07
10,000°R < T < 50,000°R			-0.60638168-12	
Region III	3	-34.1074	0.27437167-02	-0.4435-07
50,000°R < T < 90,000°R			0.20483333-12	

The above equations were coded in FORTRAN V to determine the temperature profile across the core of a gaseous core nuclear reactor. The Georgia Tech Univac 1108 digital computer was employed because of its inherent speed and ease of programming.

The computer code consists of a main program and two subroutines, DEQG and RKG. The main program controls the input and output of all data and the calculation of the edge heat flux, brightness temperature, and edge temperature. The subroutine RKG is a four-pass, fourth-order Runge-Kutta integration routine which integrates the differential equations contained in subroutine DEQG.

Input into the main program is through two namelist qualities, INPUT and ARREY. The namelist statement was chosen for ease of data manipulation. In a parameter study, usually only 1 or 2 variable quantities are changed per case and with the namelist usage only they must be changed. This results in computer time savings when many cases are run. Under INPUT the following input data are read: polynomial coefficients in Q expression (watts/m^3), core edge and containment wall radii (m), wall temperature ($^\circ$R), wall emmissivity, pressure (atm), mole fractions of uranium and hydrogen, integration and print increments, region boundaries ($^\circ$R) in the absorption coefficient polynomials for uranium and hydrogen. Under ARREY input the absorption coefficient polynomial degree and coefficients (cm^{-1}) are read. The output of these namelist input data is through conventional namelist output modes. All input data needed in the DEQG subroutine are stored in common.

The initial calculations in the main program are the edge heat flux and brightness temperature by Eqs. 4 and 11, respectively. Next the edge temperature is determined iteratively by Eq. 14. The iterative scheme is basically a difference halving approach. The edge temperature T_e is approximated by an initial guess of $T_e = 0.7\ T_b$. With this value of T_e, the right hand side (RHS) of Eq. 14 is evaluated. The polynomials previously determined are used for the calculation of $K(T_e)$. The value of T_e is compared with the value of the RHS and if the difference is less than a tolerance of 10^{-2} the iteration is halted. If the difference is not less than the tolerance, iteration continues. The magnitude of T_e is compared to that of the RHS. If T_e is less than the RHS in absolute magnitude, T_e is replaced by $T_e + \Delta T$ where T is initially set equal to 20°R. However, if T_e is greater than the RHS, T_e is replaced by $T_e - \Delta T$ where $T = 10°R$. Once this new value of T_e is determined the RHS of the equation is recomputed and all the comparison tests are rerun. The new value of T_e is again determined by $T_e = T_e + \Delta T$ but ΔT is cut in half each time T_e and RHS alternate in greatest magnitude; hence the half difference techanique. Once the difference between T_e and RHS is less than the tolerance, iteration halts and printout of q_e, T_b, and T_e occurs.

Finally, the temperature profile is calculated across the core as a function of radius from the core edge inwards toward the center. The DEQG subroutine is called to compute the initial value of $T'(r_e)$ as given by Eq. 7. Subroutine RKG is then called with a negative integration increment $\Delta r'$ such that the independent variable r' is

decremented from 1 to 0 in steps of r'. The variable r' is a dimensionless radius defined as (r/r_e) such that it is 1 when $r = r_e$ and 0 when $r = 0$. In essence RKG calls DEQG four times in its determination of T' and T at each increment of r'. After RKG makes its last pass through DEQG it returns to the main program when output occurs. The output lines consist of three variables--r, r', and T. The increments at which r' is printed are determined by ΔP which is equal to multimples of the absolute value of $\Delta r'$. When r' falls below zero, computation is terminated and control is returned for initialization of the next data case. If no other data cases follow, run termination results. For $\Delta r = -0.01$ and $\Delta P = 0.01$, run times are approximately 1 second per case and convergence is assured.

An accuracy check was performed on the computer program by running data cases presented in Ragsdale and Kascak.[42] Figure 4 on page 23 of their report shows $T.T_b$ versus r' for values of τ equal to 0.1, 1, 100, and 1000. The volumetric heat generation rate was assumed uniform and the absorption coefficient assumed constant. Their cases did not have a containment vessel around the gas volume which requires $T_w = 0$ and $\varepsilon_e = 1.0$. These four cases were rerun on the current computer program and the results were identical. Plots of these curves are given in Fig. 48. Since identical results were obtained for these cases, it is tacitly assumed that the current program will give valid results when the absorption coefficient is a function of temperature, when there is a non-uniform volumetric heat generation rate, and when the containment vessel wall temperature is constrained.

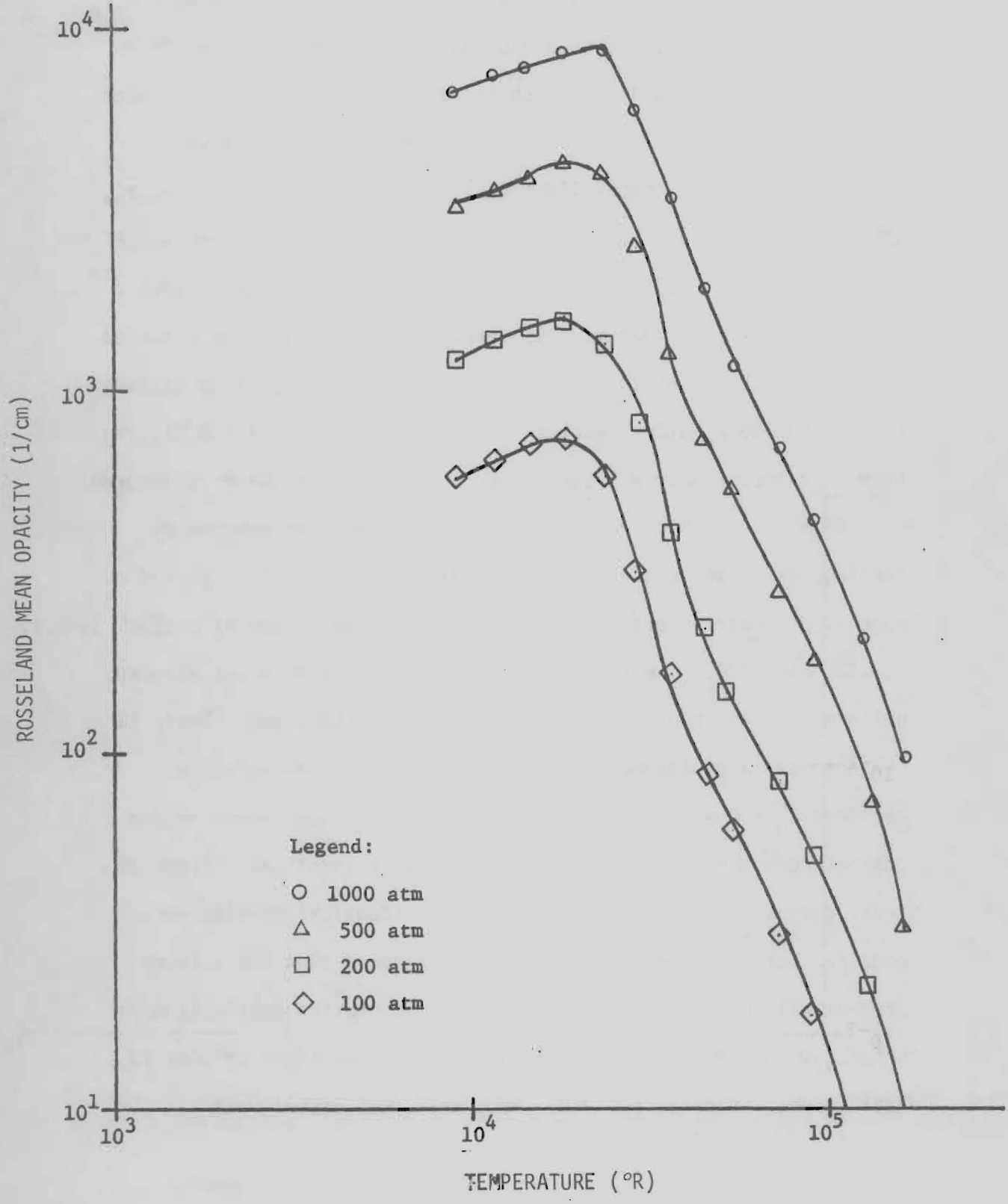

Figure 46. Rosseland Mean Opacity versus Temperature for Uranium[43].

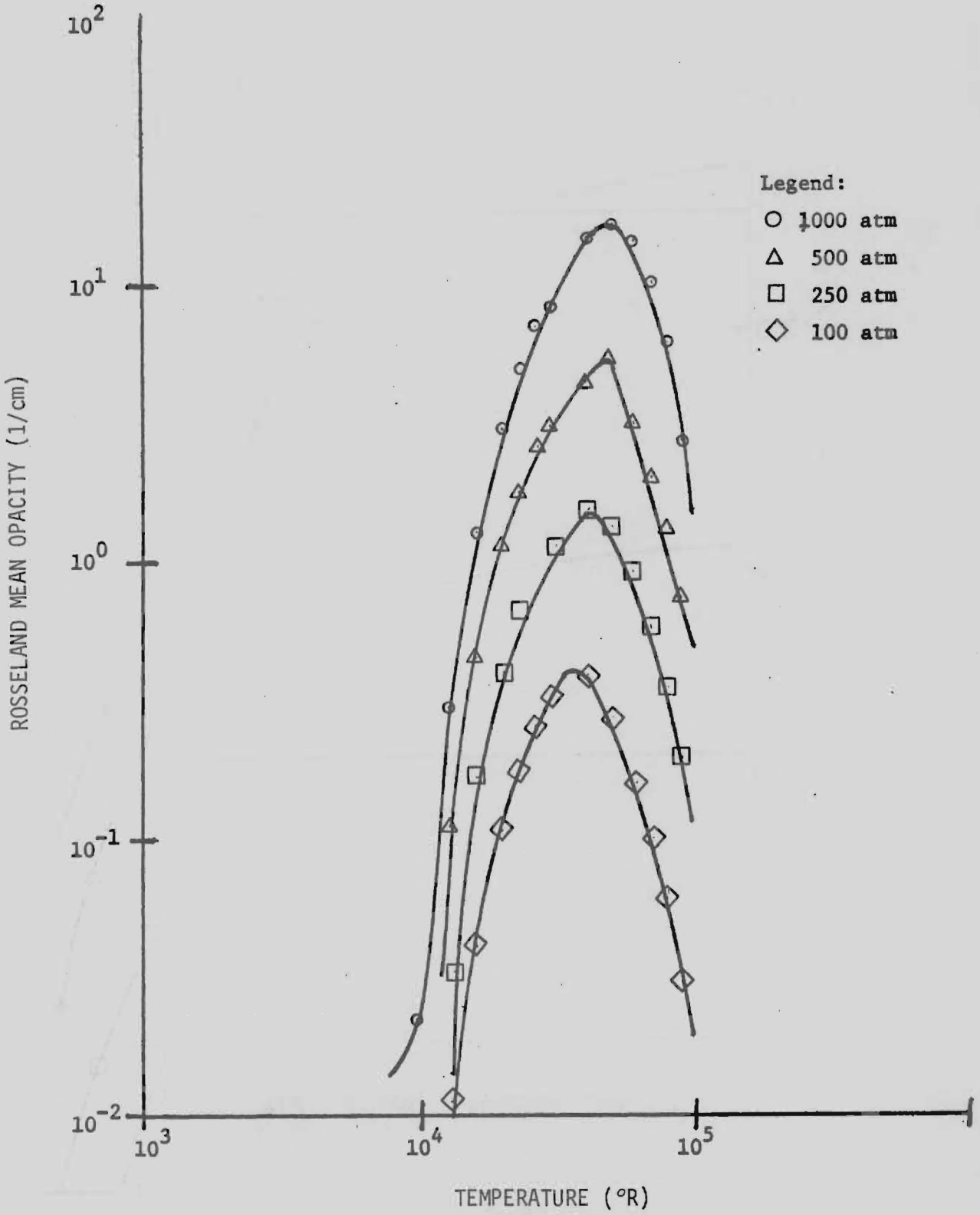

Figure 47. Rosseland Mean Opacity versus Temperature for Hydrogen[44].

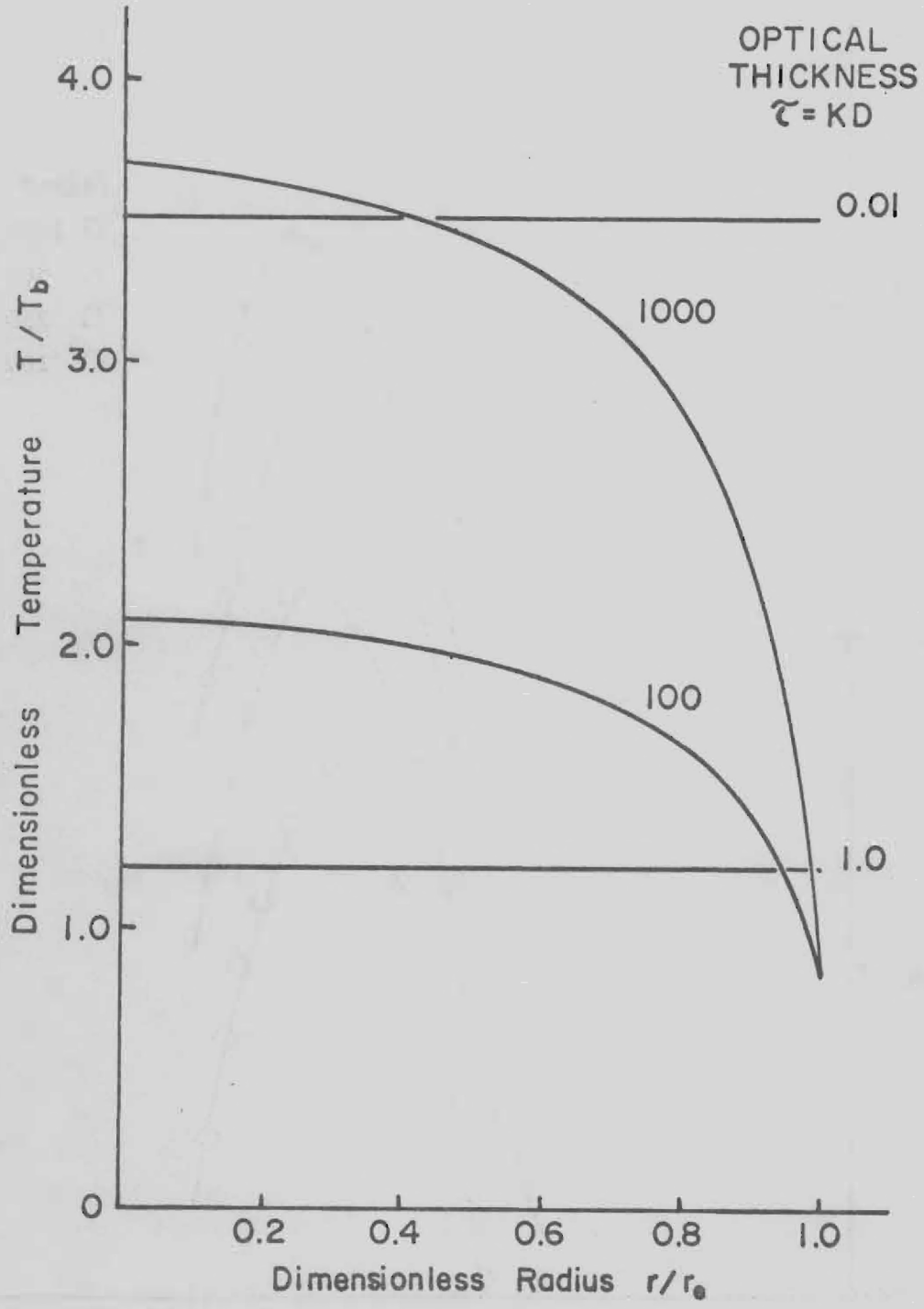

Figure 48. Dimensionless Temperature Profile in Gas Core Reactor with Perfect Containment.

REFERENCES

REFERENCES

1. G. R. Seikel, and L. D. Nichols, "The Potential of Nuclear-MHD Electric Power Systems", NASA TM X-67829, June 1971.

2. R. R. Holman and S. Way, "Exploring a Closed Brayton Cycle MHD Power System Applying Nerva Technology", AIAA Paper No. 70-1225, October 1970

3. Y. S. Tang, J. S. Stefanko, P. W. Dickson, and D. W. Drawbaugh, "An Engineering Study of the Colloid-Fuel Reactor Concept," Journal of Spacecraft and Rockets, Vol 8, No. 2, February 1971

4. B. N. Truman, J.A. Kyslinger, and J. M. Ravets, "An Analysis of the Operating Characteristics of the Colloid Core Reactor", AIAA Paper No. 72-1094, December 1972.

5. W. A. Carbiener and R. A Robinson, "Experimental Investigation of Heat Release in a Particle-Seeded Vortex", Battelle Columbus Labrotories, (Quarterly Progress Report, contract F33615-73-C-4027), January 1973.

6. Rodgers, R.J., Latham, T. S. and Clark, J. W., " Analytical Design and Performance Studies of the Nuclear Light Blub Engine", United Aircraft Research Laboratories Technical Report L-910900-16, September 1972.

7. McLafferty, G. H., "Gas Core Nuclear Rocket Engine Technology Status", Journal of Spacecraft and Rockest, 1, No. 12, 10, 1391, December 1972.

8. Research on Uranium Plasmas and Their Technological Applications edited by K. Thom and R. T. Schneider, published by the NASA Scientific and Technical Information Office, NASA SP-236, January 1970.

9. 2nd Symposium on Uranium Plasmas: Research and A pplications, published by the AIAA, November 1971.

10. J. D. Clement and J. R. Williams, "Gas Core Reactor Technology", Reactor Technology, 13, No. 3, 226-51, Summer 1970.

11. R. G. Ragsdale, "To Mars in 30 Days by Gas Core Nuclear Rocket", Astronautics 10, No. 1, 65-71, January 1972.

12. T. S. Latham and R. J. Rodgers, "Analytical Design and Performance Studies of Nuclear Furnace Tests of Small Nuclear Light Blub Models, "United Aircraft Recearch Laboratories Report No. L-910900-17, September, 1972.

13. J. R. Williams, Y. Y. Yang, K. D. Kirby, and J. D. Clement, "Exploratory Investigation of an Electric Power Plant Utilizing a Gaseous Core Reactor with MHD Concersion", ANS Nuclear Power for Tomorrow Conference, August, 1972.

14. J. R. Williams, Y. Y. Yang, K. D. Kirby, and J. D. Clement, "Exploratory Investigation of an Electric Power Plant Utilizing a Gaseous Core Reactor with MHD Conversion", Proceedings of the 7th IECEC, September, 1972.

15. R. J. Rosa, Magnetohydrodynamic Energy Conversion, McGraw-Hill Book Company, Inc. New York, 1968.

16. J.R. Williams and S. V. Shelton, "Gas-Core Reactors for MHD Power Systems", Proceedings of the Symposium on Research on Uranium Plasmas and their Technological Applications University of Flordia, January, 1970.

17. J.R. Williams, J. M. Kallfelz, and S. V. Shelton, "A Parametric Survey of a Gas Core Reactor-MHD Power Plant Concept, "Energy 70:Proceedings of the Intersociety Energy Conversion Engineering Conference, Las Vegas Nevada, September 21-25, 1970.

18. J. R. Williams "A Study of a Gas Core Reactor-MHD Power Plant Concept", Trans. Am. Nucl. Soc., 13, No. 3, 446-7, November 1970.

19. J. R. Williams, "A Gaseous Core Reactor for MHD Power Generation", Proceedings of the Frontiers of Power Technology Conference, Stillwater, Oklahoma, October 1971.

20. J. M. Kallfelz and J. R. Williams, "Exploratory Calculations for a Gaseous Core Breeder Reactor", Proceedings of the 2nd Symposium on Uranium Plasmas: Research and Applications, Georgia Tech, Atlanta, Georgia, November, 1971.

21. J. R. Williams and R. J. Rosa, "A Gaseous Core Reactor with MHD Conversion for Electrical Power Generation, Trans. Am. Nucl. Soc., 14, No. 2, October 1971.

22. W. C. Brown, "Transportation of Energy by Microwave Beam", Proceedings of of the 1971 IECEC, Boston, Mass. August 1971.

23. J. Mockovciak, Jr."A Systems Engineering Overview of the Satelite Solar Power Station", Proceedings of the 7th IECEC, 712-19, September 1972.

24. C. L. Whitmarsh, Jr., "Neutronics Analysis of An Open-Cycle High-Impulse Gas-Core Reactor Concept, "NASA TM X-2534, April, 1972.

25. J. F. Kunze, et.al., "Benchmark Gas Core Critical Experiment, " Nuclear Science and Engineering: 47,59-65 (1972).

26. R. E. Hyland, "Evaluation of Critical Mass for Open-Cycle Gas-Core Rocket Reactors," Nuclear Technology, Vol. 12, October, 1971.

27. D. A. Meneley, et al., "MACH-1, A One-Dimensional Diffusion Theory Package," ANL-7223 (1966).

28. B. J. Toppel and I. Baksys, "The Argonne-Revised THERMOS Code," ANL-7023 (1965).

29. I. I. Bondarenko, ed., Group Constants for Nuclear Reactor Calculations, Consultants Bureau, New York (1964).

30. R. W. PATCH, "Thermodynamic Properties and Theoretical Rocket Performance of Hydrogen to 100000 K and 1.01325 x 10^{8} N/M^{2}," NASA SP-3069, 1971.

31. R. F. Kubin and L. L. Presley, "Thermodynamic Properties and Mollier Chart Hydrogen from 300°K", NASA SP-3002, 1964.

32. M. W. Rosenthal, et al., "Molten-Salt Reactors--History, Status, and Potential," Nucl. Appl. and Tech., 8, Feb. 1970, p. 107.

33. R. W. Patch "Thermodynamic Properties and Theoretical" Rocket Performance of Hydrogen to 100000°K NASA SP-3069, 1971.

34. W. M. Kays and S. L. London Compact Heat Exchangers second edition, 1964.

35. Satellite Solar Power Station: Systems Engineering Report, Grumman Aerospace Corporation, Bethpage, New York, Report No. ASP 583-R-8, November 1971.

36. R.G. Ragsdale, "High Specific Impulse Gas-Core Reactors," NASA TM X-2243, March 1971.

37. R.G. Ragsdale, "Some Fuel Loss and Weight Estimates of an Open-Cycle Gas-Core Nuclear Rocket Engine," NASA TM X-52775, June 1970.

38. W. R. Durkee and F. B. Damerval, "Nuclear Rocket Experimental Engine Test Results," AIAA Paper No. 70-709, June 1970.

39. Y. S. Tang, J. S. Stefanko, P. W. Dickson and D. W. Drawbough, "An Engineering Study of the Colloid Fueled Reactor Concept," AIAA Paper No. 70-688, June 1970.

40. F. J. J. Stekly, R. J. Thome, R. F. Cooper and R. Pope, "Superconducting Saddle Magnet Design Considerations," Proceedings of the 12th Symposium on the Engineering Aspect of Magnetohydrodynamics, March, 1972.

41. Haller H.C. and Leiblein, "Analytical Comparison of Rankine Cycle Space Radiators Constructed of Central, Double and Block-Vapor-Chamber Fin-Tube Geometries," NASA TN-D-4411, 1968.

42. Ragsdale, Robert G. and Albert F. Kascak, "Simple Equations for Calculating Temperature Distributions in Radiating Gray Cases," NASA TN D-5226, May 1969.

43. D. E. Parks, G. Lane, J. C. Stewart, and S. Peyton, "Optical Constants of Uranium Plasma," NASA CR-72348, GA-8244, February 1968.

44. Patch, R. W., "Interim Absorption Coefficients and Opacities for Hydrogen Plasma at High Pressure," NASA TM X-1902, October 1969.

45. Carnahan, Brice, H. A. Luther, and James O. Wilkes, "Applied Numerical Methods," John Wiley & Sons, Inc., New York, 1969.